ELECTRON EMISSION FROM SURFACES RESULTING FROM LOW ENERGY POSITRON BOMBARDMENT

by

SAURABH MUKHERJEE

Presented to the Faculty of the Graduate School of

The University of Texas at Arlington in Partial Fulfillment

of the Requirements

for the Degree of

DOCTOR OF PHILOSOPHY

THE UNIVERSITY OF TEXAS AT ARLINGTON

December 2008

ACKNOWLEDGEMENTS

I would like to express my gratitude to my dissertation supervisor, Alex Weiss , who introduced me to the wonderful world of positrons. Special thanks for all the discussions that we had over endless cups of coffee. Thanks to Dr. Ali Koymen, Dr. Suresh Sharma, Dr. Nail Fazleev, and Dr. Asok Ray for their excellent suggestions and advice.

My deepest gratitude towards Manori for teaching me about UHV and surface physics and above all having patience with me when I would ruin the vacuum. My heartfelt thanks to Doug for providing me with all the MP3 CD's that I could name and the honest advice.

Thanks to Maria for being the sounding board for all my crazy ranting and the discussion about Mircea Eliade. Special mention must be made of Brian for teaching me the "hammer method" of making UHV electronics work.

This list will not be complete without the mention of some of wonderful colleagues I had- Yogi, Tommy, Debrup, Arnab, Souptik, Karthik, Ajani. Thanks for making my stay here cheerful.

Special mention should be made of the wonderful administrative staff in physics- Margie, Amy, Fran , Stacy and Caye. Thanks for making this our home away from home.

Finally, I would like to thanks my parents- Gour Shankar and Aparna- for their support and encouragement.

November, 2008

ABSTRACT

ELECTRON EMISSION FROM SURFACES RESULTING FROM LOW ENERGY POSITRON BOMBARDMENT

Saurabh Mukherjee, PhD.

The University of Texas at Arlington, 2008

Supervising Professor: Alex H. Weiss

Measurements of the secondary electron energy spectra resulting from very low energy positron bombardment of a polycrystalline Au and Cu (100) surfaces are presented that provide evidence for a single step transition from an unbound scattering state to an image potential bound state. The primary positron energy threshold for secondary electron emission and energy cutoff of the positron induced secondary electron energy peak are consistent with an Auger like process in which an incident positron make a transition from a scattering state to a surface-image potential bound while transferring all of the energy difference to an outgoing secondary electron. We term this process: the Auger mediated quantum sticking effect (AQSE). The intensities of the positron induced secondary electron peak are used to estimate the probability of this process as a function of incident positron energy. Positron annihilation induced Auger spectra (PAES) of Cu and Au are presented that are free of all primary beam induced secondary electron background. This background was eliminated by setting the positron beam energy below AQSE threshold. The background free PAES spectra obtained include the first measurements of the low energy tail of CVV Auger transitions all the way down to zero kinetic energy. The integrated intensity of this tail

is several times larger than Auger peak itself which provides strong evidence for multi-electron Auger processes

TABLE OF CONTENTS

APPENDIX

LIST OF ILLUSTRATIONS

LIST OF TABLES

CHAPTER 1

INTRODUCTION

1.1 Overview

Positron annihilation induced Auger electron spectroscopy (PAES) has been shown to be a useful tool in analyzing the chemistry of technologically important surfaces [1a-1c,39-50]. PAES has been used to study ultra thin film growth, surface alloying and intermixing, the growth of self assembled nano-structures[1a], and studies adsorption[1b] and passivation[1c]. In PAES the core hole is created by positron tunneling into the core region and annihilating with a core electron. Weiss et al. [56] have predicted that due to the fact that the core holes necessary for the Auger process are excited by an annihilation process (and not impact ionization as in conventional Auger techniques) it should be possible to excite the Auger process with a positron incident on the sample at arbitrarily low energies. Till now PAES studies have all been performed with positron beam energies on the order of 10's of eV. The use of these energies was necessitated by the limitations associated with the charged particle optics of the beam transport system. For the measurement reported in this dissertation, the beam optics was optimized for very low beam energy operation. This permitted PAES measurements to be performed using beam energies an order of magnitude lower than in previous experiments. Measurements performed with the very low energy positron beam settings developed made it possible, for the first time, to observe a direct one-step transition from an unbound positron scattering state to the bound image potential surface state. The use of very low positron beam energies also permitted the first measurements of Auger spectra that were completely free of primary beam induced secondary electron background

1.1.1 Quantum Sticking of Positrons-Single Step Transition into the Image Potential Surface State

The measurements reported in Chapter 3 provide direct evidence for a one step process in which a positron makes a direct transition from the scattering state to the image potential bound state. This process is referred to as positron sticking to surfaces [18]. The sticking process is treated here quantum mechanically and is justified based on the consideration of the incident particle wavelength and the potential well width. The incident positrons of energy 1eV have wavelength (λ_{dB}) 12Å which is almost an order of magnitude larger than the image potential induced surface state well width (W_{ss}), 2Å. We have shown that the transition from the scattering state to the bound state is accompanied by the creation of an electron hole pair in which the electron has sufficient energy to leave the surface. This process may be thought of as a form of Auger transition where the incident positron makes a transition from the scattering state to the image potential bound state and creating a secondary electron in the process. Hence the process has been termed as Auger mediated quantum sticking.

Quantum mechanically the deciding factor is the de broglie wavelength of the particle, λ and the width of the potential well, λ_C. The quantum limit is defined as when $\lambda >> \lambda_C$ [3]. In the experiments reported here the positron energy is in the range of 1.5eV-7eV and this corresponds to λ in the range of 10-4.6A while the image potential induced surface well has width of 2A. Hence for most of the range of energies considered in the measurements reported in this dissertation, we can consider the positron interaction with the surface to be dominated by quantum effect.

As the particle approaches the potential well at the surface, the wavelength mismatch at the boundary results in reflection. A detailed analysis shows that $S_0 = S(0,0)$ is 0 as $E \to 0$. The incident particle in case of $E \to 0$, will end up getting stuck to the surface. Hence the classical and quantum mechanical approach are at odds with each other in the low energy regime. Mills and coworkers [4] found that the Positronium (Ps) sticking probability on

cold surface goes to 1 in the vanishing energy limit. They proposed that due to coupling to higher order virtual processes the effective mass changes leading to an increase in coupling to inelastic processes and in situations where the inelastic loss channel is due to phonon creation or electron-hole pair creation, Λ is very close to 0. In such a case, they claim S_0 is 0.

The research done here shows that in the energy range of 2.25eV to 7eV, positron sticking to the surface is associated with the electron –hole pair creation. The relation of the secondary electron peak to the surface density of states is explored as is the feasibility of using this phenomenon as a probe of the surface density of states.

1.1.2 Background Free Auger Measurements

The second part of the dissertation deals with the electron emission that follows after with the sudden creation of a core hole in solid. The background free Auger spectrums were obtained by lowering the incident positron energy below the secondary electron emission threshold. The resulting spectra are devoid of the primary beam induced secondary electrons.

Once created, a core hole may decay via radiative(X-ray emission) or a non-radiative transition (the Auger process).For core levels with less binding energy($E_b < 1000eV$) the Auger process is dominant while for higher binding energy core electrons X-rays emission dominates. However, in rare gases, another phenomenon called Double Auger occurs with some frequency [5]. Carlson and Krause [5] were the first to demonstrate how an excited atom with a core hole can relax via simultaneous emission of two electrons. The usual energy of the Auger electron, in this case, was to be shared asymmetrically by both the electrons. They described the probability of such a process as the square of the transition matrix, M_d [51], which is given by,

$$M_d = \int \psi_f(r_1, r_2, r_3)\left(\frac{1}{r_{12}} + \frac{1}{r_{13}} + \frac{1}{r_{23}}\right) \times \psi_i(r_1, r_2, r_3) d\tau_1 d\tau_2 d\tau_3 \qquad 1.1$$

They explained there observations by treating the outgoing electrons as due to the shake-off process [6]. Shake-off process happens when an inner core electron is knocked out resulting in a sudden change of the nuclear charge as seen by the other electrons [7]. These shake off phenomena appear as satellite structures in the resulting photoelectron spectra.

Most of the research related to the shake –off phenomenon deal with inner or deep core levels and hence the incident beam energy used is in keVs. The shake-off phenomena associated with shallow core states have not yet been studied because of the secondary electron background issues. In conventional electron induced Auger spectroscopy the core hole is created by exciting the bound electron with electrons of energy much higher than the binding energy of the core electron. In such an experiment, the Auger peak sits on a background consisting of electrons from the beam (primary electrons) and secondary electrons from the sample. This background is mostly fitted with a polynomial [8, 9] and subtracted to reveal the nature of the Auger peak. The drawback of this method of background subtraction is that it neglects the various intrinsic processes associated with the Auger process including- shake off, spectator Auger process etc. In case of positron annihilation induced Auger, both the abovementioned channels of secondary electron production are not present and hence the true contribution from sudden appearance of the core hoe can be explored. In PAES, the background is eliminated by using beam energy less than the excitation threshold for secondary electrons. Hence the only source of the background is the inelastic scattering of the Auger electrons with the sample surface. Such a spectrum can be compared to other techniques like Auger photoelectron coincidence technique. In APECS, the Auger electron is detected in coincidence with the corresponding photoelectron. This reduces the background but does not completely eliminate it. Jensen and coworkers [10] have carried out such experiments on Al surface and looked at the low energy tail (LET) associated with the Auger peak. They concluded that the observed large intensity spectral weight in the LET is due to intrinsic process associated with the creation of the core hole. The minimum measured energy of the LET was

~40eV. Here we present PAES data in which the LET has been measured up to 0eV. The various factors contributing to LET like the inelastic scattering of the Auger electrons, accidental background and beam induced secondary electron have been discussed.

1.2 Positron spectroscopy of solids

The positron has been employed in a variety of techniques to study the physical, chemical and electronic properties of solids. When a positron is incident upon a solid, there are various channels open to it. The most prominent are – Positronium formation, positron trapping in defect or surface state and positron reemission. These different channels may be exploited to extract chemical and electronic properties of solids. The various techniques are shown in table 1.1. Two of the principal techniques are Positronium lifetime spectroscopy and 2D Angular correlation of annihilation radiation (2D ACAR). In the lifetime experiments the incoming positron is tagged using various signals (e.g. detection of secondary electron generated by the positron when it hits a surface or of the gamma ray associated with positron production). Then the time delay from the signal indicates the START of the positron interaction with the sample and the annihilation signal from the gamma ray is measured and used to find positron lifetime. The lifetime data is then correlated to the defect structure of the sample. In the 2D ACAR the angular deviation between the two gamma rays emitted when the positron annihilates with a valence electron is measured and is used to map the Fermi level.

There are many channels open to positrons when they encounter a surface. In the high energy regime (>100eV) the incident positrons penetrate into the bulk, thermalize by phonon excitaition and then diffuse. The mean distance that thermalized positrons can diffuse before annihilating is given by $\sqrt{D\tau}$, where D is the diffusion constant and τ is the lifetime of positron in a solid. This diffusion length is typically around 1000A and consequently there is a high probability that a positron will encounter the surface. Once the thermalized positron reaches the surface, it can undergo various processes. The various processes possible are- Positronium formation, positron reemission, trapping in the image potential induced surface state. These

three processes occur with roughly equal probability. At low energies (~1eV) another process becomes important in addition to the above mentioned ones. This is described in the figure 1.1.

Table 1.1 Techniques using positrons as probes

Technique	Output Data	Information obtained
Positron/Positronium Lifetime Spectroscopy	Distribution of measured positron lifetime	Concentration and types of defects
2D ACAR	Angular distribution of annihilation gamma ray	Fermi surface /electronic properties
LEPD	Intensity of diffracted Positrons from crystal surfaces as a function of incident beam energy	Surface structure
Positron annihilation induced Auger electron spectroscopy	Energy distribution of Annihilation induced Auger electrons	Surface chemistry
Doppler Broadening Spectroscopy	Energy distribution of annihilation Gamma rays	Defect concentration and identification of chemical environment of defects

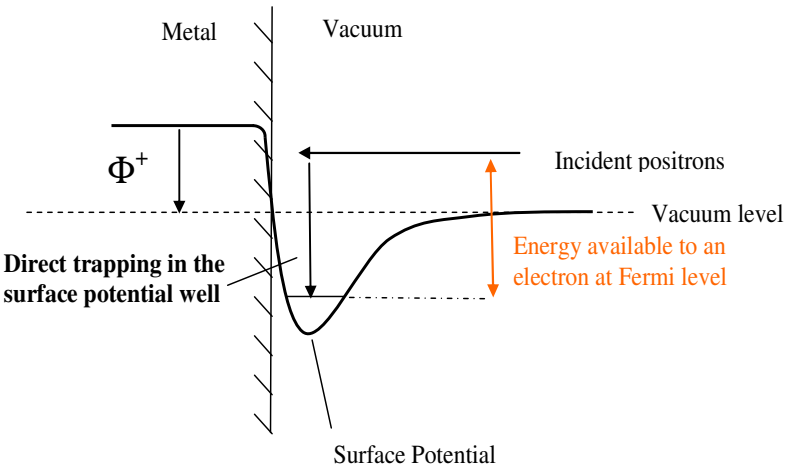

Figure 1.1 The slow positrons may be directly trapped in the surface state resulting in the release of an electron with the residual energy.

In this process the incident positron makes a transition from the scattering state to the image potential induced surface state. This transition may be thought of as a type of Auger mediated sticking.

1.3 Positron Work Function

The terms contributing to positron work function is shown schematically in fig1.2. Most of the positronic properties of solids can be derived from their electronic counterpart and hence the positron work function is quite equivalent to the electronic work function. In the jellium model the electron density spills out of the surface towards the vacuum and leads to the creation of a surface dipole whose corresponding potential step is represented by $\Delta\varphi$. This term along with the chemical potential, μ^-, relative to the mean electrostatic potential in the bulk gives rise to the electron work function

$$\Phi^- = \Delta\varphi - \mu^- \qquad 1.2$$

For positrons the signs are reversed. The $\Delta\varphi$ term is almost cancelled by the correlation potential V_{corr} . Hence the positron work function is given by

$$\Phi^+ = -\Delta\varphi - \mu^+ \qquad 1.3$$

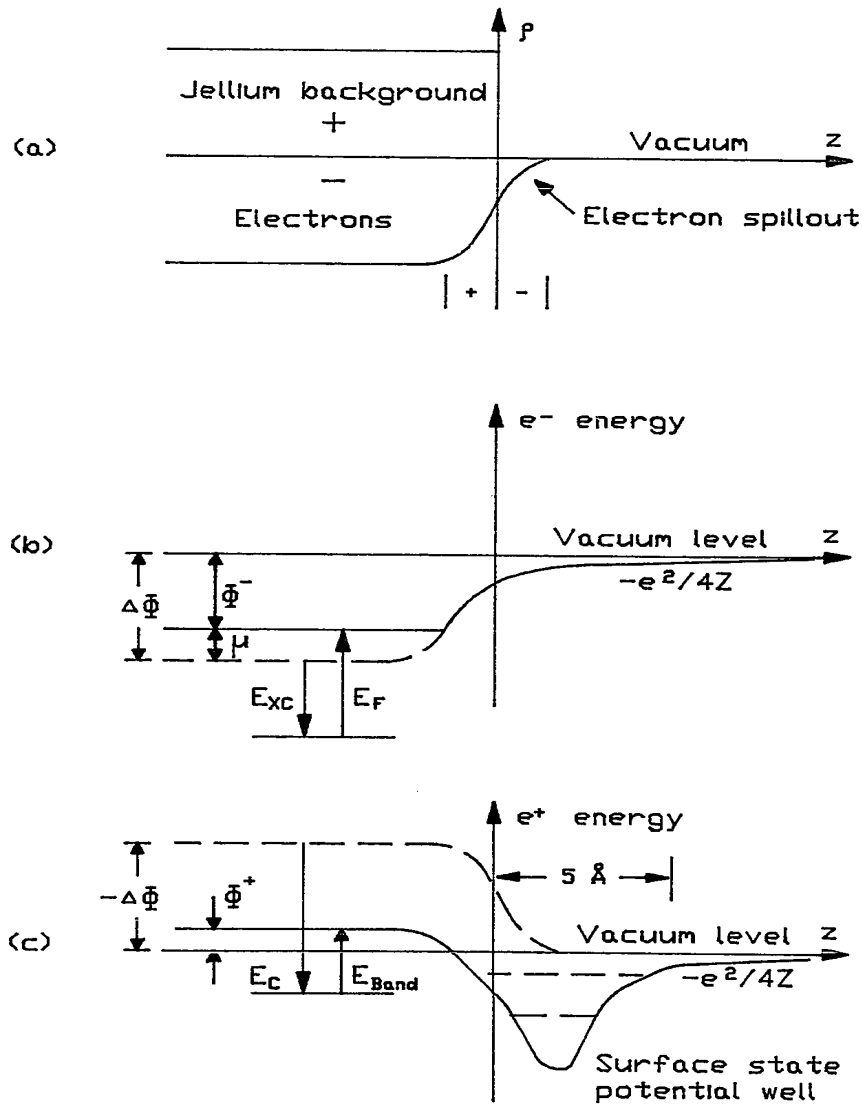

Figure 1.2 Schematic diagram showing terms contributing to the positron work function [11].

The positron chemical potential is given by

$$\mu^{+} = V_{corr} + V_0 \qquad 1.4$$

where V_0 is the zero point energy due to the positron-positive ion core interaction and causes the positrons to be repelled from the ions.

The zero point potential term arises due to the repulsion of the positron by the ion cores. The correlation term arises due to the enhancement of the electron density around the

positron which leads to the lowering of the total energy of the system. Due to the near cancellation of the dipole term by the correlation term, the positron work function is almost zero and sometimes negative. In the case of a metal with a negative positron work function there is spontaneous emission of positrons at thermal energies.

1.4 Image potential induced surface state

The Image potential induced surface state (hence forward referred to as surface state) has contribution from two factors- (a) the Correlation potential, $V_{Corr}(z)$ and (b) the Hartree potential, $V_H(z)$. Hence the potential can be written as,

$$V_{e^+}(z) = V_H(z) + V_{Corr}(z) \qquad 1.5$$

In the vacuum, the correlation part is modeled as the image potential and is given by,

$$V_{Corr}(z) = V_{im}(z) = \frac{-1}{2(z - z_{im})} \qquad 1.6$$

where z_{im} is the distance of image charge from the surface .This potential does not hold true for $z = z_{im}$ and hence the lower boundary for this is taken as the Positronium binding energy, 6.8eV.

The Hartree potential is defined as the superposition of the coulomb potential from all the surrounding atoms and is given by $V_{coulomb}^{atom}(|r - R|)$ where R is the positron of the atom.

1.5 Positron Annihilation induced Auger electron Spectroscopy(PAES)

PAES was developed by Weiss and coworkers in 1988[12]. In PAES, the core hole excitations that results in Auger electron emission are created by the matter- antimatter annihilation (see fig1.3).

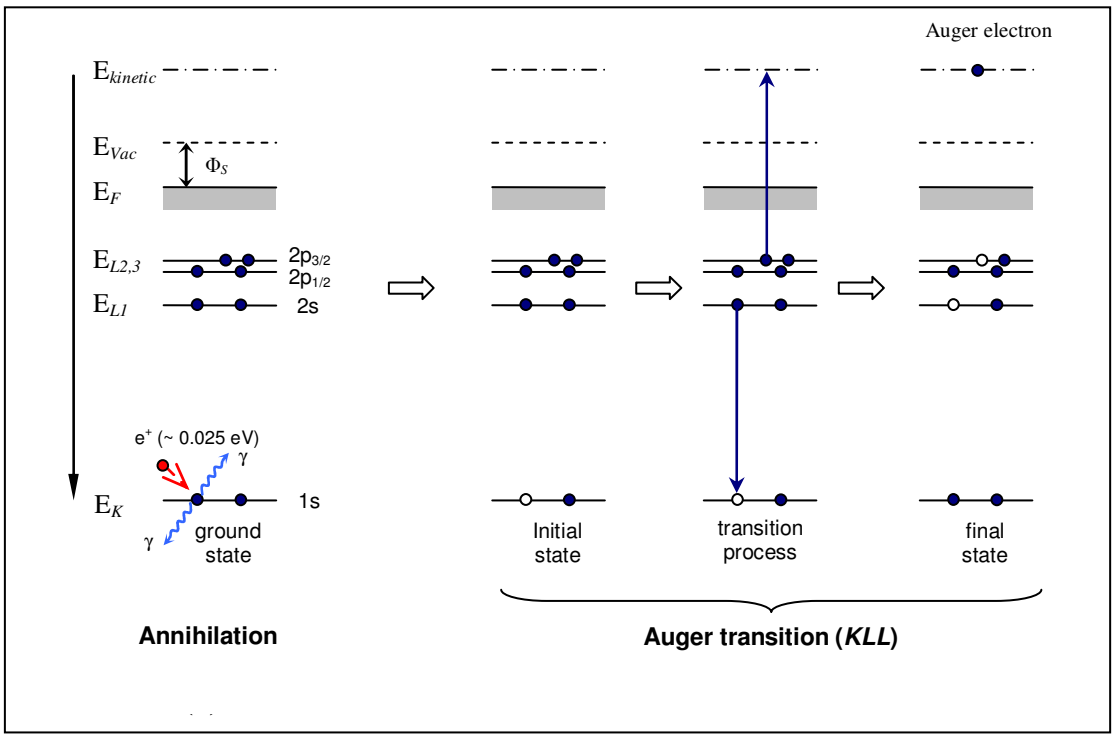

Figure 1.3 Schematic of the positron annihilation induced Auger electron (PAES process).

In a conventional Auger spectroscopy, like Electron induced Auger electron Spectroscopy (EAES), the beam consists of electrons in keV range. This high energy beam is used to knock the core electrons out by energy exchange. Consequently the incident beam energy must exceed the core electron binding energy. The main drawback in such a process is that the ratio of the Auger electron signal to the background due to secondary electron is very low. In PAES the beam energy is kept below the Auger excitation energy and hence the secondary electron background is greatly reduced giving rise to the high signal to the background ratio. Another advantage in using PAES is high surface selectivity. As the incident positron energy is in the order of tens of eV's , the positron is being stopped very close to the surface. The positron in

the sample loses energy by electron-hole pair and phonon creation and quickly attains the lowest energy possible given by the positron work function. For most of the metals this is very close to 0. Once the positron attains the lowest energy state, it undergoes random walk and ends up encountering the surface.

Once at the surface, the positron has a high probability of becoming trapped at the surface state potential. The trapped positron annihilates with the core electron of the surrounding atoms and hence almost the entire signal comes from the top most layers [13]. The fraction of PAES signal coming from the second and third layer of atoms of a low miller index plane can be estimated easily. If we assume a 1-D potential step at the surface the positron wave function is found to decay exponentially into the bulk be roughly given by e^{kz}. Here z is the distance from the surface into the vacuum which becomes more negative with increasing distance into the bulk and $k = [2(E_b - \phi^+)]^{1/2}$.Hence the ratio of the Auger intensity from the second and third layer is proportional to the ratio of the positron density between these two layers and can be written as e^{-2kd} ,where d is the interlayer spacing between the atoms. Using the values of $E_b - \phi^+ \approx 0.1$ a.u. and $d \approx 3$ a.u, this ratio turns out to be ≈ 0.07. Hence the signal coming from the second and the third layer is almost negligible.

CHAPTER 2

EXPERIMENTAL DETAILS

2.1 Overview

The experiments reported in this dissertation were performed using the UT Arlington Time of Flight-Positron annihilation induced Auger electron Spectroscopy (TOF-PAES) system which has been described in detail in dissertation of S. Xie [15]. The main parts of the system include a positron source, a low energy positron beam transport system, Time of flight tube, detectors and electronics for timing spectroscopy. The unique feature of the system is that the time of flight is measured without using a pulsed beam. Due to the low intensity of the radiation source, the incoming beam is, in a sense, naturally pulsed. The time between the incident positron and the detection of the electron is a few μ sec. A 100 mCurie source will produce positrons with an average time difference between the consecutive positrons of 3 μ secs. Hence at any instant, on the average, there is only one detected positron in the sample. At the same time the lifetime of positron is ~10^{-10} sec. On the average only a small fraction of incident positrons(~5%) will produce Auger electrons. Hence only one Auger electron , with flight time of 0.2μsec, will be present in the TOF flight path. Thus the TOF technique can be utilized without knowing the exact time difference between two consecutive positrons. The Time of flight technique , in which all the outgoing electrons are collected simultaneously, has been shown to be more efficient for the detection of very low energy electrons as compared to the conventional Cylindrical Mirror Analyzer(CMA) in which only a small range of energies is collected at one time[16]. The magnetic bottle field used in our spectrometer contains the additional advantage of collection over nearly 2π solid angle while for the CMA the acceptance angle is only 0.2π. This property has been exploited in studying the low energy tail of the Auger. The schematics of the spectrometer are shown in fig 2.1.

2.2 Positron beam

Positrons are made in our lab by using Na-22. It has a half life of 2.5 years and hence the intensity of the positron beam is, for all practical purposes, constant during a typical experimental run of one or two weeks. The Na-22 undergoes a nuclear reaction to produce positrons via the following equation

$$^{22}_{11}Na \rightarrow ^{22}_{10}Ne + \beta^{+} + \nu \qquad 2.1$$

where β^{+} is the positron, ν is the neutrino. The positrons emitted in this reaction have very high energy with mean energy of 178 keV and width 545 keV. This requires moderation of the positrons to make a slow positron beam. The high energy positrons are moderated by using a 1μm thick and 9 mm diameter polycrystalline tungsten (W) foil. The source sits on a stainless steel disk and is insulated from the moderator by macor insulations. Electrical connection to the source is made by a thin film of copper deposited on the steel disk. The source moderator assembly is shown in fig 2.2. For the thin film moderator used in our experiments, the ratio of the moderated positrons to the total positrons implanted in the moderator is determined by the ratio of positron diffusion length and the thickness of the moderator. The other factors that affect this ratio are self absorption and the solid angle seen by the moderator. The efficiency of our moderator is ~ 10-4. The reason for choosing W as the moderator is that it has high negative positron affinity and it stays clean for a long time even in high vacuum conditions.

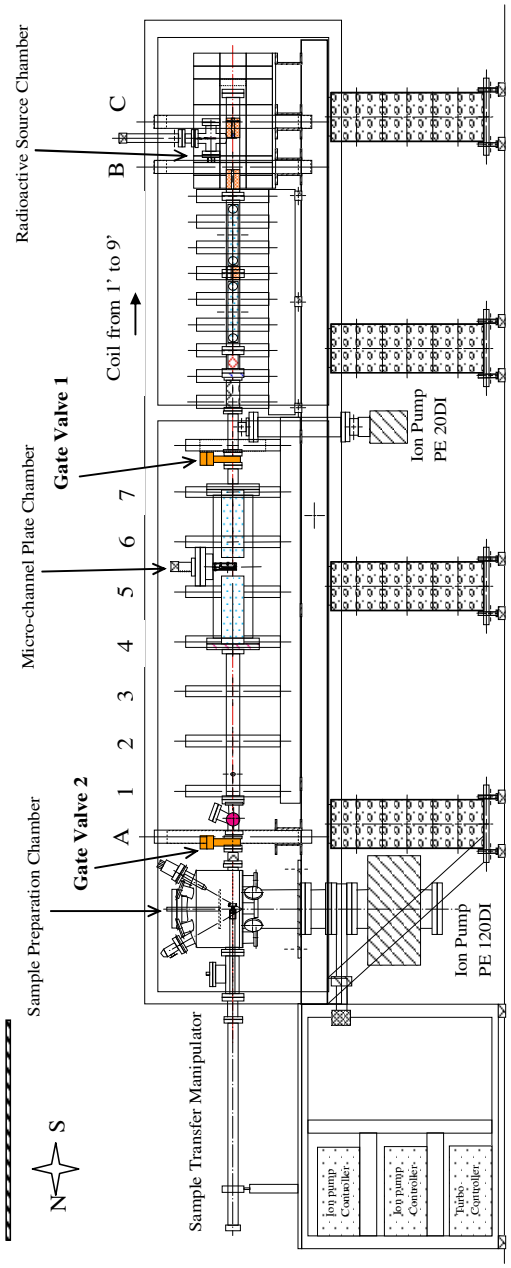

Figure 2.1 Time of flight Positron Annihilation induced Auger Spectrometer at UTA (TOF-PAES) [15].

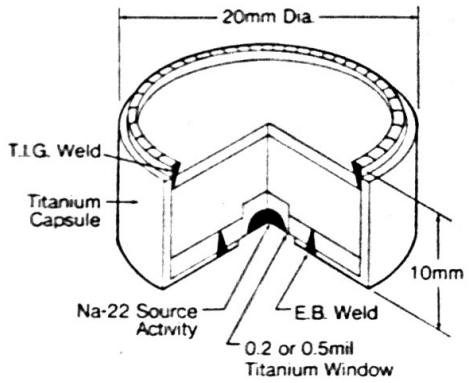

Figure 2.2 Source-assembly [15].

Due to the high energy of the incident positrons on the moderator, most of them pass through the moderator without losing any energy. These high energy positrons also produce a large number of secondary electron. The unmoderated positrons and secondary electrons are the major background present in the unfiltered beam. The moderated positrons have energy equal to the positron work function of W. They are emitted in a cone with half angle given by the ratio of thermal energy and the work function. The slow positrons from the moderator are extracted by a grounded grid in front of the moderator.

The next stage involves with removal of the fast positrons, gamma rays and fast electrons (secondary). This section contains two tungsten barriers “B” and “C” and two sets of $E \times B$ plates. The hole in barrier B is used to collimate gamma rays, fast positrons and the fast secondary electrons from the source and the moderator. This is followed by 2 sets of $E \times B$ plates and is shown in fig 2.3.

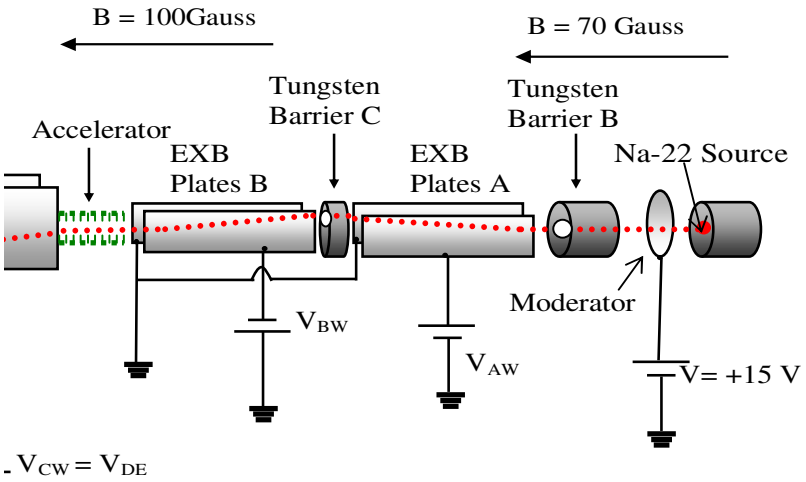

Figure 2.3 Schematics showing $E \times B$ plates A and B. They are separated by tungsten barrier C with an off-center hole in it.

Each set of $E \times B$ plates (A& B) consist of two stainless steel plate with the tungsten barrier C which is mounted between $E \times B$ plates A and B. The potential on the $E \times B$ plates are set to deflect the low energy positrons through the off centered hole in tungsten barrier C. Gamma rays are not deflected and hence are blocked by the barrier C. The voltages on the plates are asymmetric meaning that the voltages on the two plates of each set were not set equal and opposite. The use of asymmetric voltages results in a net acceleration or deceleration of a charged particle entering the region between the plates.

Charged particles moving through the $E \times B$ plates are deflected according to

$$y = \frac{(V_2 - V_1)}{d} \cdot \frac{L}{2B} \sqrt{\frac{m_{p,e}}{2[E_K - q_{p,e}(\frac{V_2 - V_1}{2})]}} \qquad 2.2$$

where V_2 or V_1 are the potential on each plate, B is the uniform magnetic field produced by the current carrying coils, E_K is the kinetic energy of positron or electrons before entering the $E \times B$ plates, L is the length of the plates, $q_{p,e}$ is the electronic or positronic charge, y is the

drift of the charged particle in the direction perpendicular to both the magnetic and electric field, $m_{p,e}$ is the mass of positron or electron. The following arguments assume that the charged particles are travelling along the axis of the tube. From the above equation it can be seen that an electron entering in the plate region will see an attractive potential while a positron sees a retarding potential. Hence while the kinetic energy of electron will increase that of positron will decrease resulting in more deflection of positrons as opposed to the electron. So the electrons of same energy before the $E \times B$ region are not deflected enough to make it through the barrier C. When the positron travels to the plate B region, they see an attractive potential as opposed to that in A region. Hence they will speed up and they will be deflected less. This repositions the initially axial positron back to the axis. Hence the unsymmetrical voltage can be used to prevent most of the secondary electrons from being transmitted. The positive potential along the axis of the plates "A" region was set close to the positron beam energy resulting in a large deflection of the positrons compared to the electrons .This source, moderator and the $E \times B$ plates are housed in the Source tube. They are biased with respect to the source tube which in turn may be biased with respect to the sample. This is useful in extracting the low energy positrons as the transmission of the spectrometer is not tuned for them.

The beam coming out of the $E \times B$ plate B next travel through an accelerator section made of 9 parallel plate metallic discs with 3/4"centered hole through them. The plates are biased using 5MΩ resistors. In the experiments reported in this dissertation, the source tube was biased at -15V and the accelerator section acted to slow the positrons down.

The next stage in the beam transport includes the $E \times B$ plates C and D with Multi channel plate in between them (figure 2.4). Here the low energy positron beam is bent around the MCP. There are two reasons for this arrangement- one, this act as an energy filter and secondly this helps in directing the electrons coming from the sample towards MCP. The voltages used in the $E \times B$ plates- A, B, C and D for various energies is given in table 2.1.

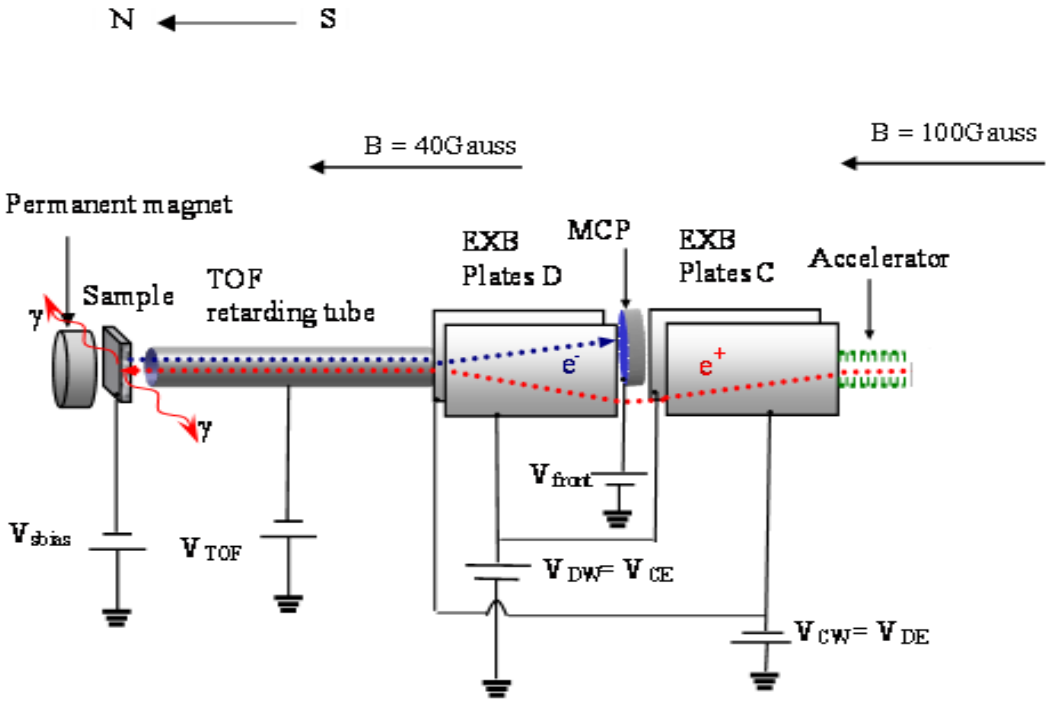

Figure 2.4 Schematics of $E \times B$ plates C and D with MCP between them. The positrons detour around the MCP while the electrons are detected by it.

Table 2.1 Voltages on the various $E \times B$ plates

E x B Plate	Applied Voltage (V)	
A	$V_{AE} = 0$	$V_{AW} = +6.5$
B	$V_{BE} = 0$	$V_{BW} = -83.0$
C	$V_{CE} = +3.6$	$V_{CW} = 0$
D	$V_{DE} = 0$	$V_{DW} = +3.6$

Table 2.2 Moderator voltages for various energy

Beam Energy(eV)	1	2
Moderator Volt(V)	-0.88	0
Source Tube (V)	-15	-15

Table 2.3 Parameters of coils that maintain axial magnetic field in positron beam path

Coil group index	Name of the coil	Inside Diameter (inch)	Number of turns	Current going through the wire (A)	Voltage (V)	Magnetic field (Gauss)
1	A	20	363	5.00	13.08	40
2	1	10	226	3.00	2.53	40
	2	10	226	3.00	2.59	40
	3	10	226	3.00	2.10	40
	4	10	226	3.00	2.51	40
	5	10	226	3.00	2.33	40
	6	10	226	3.00	2.76	40
	7	10	226	3.00	2.54	40
	8	10	226	3.00	2.48	40
3	1`	4.5	320	3.00	3.46	100
	2`	4.5	320	3.00	3.46	100
	3`	4.5	320	3.00	3.45	100
	4`	4.5	320	3.00	3.44	100
	5`	4.5	320	3.00	3.45	100
	6`	4.5	320	3.00	3.46	100
	7`	4.5	320	3.00	3.46	100
	8`	4.5	320	3.00	3.46	100
	9`	4.5	320	3.00	3.49	100
4	B	20	159	12.00	15.14	70
4`	C	20	510	7.00	27.4	70

2.3 TOF tube

The time of flight tube is normally used to slow down the emitted electrons from the sample in order to increase their flight time, *t*, and to thus decrease the resolution limiting term $\Delta t / t$ where Δt is the fixed timing resolution of the detection system. Another important use of the TOF tube is to remove the primary beam induced secondary electrons which contribute to the Positronium induced background. The time of flight of an electron is related to the energy by

$$t = l / \sqrt{2mE}$$

$$|dE| = \frac{ml^2}{t^3} dt \qquad 2.3$$

Thus a longer flight time leads to better energy resolution. This can be achieved by increasing the negative voltage in the TOF tube to reduce the energy of the electron while inside the TOF tube and hence increase their flight time. Another observation from the above relation is that increasing the length of TOF tube will lead to better the resolution.

As alluded to above the retarding tube is useful for the reduction of Positronium induced background. This arises when the incident positron kicks out a secondary electron and then forms Positronium. The ortho component of Positronium is long lived (~10^{-7} sec) and its decay rate is modeled as exponential decay. The electron energy is determined in reverse timing mode by

$$t_{measured} = t_{STOP} - t_{START} = t_{delay} - t_{tof} - t_{\gamma} \qquad 2.4$$

where $t_{measured}$ is the time of flight of the electron measured by the spectrometer, t_{STOP} is the stop signal provided by the detection of the gamma photon, t_{START} is the signal provided by the detection of the electron by the MCP, t_{delay} is the duration by which the gamma ray signal is delayed, t_{tof} is the actual time of flight of the electron and t_{γ} is the time of the detection of the gamma photon after the secondary electron has been kicked out. For secondary electron with Positronium formation

$$t_{measured} = t_{delay} - t_{tof} - t_{\gamma}$$

If the γ ray comes out at the same time as the electron then the above equation holds. But due to the long decay time of the ortho Positronium, the above equation is modified as

$$t_{measured} = t_{delay} - t_{tof} - t_{Ps} \qquad 2.5$$

This means that the Positronium decay will produce an exponentially decaying background with maximum at the channel corresponding to the slowest electron (which is same as the sample bias). This Positronium background can be removed by using a bias on the TOF tube that is sufficient to repel all of the secondary electron. To do this the bias should be more than the maximum of the secondary electron energy

$$e|V_{TOF}| \geq E_{beam} - 2eV_{sample} \qquad 2.6$$

While this can remove most of the Positronium induced background, there is still some background present due to the electrons coming from the source region. A conservative estimate of this can be made by calculating the accidental count rate. In the experiments described in this dissertation, TOF tube was grounded.

2.4 Detection system

There are two types of signals in TOF-PAES- One from the detection of the Gamma rays and the other from the detection of electrons (secondary and Auger). The gamma rays are detected by a Barium Fluoride detector (BaF2) and a Sodium Iodide detector (NaI). The electrons are detected by the Micro channel plate (MCP). The BaF2 detector is used to detect the annihilation gamma rays. The choice of BaF2 as the STOP signal is due to better timing resolution as compared to the NaI .On the other hand NaI (Tl) gives better energy resolution and hence is used to monitor the Positronium fraction. The schematic of the gamma ray detectors with respect to the sample is shown in fig 2.5

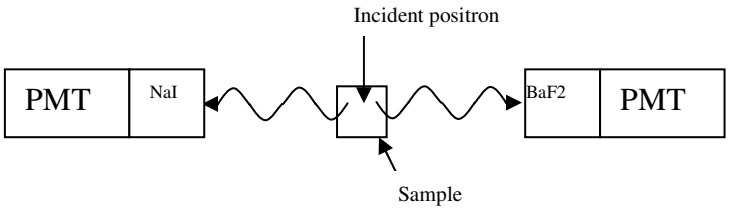

Figure 2.5 Arrangement of sample, BaF2 and NaI(Tl) detectors.

This shows that both the detectors can be used as Triple coincidence (described in section 2.5.2). Since the solid angle seen by both the detectors is same and they are at 180^{o} to each other, there is no additional loss due to solid angle consideration. Only matter of concern here is the efficiency of the detectors. Hence the total detection efficiency in triple coincidence, ε_{TC} , is given by $\varepsilon_{TC} = \varepsilon_{BaF2}.\varepsilon_{NaI}$. The reason for the increased energy resolution of NaI (Tl) is due to the higher density and Z(Z=53). The rising time of the pulse (time taken to go from 10% to 90% of maximum) from BaF2 is 2nsec .

The electrons are detected by MCP. It is an array of 10^4-10^7 micron size channels made from lead glass and oriented parallel to each other. Each channel is coated with a material with low electron work function. The grid in front of the MCP is biased to +220V to avoid detecting the positrons. The back side is biased to +2200V. This is to ensure that the detection efficiency of the electrons incident upon the MCP is not dependent on the incident electron energy. The incident electrons are accelerated by the large positive bias and in process knock out secondary electrons. This results in a cascade effect resulting in ~10^6 -10^7 electrons being collected by the MCP anode. The anode is kept at 2460 V. The resulting pulse has a rise time of ~2nsec. Another important consideration of the MCP is the dead time which is critical for the experiments where two electrons separated by nsec are to be detected.

2.5 TOF Data Acquisition System

The data acquisition described in this section corresponds to three types of experiments done in this dissertation- 1. Normal TOF-PAES 2.Triple coincidence-TOF-PAES 3.Multi STOP TOF-PAES

2.5.1 TOF-PAES Data Acquisition

The schematics of the normal TOF-PAES is shown in fig 2.6. When a positron annihilates with a core electron, it gives out a gamma ray and an Auger electron. These two processes are femtosecond apart. This is about a million times shorter than the flight time of the

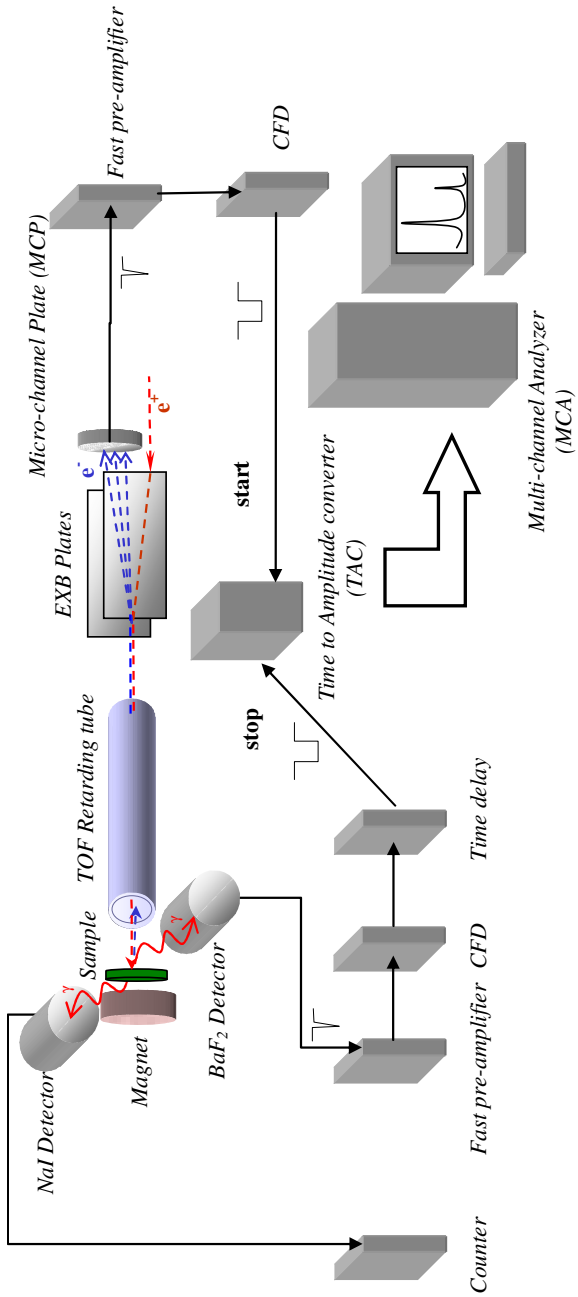

Figure 2.6 Schematics of timing electronics for TOF-PAES system.

Auger electron. Hence the emission of the gamma ray and the Auger electron are considered to occur simultaneously.

The gamma rays are detected by BaF2 detector whose output signal is fed into a Constant fraction discriminator (CFD, Canberra 2126). The output of CFD goes to Gate and Delay generator (Ortec, 416A). The output of the Gate and delay generator is used as the STOP pulse in the Time to amplitude convertor (TAC, ORTEC 437A). The Auger electron incident on the MCP produces a fast negative pulse which is fed to a fast preamplifier. Output of the preamplifier is fed to CFD and its output goes to the START of the TAC. The reason for selecting the MCP signal as the START is that the count rate of the BaF2 is almost 10 times that of the MCP. Since the accidental count rate is proportional to the true count rate , there will be more false STARTS. This will increase the dead time of the TAC, hence the MCP signal is used as the START. Another thing to be considered is the situation when the count rate is low. When the count rate is low the accidentals go as inverse of the true counts. Hence in our case it will not matter if the BaF2 signal be used as the START as the positron source is 4mCi strong. The incident Auger electrons on the anode of the MCP stimulate fast negative pulse which has a response time less than 1 ns on the cathode of the MCP and it will be the input signal to the preamplifier. The output pulse of the preamplifier goes through the second constant fraction discriminator. The output signal of the CFD is the start signal for the TOF coincidence measurement. The TAC gives out a pulse with amplitude proportional to the time difference between the START and the STOP. This pulse is analyzed by the Multi channel analyzer and converted to digital form. The pulse height is used to bin the signal in specific memory location called channels. The counts in channels are then incremented to get a histogram in channel numbers.

2.5.2 Triple Coincidence Measurements

The setup for this is essentially the same as that of normal TOF-PAES with the difference that the NaI signal is gated to the START of TAC (BaF2 signal). The gamma rays

emitted when the positron annihilates in the sample surface are 180^{o} apart. This is due to the fact that positron in solid always decays via 2 gamma emission. Hence when a positron annihilates with a core electron resulting into Auger emission, there are two gamma rays emitted. One of them is detected by the BaF2 detector while the other is detected by NaI(Tl) detector stationed 180^{o} opposite to the former. The block diagram is shown in fig 5. The problem with this is that the preamplifier of the NaI (Tl) is slower. Hence the BaF2 signal has to be delayed. Surprisingly this did not result in reduced count rates as expected by dead time and efficiency of the detectors logic. This experiment has another advantage that long lived Positronium component will not be recorded in this setup and hence there is no Positronium induced background.

2.5.3 Multi Stop TOF-PAES

This experiment was set up to study the low energy electrons in Auger emission. The setup for this experiment is shown in fig 2.7. The BaF2 signal is stretched in time and gated with the START of the TAC. The MCP signal is split into two. One goes to the START and is not delayed while the other one goes to the Gate and Delay generator (ORTEC, 416A). This is the STOP of the TAC. In this way the absolute energy of both the electrons will not be measured and only the energy difference between them will be.

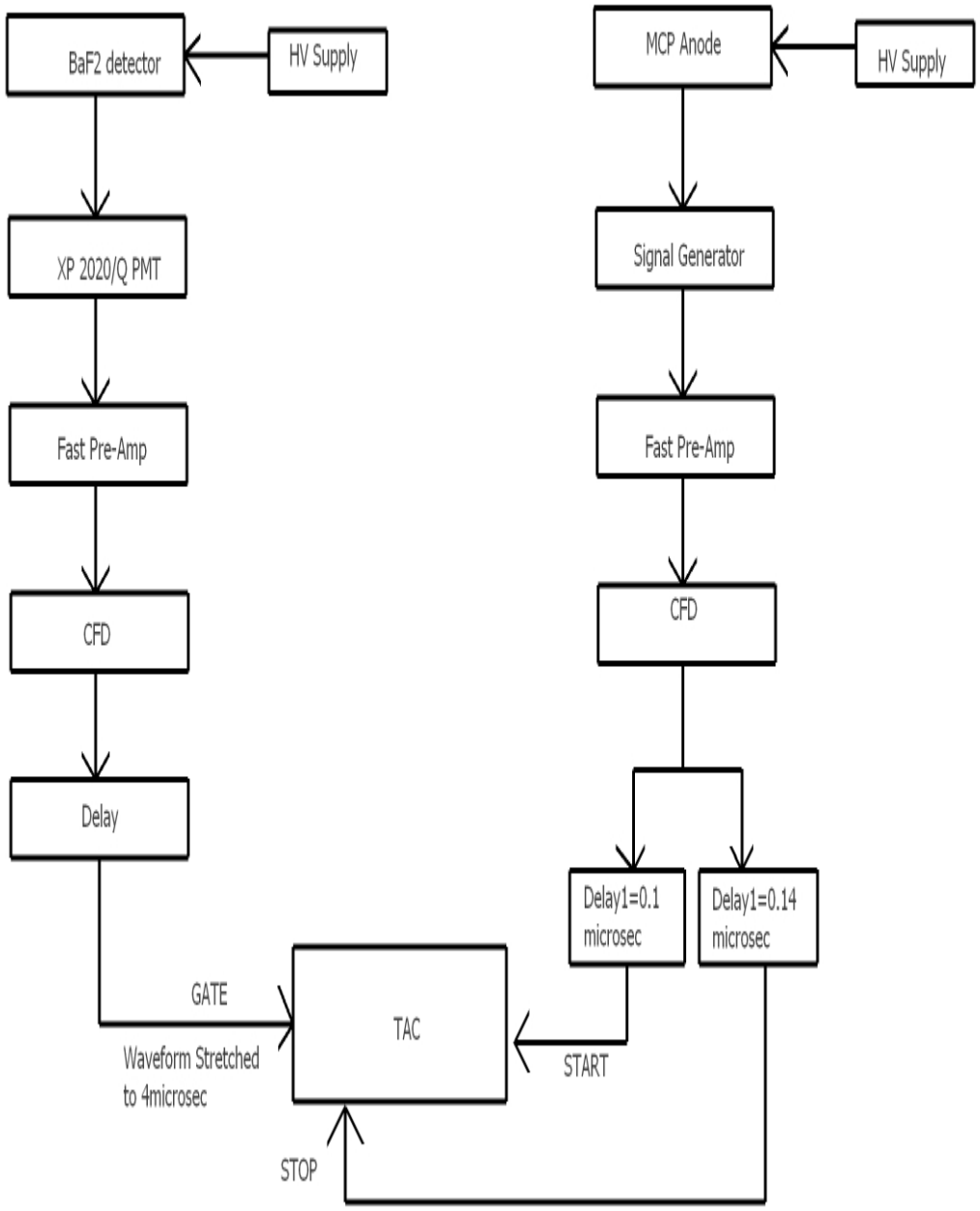

Figure 2.7 Electronic setup for signal processing in multi stop TOF-PAES.

2.6 Time to Energy Conversion

The calibration of TOF-PAES is done by looking at the secondary electron peak as a function of the sample bias. The beam energy is ramped by putting a negative bias on the sample. The electrons leaving the sample go through the TOF tube, EXB plates and then strikes the MCP. In case of high energy electrons (>20eV) the mean potential between the EXB plates does not affect the travel time much. This can be realized by using eq 2.2. For high energy electrons the denominator under the square root is given by $2E_K$ and hence the electrons travel with miniscule change in their longitudinal speed. In such a case the time of flight is related to energy as, $t \sim 1/\sqrt{E}$. The relation between the channel number and the energy follows the same trend as the time of flight and energy. The usual process of calibration followed is to fit the peak channel number as a function of the sample bias. The reasoning for this is that irrespective of the beam energy, the lowest energy that an electron will have coming out of the sample is the bias on the sample. The relation between the channel number and energy is given by

$$\#=\#_0+\frac{P1}{\sqrt{E-P2}} \qquad 2.7$$

Hence the process that is followed here is as such- the data in channel space is obtained. Then the background is subtracted from the channel spectrum. The channel number where the spectrum starts to rise above the background is taken as corresponding to the sample bias. The resulting plot of $E^{-1/2} vs \;\; t_d - t_{tof}$ is fitted with a straight line giving a relation between energy and #. This situation breaks down when we are dealing with low energy electrons. This can be explained by considering the status of the electron in the EXB plates. The potential used in the plates is shown in table. As can be seen that the potential at the centre of the plate is positive. This speeds up the incoming positrons and hence the time of flight measured is shorter than

what one would expect if the effects of EXB are neglected. Hence the total time of flight of an electron can be written as the sum of 2 parts, $t = t_{tof} + t_{E\times B}$. In terms of the electron energy,

$$t = \frac{l_1}{\sqrt{\frac{2}{m}E_{Auger}}} + \frac{l_2}{\sqrt{\frac{2}{m}(E_{Auger} + eV_{mean})}}. \qquad 2.8$$

In cases where $E_{Auger} > eV_{mean}$, then the second term can be simplified to as $t_{E\times B} = \frac{l_2}{\sqrt{\frac{2}{m}E_{Auger}}}$.So for high energy electrons, the $E^{-1/2} vs \;\; t_d - t_{tof}$ plot is essentially linear. But in case of low energy electrons, the plot deviates from a straight line. This discrepancy can be addressed by empirically fitting the calibration curve by a function to mirror the effect of the EXB plates. This is given by eq

$$E^{-1/2} = E_0^{-1/2} + A_1 \exp(-(\#-\#_0)/\#_1) + A_2 \exp(-(\#-\#_0)/\#_2) \qquad 2.9$$

Here $\#= C(t_d - t_{tof})$ where C is a constant, E_0, A_1, A_2, $\#_1$, $\#_0$, $\#_2$ are the fit to constant. As can be seen for high energies the exponential can be expanded in taylor series and retaining only the linear terms, giving rise to the linear dependence. The resulting fits for copper and Gold are shown in Fig 2.8, 2.9 and 2.10.

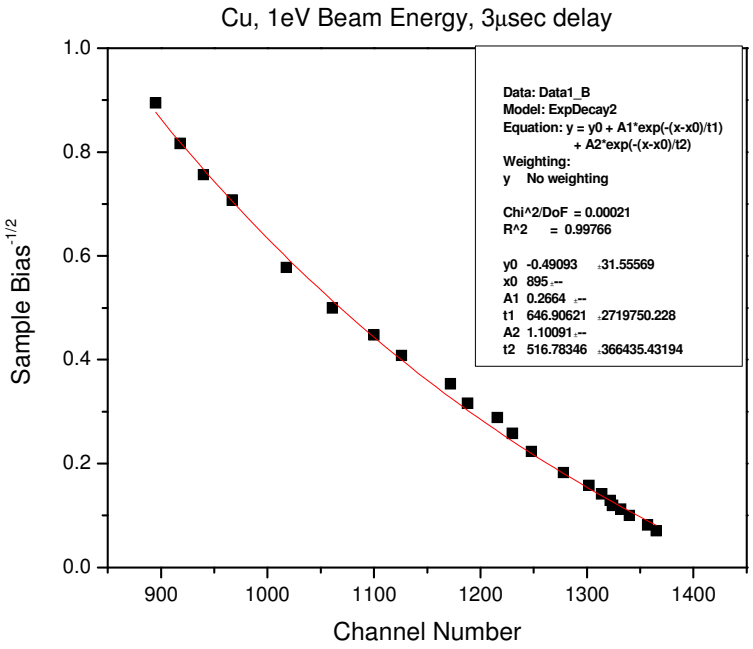

Figure 2.8 Calibration curve for Cu with 1eV positron beam. Exponential decay has been used in place of the straight line fit to reflect the effect of EXB plates.

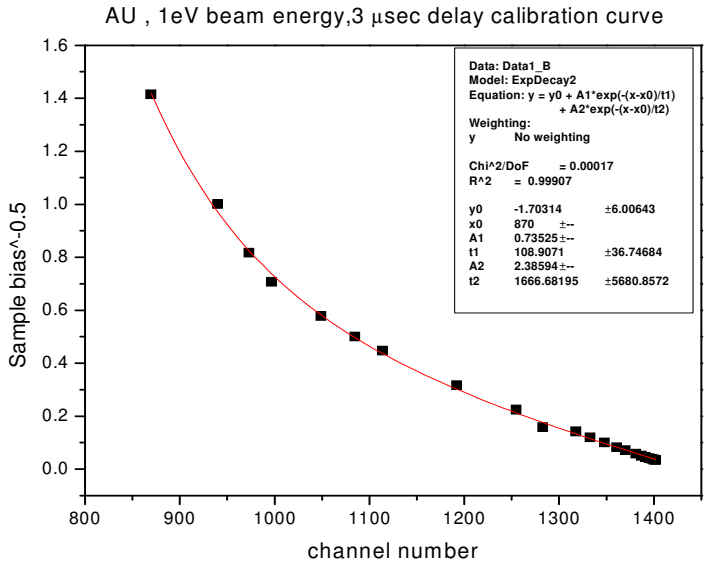

Figure 2.9 Calibration curve for Au with 1eV positron beam

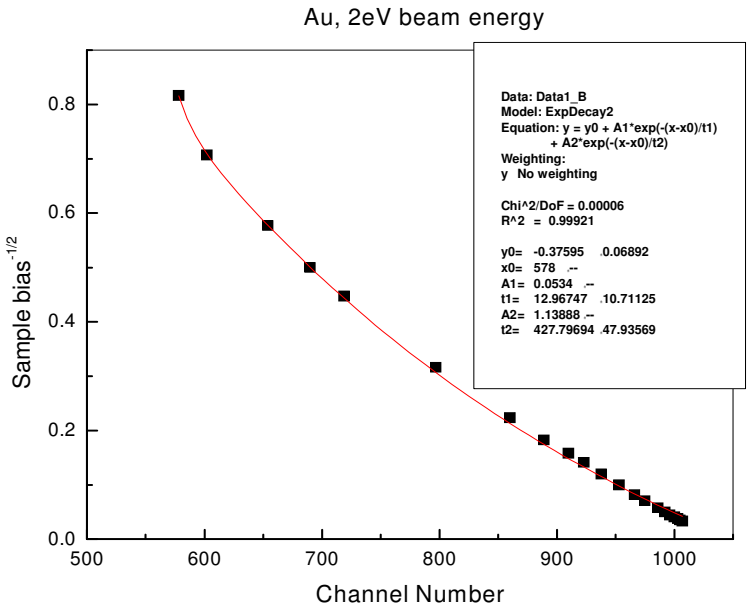

Figure 2.10 Calibration curve for Au with 2eV positron beam.

The effect of the change in the voltage of EXB can be seen in the change in channel numbers (and hence time of flight) for same sample bias. If it is assumed that the channels correspond to the same time then the resulting effect in timing can be easily observed. Once the relation between E and # is known the resulting relation between $N(\#)$ and $N(E)$ can be obtained by assuming that area under the peak is conserved in conversion. Hence $\int_{\#_1}^{\#_2} N(\#)d\# = \int_{E_1}^{E_2} N(E)dE$

where E_1 and E_2 correspond to $\#_1$ and $\#_2$ respectively. $\int_{\#_1}^{\#_2} N(\#)\frac{d\#}{dE}dE = \int_{E_1}^{E_2} N(E)dE.$

Thus $N(\#)\frac{d\#}{dE} = N(E)$. Another problem with a straight line fit is that when the channel spectrum is converted to the energy spectrum, the high energy peaks (>40eV) which were visible in the channel spectrum are not present.

2.7 Sensitivity of TOF-PAES to low energy electrons and the beam energy used

Up until the research reported in this dissertation all the measurements of electron energy in TOF-PAES were restricted to kinetic energy more than 20eV. Consecutively it was important to adjust the setting of the T-O-F detection system to ensure efficient detection of very low energy electrons. Assuming that the transmission of electrons upto the $E \times B$ plates were independent of energy, the critical factor in the electron transport is their motion in $E \times B$ plates D (figure 2.4). If the electric field is too large, the electrons get deflected too much and miss the MCP. Since the same electric field deflects the positrons across the MCP, the field has to be such that it allows only the low energy positrons to pass around the MCP while allowing electrons of all energies are detected by the MCP. In the experiments carried out in this dissertation, the ability of the spectrometer to detect the low energy electrons is verified using an incident beam energy 2eV (fig 2.11). Once efficient transportation was confirmed, the voltages on $E \times B$ plates D were kept the same while the beam energy was reduced by lowering the moderator voltage. Figure 2.11 shows the channel spectrum at different sample biases while the incident beam energy is 2eV. The TAC range here was 4 μ sec. The channel spectrum has two peaks- the secondary electron peak at lower channel numbers and the Auger peak at higher channel numbers. The low energy edge of the secondary electron peak represents the electrons coming out with energy $-eV_S$, where V_S is the sample bias.

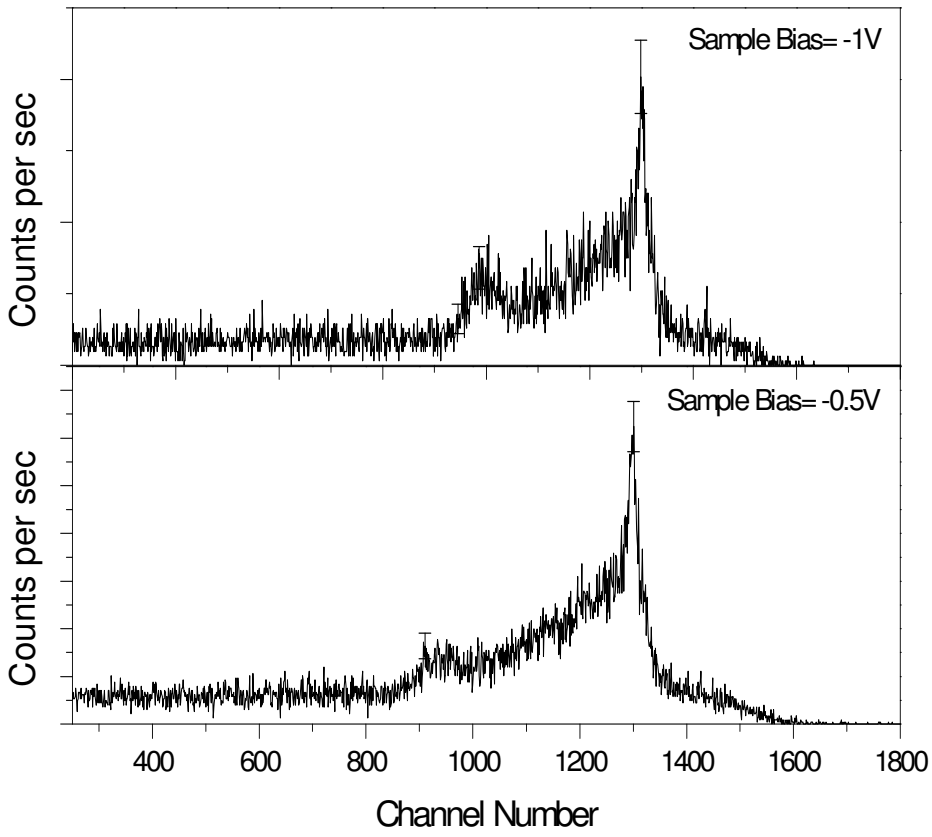

Figure 2.11 Comparison of TOF spectra showing the secondary electron peak with different sample bias. The positron beam energy is 2eV. 1 channel corresponds to 4μsec.

As can be seen in fig 2.11, the low energy edge (lower channel number) of the secondary electron moves to lower channels. This means that the 0.5eV electrons are deflected by the right amount so that they are hitting the MCP and hence spectrometer is sensitive to low energy electrons. Fig 2.12 shows the channel spectrum corresponding to 2eV positron beam while the sample is maintained at different bias. The time range of the TAC in this figure is 4 μ sec.

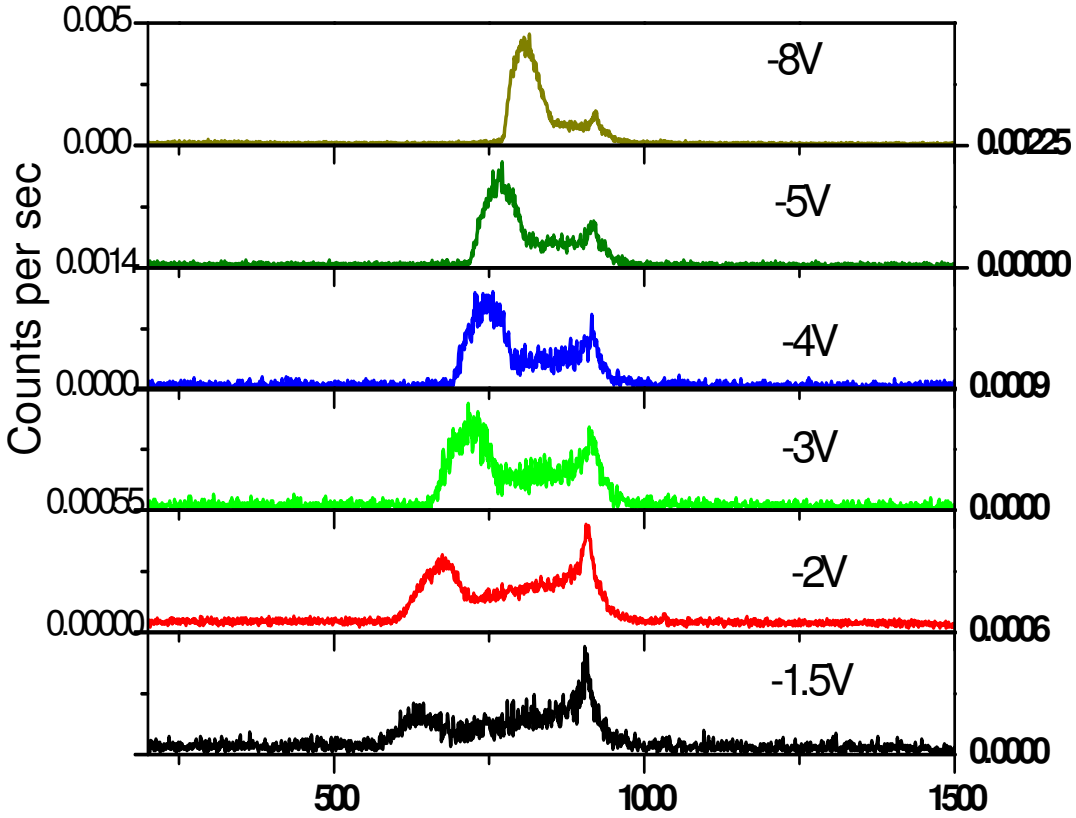

Figure 2.12 Channel spectrum of Gold with 2eV positron beam. 1 channel corresponds to 4μsec.

The beam energy was measured by reflecting the positrons off the potential on the TOF tube while the sample is biased to -60V. The coincidence counts were measured as a

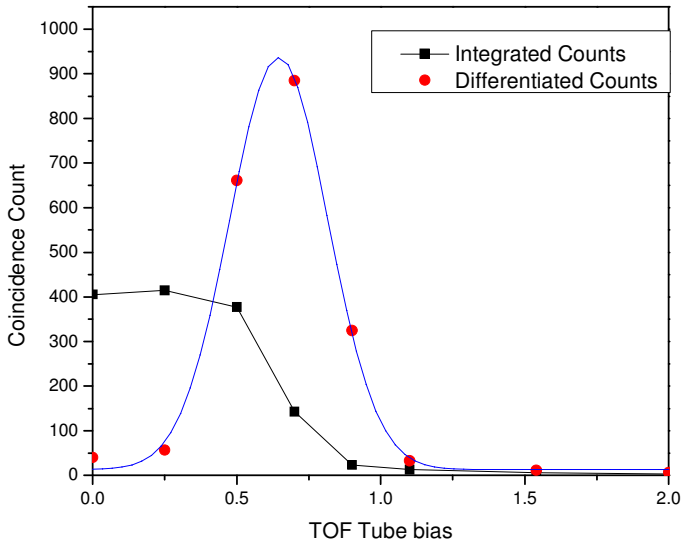

Figure 2.13 Beam energy for Moderator voltage of -0.88V and $E \times B$ plates voltages as shown in table 2.1.

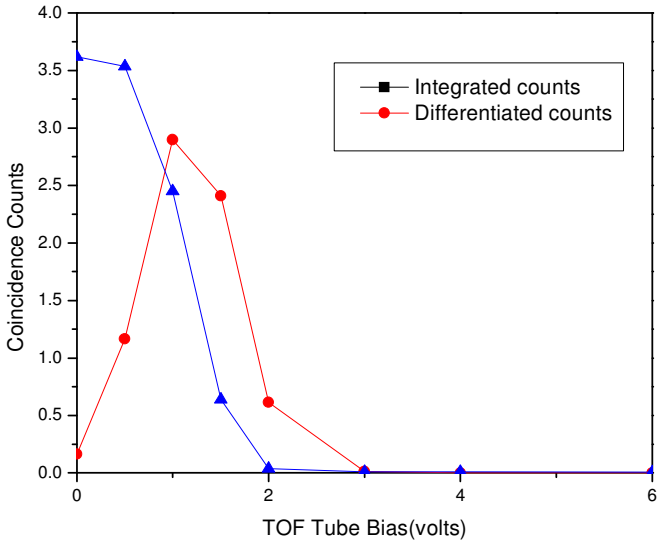

Figure 2.14 Beam energy for Moderator voltage of 0V and $E \times B$ plates voltages as shown in table 2.1.

function of the TOF tube bias and are plotted for two different moderator voltages in fig 2.13 and 2.14. It is to be noted that the voltages on $E \times B$ plates –C and D were same for these two beam energies.

2.8 Focusing of electrons and reflection of positrons by the permanent magnet behind the sample

The TOF-PAES uses a magnetic bottle spectrometer for redirecting the transverse motion of the outgoing electrons back towards the axis of the spectrometer. This property is used to collect all the electrons from 0 to π and is important for detection of the low energy electrons. The Magnetic bottle spectrometer was first developed by Kruit et al [57]. The physics of this process can be understood by invoking conservation of angular momentum. Let the electron start from the sample surface with speed v_o and at an angle θ_i to the surface normal in the region1where the magnetic field is B_i and in the region 2 where the field is B_f and the angle to the normal is θ_f .This is shown in figure 2.15. The electron undergoes helical motion bounded by the magnetic field lines. The initial angular momentum is given by

$$L = I\omega \qquad 2.10$$

where, $\omega = \frac{eB}{m}$. Hence the angular momentum can be written as,

$$L = \frac{m^2 v^2 \sin^2 \theta}{eB} \qquad 2.11$$

By applying conservation of angular momentum, θ_f and θ_i will be related as,

$$\frac{\sin \theta_f}{\sin \theta_i} = \left(\frac{B_f}{B_i} \right)^{1/2} \qquad 2.12$$

When the electrons go from the strong field at the sample into the weaker field region of the T-O-F drift tube the angle, θ is reduced. This is the reason of using the permanent magnet behind

the sample. In our case B_f is 40 G and B_i is 504G for Cu sample. The resulting ratio is~1/10 which indicates that the most of the transverse momentum is transferred to the longitudinal momentum. The maximum value θ_f can have, is given by $\theta_f = \sin^{-1}\left(\frac{B_f}{B_i}\right)^{1/2}$.

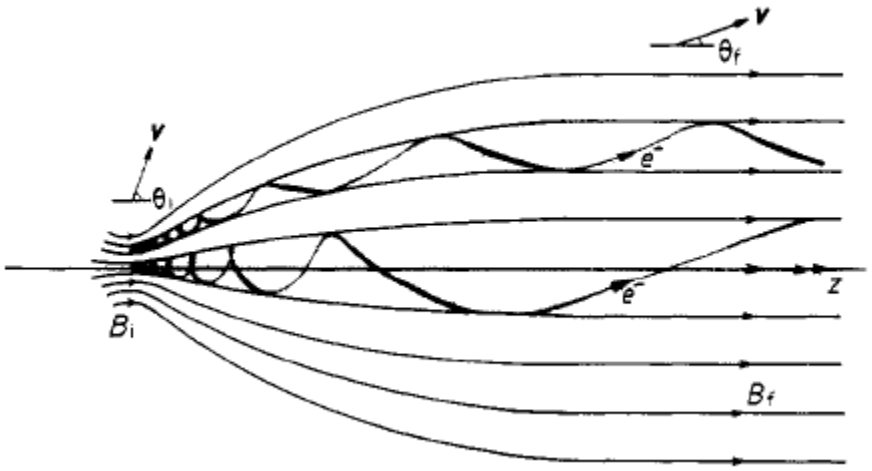

Figure 2.15 Focusing of the outgoing electrons by the magnetic bottle type field.

For positrons approaching the sample θ is increased. If eq 2.12 gives a value of $\sin\theta_\perp > 1$, then the incident positrons are reflected (see fig 2.16). Let the incident positron have a velocity components, $v_{\parallel 0}$ parallel to the B field at z=0(B_0) and $v_{\perp 0}$ perpendicular to the B field. Let the corresponding values at z>0 be $v_\parallel, v_\perp$ and B. Since the B field is conservative hence $v_\parallel^2 + v_\perp^2 = v^2$. If it is assumed that the field is adiabatic which means that the rate of change of the field is slow in space or time then we can say that the quantity $p_\perp^2 / B$ is conserved. Thus

$$\frac{v_{\perp}^2}{B} = \frac{v_{\perp 0}^2}{B_0}$$

$$v_{\parallel}^2 = v_0^2 - v_{\perp 0}^2 \frac{B(z)}{B_0} \qquad 2.14$$

If we plug in the values of $B(z) = 2000G$ and $B_0 = 40G$, then we can see that for a positron to be incident on the sample, most of the initial momentum(in the region of low magnetic field intensity) should be in longitudinal direction. But the positrons with momentum in the range given by above equation will end up on the sample with angle range from0-90^o. This points to a difference between the actual experimental circumstances and the theoretical modeling in which it is assumed that the particles are incident normal to the surface.

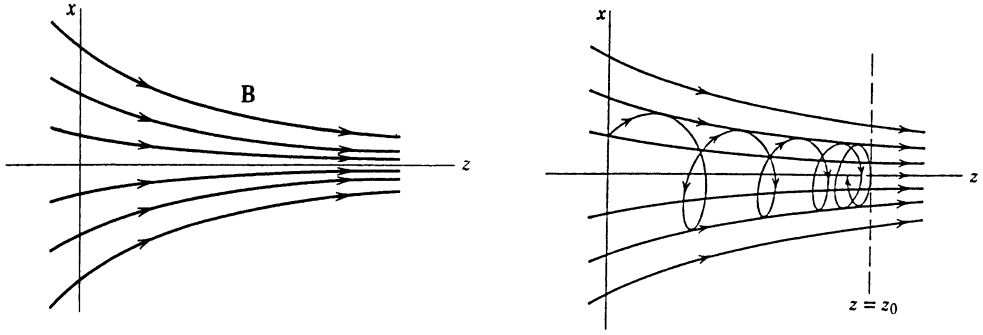

Figure 2.16 Schematics showing the field lines near the permanent magnet. The incident positron shown by the spiral lines may lose all of its transverse momentum and get reflected [17].

Fig 2.17 shows total peak area in the gamma spectrum plotted against the beam energy. As can be seen the intensity increases rapidly from -0.5V to ~-20V at which point the intensity plateaus. This can be understood in terms of a model where the positrons are reflected from the magnetic field at the sample surface (eq 2.19). The ratio of the incident positrons on the sample to the total positrons emitted from the moderator can be estimated from equation 2.14. Let the positrons emitted from the moderator have $\cos^2(\theta)$ distribution. From 2.14

$$v^2 \le v_{\perp 0}^2 \frac{B}{B_0} \tag{2.15}$$

$$v_\perp^2 + v_\parallel^2 \le v_{\perp 0}^2 \frac{B}{B_0} \tag{2.16}$$

$$E^{0V} + qV \le E^{0V} \sin^2(\theta_c) \frac{B}{B_0} \tag{2.17}$$

$$\theta_c \ge \sin^{-1}\left(\sqrt{\frac{B_0}{B}(1+\frac{qV}{E^{0V}}}\right) \tag{2.18}$$

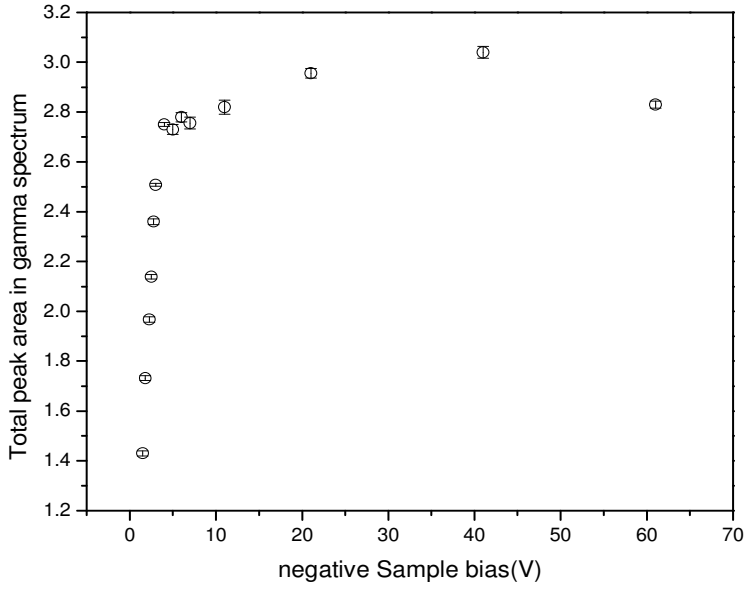

Figure 2.17 Total peak areas in the gamma spectrum (NaI detector) as a function of the incident positron energy.

Incident intensity of positrons on the sample is proportional to $\sim \int_0^{\theta_C} 3\cos^2(\theta)\sin(\theta)d\theta$. This can be written as

$$I_{incident}(V) = \left[1 - \left(1 - \left[\frac{B_0}{B}\left(1 + \frac{qV}{E^{0V}}\right)\right]\right)^{3/2}\right] \qquad 2.19$$

where E^{0V} is a fitting parameter, B_0 is the magnetic field at the moderator, B is the magnetic field at the sample due to the permanent magnet and V is the negative sample bias on the sample. The intensity thus calculated has been plotted in fig 2.18.

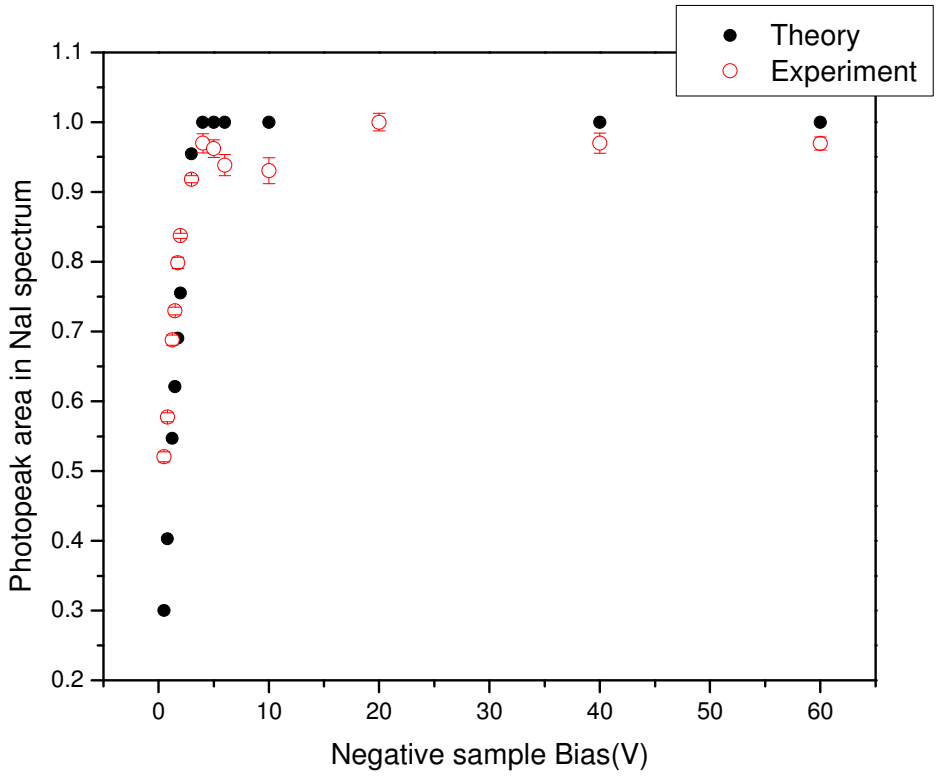

Figure 2.18 Photo peak areas in the gamma spectrum (NaI detector) as a function of the negative sample bias.

2.9 Sample preparation chamber

The sample preparation chamber consists of a stainless steel chamber and UHV pumping system. The sample manipulator is of a rack and pinion type. The sample sits at one

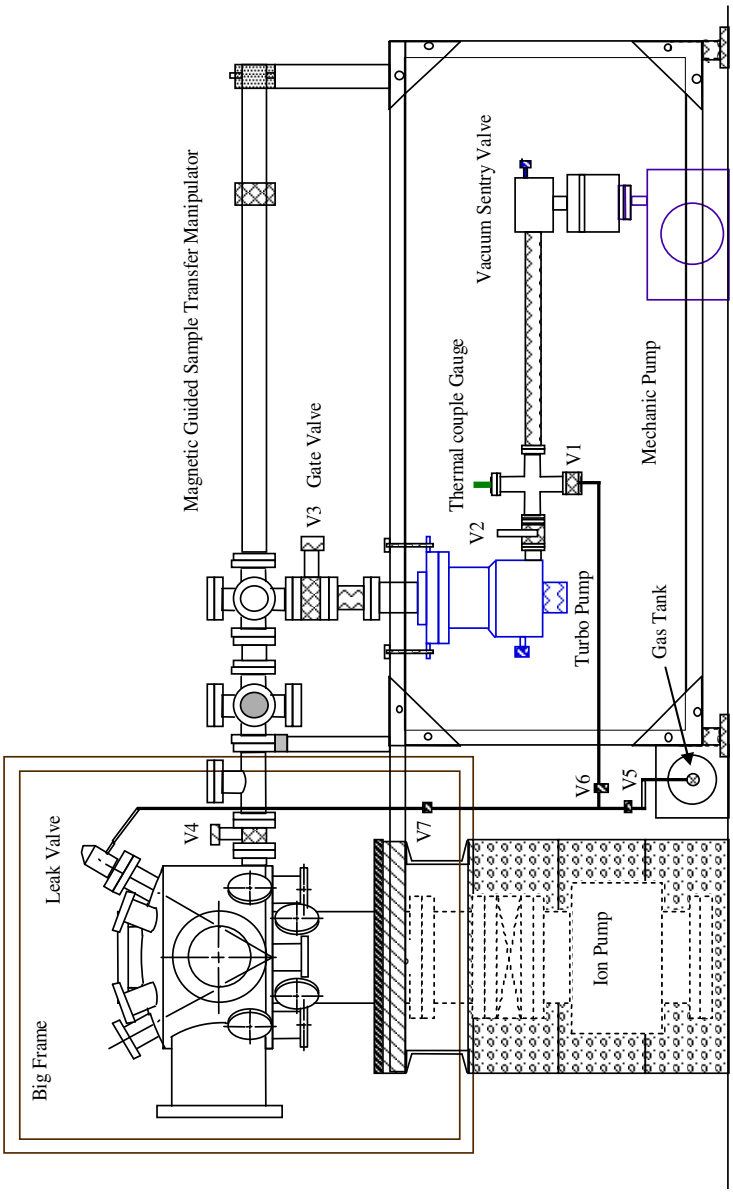

Figure 2.19 Side view of sample preparation chamber.

end of the manipulator. The sample holder consists of a Sm-Co permanent magnet, Button heater and thermocouple wires. The sample holder is electrically insulated from the rest of transfer shaft and can be biased to desired voltages. In situ cleaning of the sample is done by a sputter gun which etches the surface with kV range argon ions. The heater button can be used to heat the sample up to 1000^{o}C. Temperatures higher than 400^{o}C were measured using an ULTIMAX (UX-10) infrared thermometer. A side view of the sample chamber is shown in fig 2.19.

CHAPTER 3

AUGER MEDIATED QUANTUM STICKING OF POSITRONS TO SURFACES

3.1 Overview

Low energy positrons impinging on solid surfaces can interact via multiple competing channels including elastic or inelastic back-scattering, penetration into the bulk followed by energy loss and dropping into a bulk state, or energy loss and trapping into a surface state. Surface state trapping typically occurs as a result of the positron first penetrating into the bulk, thermalizing and then diffusing to the surface. At the surface, the positron must lose ~3 eV to fall from thermalized state in the bulk into the lower energy surface state (most likely by creating an electron- hole pair). However, calculations indicate that another process becomes important at very low incident energies in which the positron undergoes a single step transition from an unbound scattering state to an image potential bound state as shown in figure 3.1[18]. We have shown that such a transition is accompanied by the creation of an electron hole pair in which the electron has sufficient energy to leave the surface.

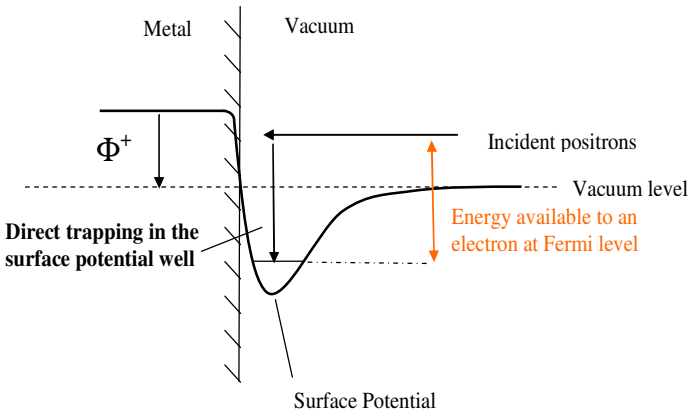

Figure 3.1 Schematics showing the direct trapping of incident positron in the surface state.

This process is analogous to the Auger transition in solids where an electron makes a transition from an occupied quantum state to an unoccupied one and giving its energy to another electron which is emitted in continuum. Here the incident positron makes a transition from the scattering state to the image potential bound state and creating a secondary electron in the process. Hence the process has been termed as Auger mediated quantum sticking.

In this section we provide direct experimental confirmation of this process through a measurement of the energies of secondary electrons emitted as result of very low energy positron bombardment. These measurements allowed us to determine the positron sticking probability as a function of incident particle energy. A narrow peak in the secondary electron spectrum was observed at incident energies well below the electron work function. The primary positron energy threshold for secondary electron emission and cutoff in the secondary electron energy spectra are consistent with a process in which incident positrons make a transition directly from the scattering state directly into a surface-image potential bound while transferring all of the energy difference to an outgoing secondary electron. The abovementioned secondary electron peak was present when the Cu sample was heated to 740 ^{o}C even though the Auger peak ($M_{23}VV$) vanished. This provides evidence that the positron sticking to the surface is generating secondary electrons even at temperatures at which positrons are desorbed from the surface state. Spectrum from the hot Cu surface (740 ^{o}C) revealed the absence of both the secondary electron peak (precluded due to energy conservation) and the Auger electron peak (surface state desorption of positrons as Positronium). The measured secondary electron yields are used to obtain estimate of positron sticking to the surface as a function of incident positron energy.

3.2 Surface sticking of neutral and charged particles

The phenomena that occur when a particle hits a surface are important both theoretically and technically. If the particle experiences scattering, then useful properties

regarding the surface structure can be extracted. On the other hand, the sticking properties of particle are important for gas phase reactions in catalytic phenomena.

The process of sticking is treated in two different ways- classically and Quantum mechanically. While these two methods provide similar results in the high energy limit, they differ qualitatively in the low energy limit. Quantum mechanics predicts that in the low energy limit the sticking probability $S = S(E,T)$ is 1 while using a semi-classical analysis [2] the sticking coefficient is 0. In the semi-classical analysis, the incident particle is treated as a classical point particle while the surface excitations which lead to energy loss are treated quantum mechanically. Because the particle is treated classically, it is assumed that it can approach arbitrarily close to the surface even in the limit of zero energy allowing it to excite the dissipative surface excitations (e.g. surface phonons, electron-hole pairs in metals) and lose enough energy to become trapped in the potential well at the surface(fig 3.1). A detailed analysis shows that this gives rise to a sticking coefficient $S = S(E,T)$ of 1 in the limit of vanishing incident particle energy.

For heavy particles (e.g. molecules) a classical or semiclassical approach may be used to model the surface interactions. For light particles like electrons, positrons or for ultra cold atoms a fully quantum mechanical approach must be used. Also for neutral particles, the interaction with the surface leads to an attractive Van der Waal type interaction, while for charged particles like positrons the interaction is Coulombic. In the classical approach, the interaction of the particle with the surface is defined relative to the range of the potential it experiences. Far away from the surface (defined relative to the range of the potential) it experiences an attractive force. But after crossing a certain threshold (again determined by the range of the potential) the particle experiences repulsion from the surface. Consecutively in the classical case of vanishing incident energy (E~0) the particle has enough time to lose energy via processes e.g. phonons, electrons hole pair, ripplons and become trapped in the potential. Consecutively the reflection probability in the case of vanishing incident particle energy is 0

while the sticking probability is 1. In the case of quantum mechanics, the wavelength of the particle increases as the particle energy goes to zero. Hence at energies $E << |V|$ there will be a wavelength mismatch between the wave in the potential and the wave coming from the vacuum. This mismatch causes the reflection of the incident particle as shown in fig 3.2

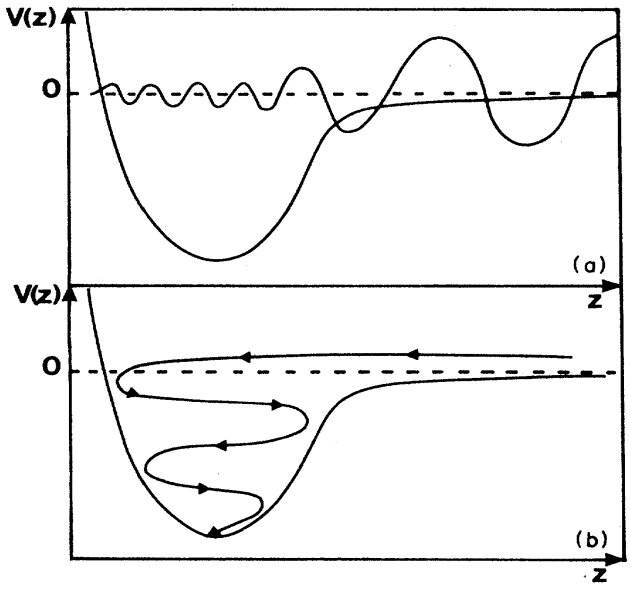

Figure 3.2 Schematics showing the amplitude mismatch at the boundary between the bound state and the scattering state as taken from reference 2 (a) causing the reflection (b) pictorial depiction of sticking in classical limit.

In the long wavelength limit, the overlap of the particle wavefunction with the potential well is small thus reducing the rate of inelastic interactions. Consecutively in the low energy limit lowest order quantum theory predicts that the particle will experience complete reflection[4,18,2]. For non-zero energies the sticking probability can be written as

$$W = \frac{2\pi}{\hbar}\sum_{F}\left\langle F\left|H_{\text{int}}\right|I\right\rangle\delta(E_F - E_I) \text{ [18]} \qquad 4.1$$

where H_{int} is the Hamiltonian describing the interaction of the particle, E_F and E_I are the final and initial state energy of the particle and F and I are the final and initial state of the particle. Here the interaction of the particle with the potential has been treated perturbatively. Also the Fermi golden rule (FGR) has been invoked. FGR gives the rate of transition of the initial state to the final state in presence of a perturbation which is long lived compared to the rate of change of the state.

3.3 Surface Sticking experiments with positrons

Low energy positrons (unlike their charge conjugate counterparts, electrons) constitute a good probe for the study of charged particle sticking to surfaces. This is due to the fact that in case of electrons, the lowest available energy state is a bulk state as opposed to a surface state. This causes the electrons to penetrate into the bulk which makes the experimental observation of surface sticking difficult. For positrons, the combination of an attractive image potential with a repulsive core potential results in positron surface state having a lower energy then the lowest bulk state. Hence the natural tendency of the positrons is to be trapped in the surface state. Also since the positron annihilates with gamma rays of characteristic energy, the detection of almost all the positrons is possible [11]. Most of the experiments related to the positrons sticking to the surface have been hampered by the various channels open to the incoming positron. A low energy positron (~1eV) can – (a) stick to the surface potential (b) form Positronium (c) get reflected (epithermal positrons) (d) go in the bulk. When it goes in the bulk , it has again similar channels open to it- (a) thermalize and then either stick to the surface, get reflected, escape as Positronium or thermalized positron (b)return to surface without losing energy and do all the things as earlier mentioned. Sorting out the signals from all these channels is difficult

In our case the capabilities of UTA TOF-PAES system provides us with a unique ability to carry out such experiments. Since the Auger signal is proportional to the positrons trapped in the surface state, surface state sticking can be monitored by directly measuring the Auger

electrons coming out of the sample. The surface state sticking will have contribution from both the positrons coming from the vacuum side and from those that penetrate into the bulk and return back.

Till now all of the experiments related to sticking of positrons to surface have utilized the positrons diffusing back to the surface after being implanted with keV energies [4,19]. Hence the experiments deal with positron incident on the potential from the metal side and not the vacuum side. It should be noted that sticking in case of atoms incident on the surface is from the vacuum side. The effective potential seen by the positrons is asymmetric depending on the direction of incidence of the positron and hence the sticking probabilities will be different. The experiments carried out in this dissertation provide a means of measuring the sticking probability of positrons incident from the vacuum side and are thus closer analogue to sticking experiments involving ultra cold atoms.

The first experiment to calculate the reflection coefficient of thermalized positrons was by carried out by Britton et al [19]. They used a keV variable positron beam incident on negative positron work function at different temperature to show that both the Ps and positron yield goes to zero as the temperature of the sample goes to zero. This was explained in terms of a one – dimensional quantum mechanical model where the positron work function is the height of the barrier. In such a case the reflection probability is given by

$$T \approx 16\frac{E}{V_0}\left(1-\frac{E}{V_0}\right)e^{-2ka} \quad [20] \qquad 3.2$$

Hence as the particle energy decreases, the transmission coefficient decreases leading to increased reflection back into the bulk.

Later Mills et al. [4] calculated the sticking probability of the Positronium on Al(111) surface. They were interested in the sticking probability of thermalized positrons, which are incident on the surface from the bulk side and are not reflected from the surface potential. In their measurements keV positrons were incident on the surface. After thermalization and

diffusion, the positrons were incident on the surface where the positrons escaped as Positronium. The resultant Positronium energy ($E_{\perp}$, the transverse component) was measured using Time of flight Positronium spectroscopy. There main observation was that the sticking coefficient $S = S(k,T)$ as $k \to 0, T \to 0, S \to S_0$. There conclusion was that $S_0 = 1$ as opposed to the prediction of the perturbation theory that $S_0 = 0$. This anomaly was explained in terms of the breakdown of the perturbation theory in the strong coupling regime[4]. They introduced a dimensionless coupling constant given by

$$\Lambda = 0.28 k_F^3 a_B^3 \left(\frac{z_c}{z_t} \right)^{1/2} \frac{e^2}{r_B} \frac{1}{E_B} \qquad 3.3$$

where z_t is the classical turning point for the bound state , $r_B \equiv (2mE_B)^{1/2}$, a_B is the Bohr radius of hydrogen atom and E_B is the binding energy of Ps on the surface. It has been suggested that when Λ is of the order unity, the perturbation theory breaks down and inelastic channel dominates over quantum reflection.

3.4 Secondary electron generation by low energy positrons

Secondary electron production under low energy positron bombardment has been the subject of several previous studies with beam energy as low as 30eV [21] and 50eV [22]. In this dissertation we present the first measurements of secondary electrons and Auger electrons emitted from a surface as a result of positrons incident with very low energy (1.5 eV to 7 eV). The electrons we are interested in here are of two different natures- a. electrons emitted as a result of annihilation induced Auger transitions and b. electrons produced as a result of energy exchanged through direct impact with the incident positrons (positron sticking induced secondary electrons).

If the positron collides with an electron in the bulk and then falls into a bulk state, the maximum energy of the secondary electrons is given by:

$$E_{K\max} = Ep - \varphi^- + \varphi^+ \qquad 3.4$$

where Ep is the kinetic energy of the positrons incident on the surface, $E_{K\max}$ is the maximum kinetic energy of the outgoing electron (as measured just outside the sample surface), φ^- and φ^+ are the electron and positron work function respectively. In order for the secondary electron to come out of the sample (E_K >0eV) Ep should be greater than $\varphi^- - \varphi^+$. For Au (Cu) the value of φ^- is ≈ 5eV (4.65eV) while φ^+ is ≈ 1eV (0.4eV) [23,24]. Hence for incident positron kinetic energies of less than ~4 (4.25) eV there should be no secondary electron generated if the positron makes a transition to a bulk state. Another possible mechanism for secondary electron production is that the incident positron forms an atom of Positronium (Ps) and transfers its kinetic energy and Ps binding energy, $E_{b\,Ps}$ ≈ 6.8 eV, to an outgoing electron. In this case the maximum kinetic energy of the outgoing electron is given by:

$$E_{K\max} = Ep + E_{b\,Ps} - 2\varphi^- \qquad 3.5$$

But unlike the above mentioned process this involves one positron and at least two electrons. In the case of Au (Cu) the incident kinetic energy of the positron must exceed ~3.2 eV (2.7eV) for this process to generate secondary electrons. Annihilation induced processes including Auger transitions and gamma-ray induced secondary electron emission can lead to the emission of secondary electrons with energies as high as the Auger transition energy and 511 keV respectively. However such processes would lead to the formation of broad secondary electron peaks.

In our studies we found a narrow secondary electron peak even when the incident kinetic energies of the positron beam were less than 3eV. This can be explained if we take into consideration a process in which the positron makes a transition directly from the scattering state into the bond surface state transferring all or most of the energy difference between the

two states to an electron that subsequently leaves the surface as a secondary electron. The maximum kinetic energy for an electron emitted in this process is given by;

$$E_{K\max} = Ep + E_{ss} - \varphi^{-} \qquad 3.6$$

where E_{ss} is the binding energy of the positron in the surface state. In such a case secondary electrons can be produced by positrons with incident kinetic energies as low as 2eV since E_{ss} for most metals is ~3eV. As will be discussed in detail below, the secondary electron peak shape and width observed in our data is consistent with the upper limit imposed by eq. 3.6 and further the integrated intensity of the secondary electron peaks indicate that a substantial fraction of the positrons incident at very low energies drop directly from the positive energy scattering state into the surface trap and transfer all of their energy to an outgoing electron.

3.5 Experimental details of secondary electron measurements

The gold sample (a 99.985% pure polycrystalline foil 25mm x 25mm x 0.025) was sputter cleaned every 12 hour with 1keVAr^{+} ions while the Cu(100) sample (a 99.9% pure single crystal 10 mm diameter x 1mm) was sputter cleaned with 1keV Ar^{+} followed by annealing at 740^{o}C every 12 hours. The TOF-PAES spectrum was used to monitor the cleanliness of the sample and showed no significant contamination of the surface in the period between sputtering. The positron intensity was monitored as a function of sample bias by a NaI(Tl) detector placed close to the sample. The incident positron energy at 0V sample bias was measured as mentioned in section 2.7. The positron energy was increased by negatively biasing the sample.

3.6 TOF-PAES spectrum from Gold and Copper

This section deals with the PAES spectrum taken with incident positron beams with maximum energy 2eV and 1eV . The positron energy mentioned here is the maximum energy of the incident beam measured with 0V sample bias(as mentioned in section 2.7). Figure 3.3 shows the PAES spectrum with the surface state induced secondary electron spectrum taken

with beam energy 2eV. Fig 3.3 and fig 3.4 show the energy spectrum normalized to the incident positron count taken at different negative sample bias for Au and Cu respectively.

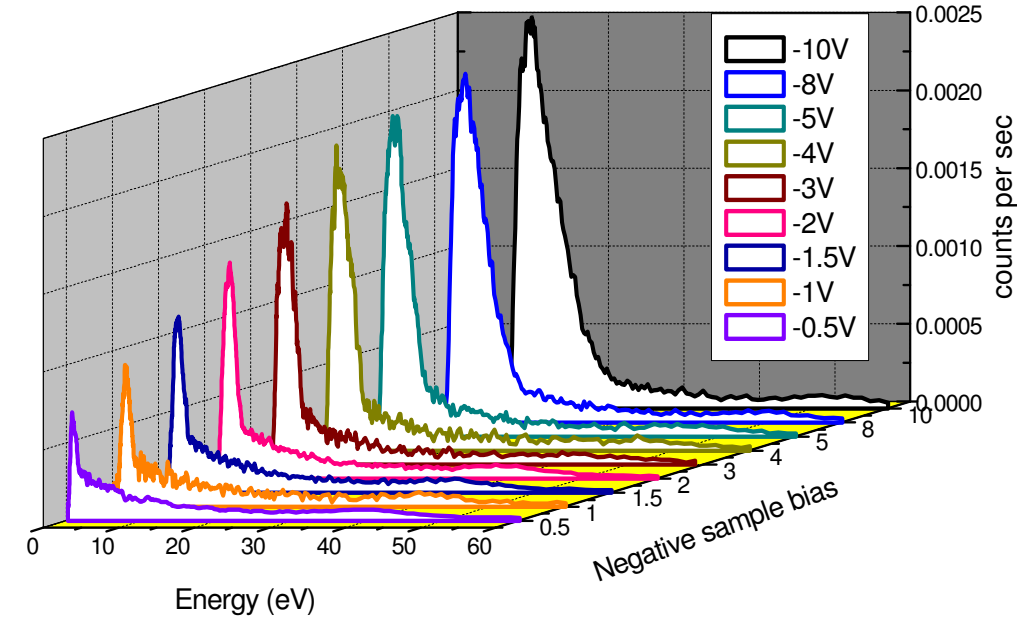

Figure 3.3 Energy spectrum of Au taken at different sample bias with maximum incident positron energy 2eV at 0V bias.

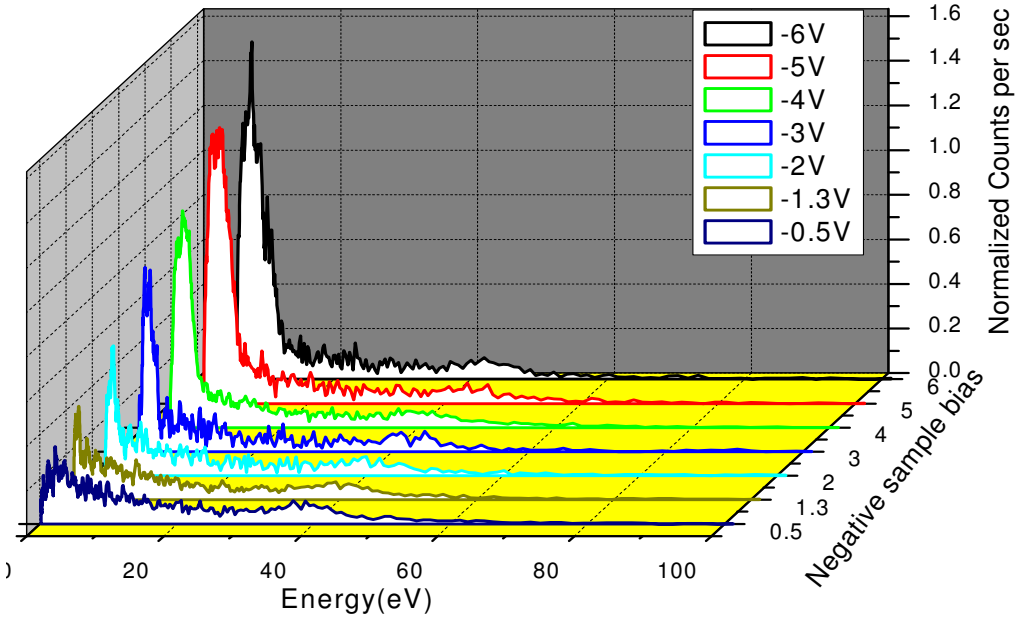

Figure 3.4 Energy spectrum of Au taken at different negative sample bias maximum with incident positron energy 1eV. All the data have been normalized to the Auger peak.

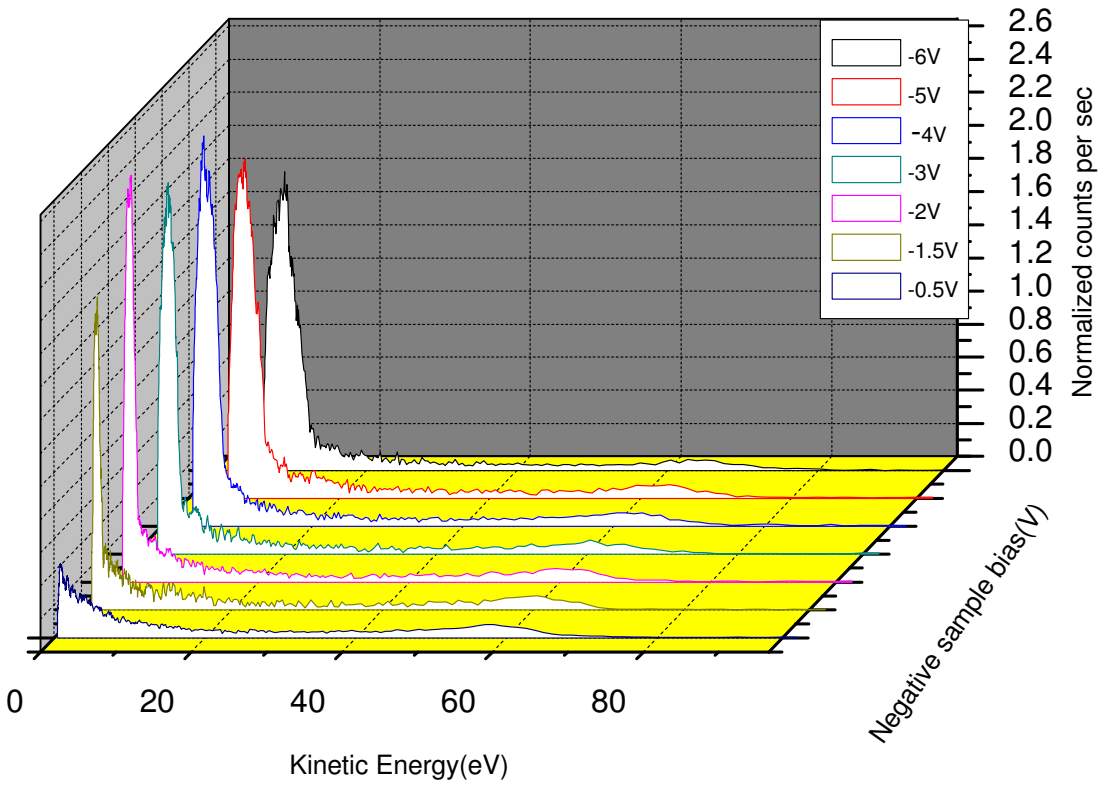

Figure3.5 Energy spectrum of Cu(100) taken at different negative sample bias with maximum incident positron energy 1eV at 0V bias. All the data have been normalized to the Auger peak.

Fig 3.6(a) shows a typical spectrum. The large peak centered at 3 eV corresponds to the positron induced secondaries due to the Auger mediated quantum sticking effect (AQSE). Fig. 3.6(b) shows the same thing except the beam energy is below the threshold for secondary electron emission E_{th}.

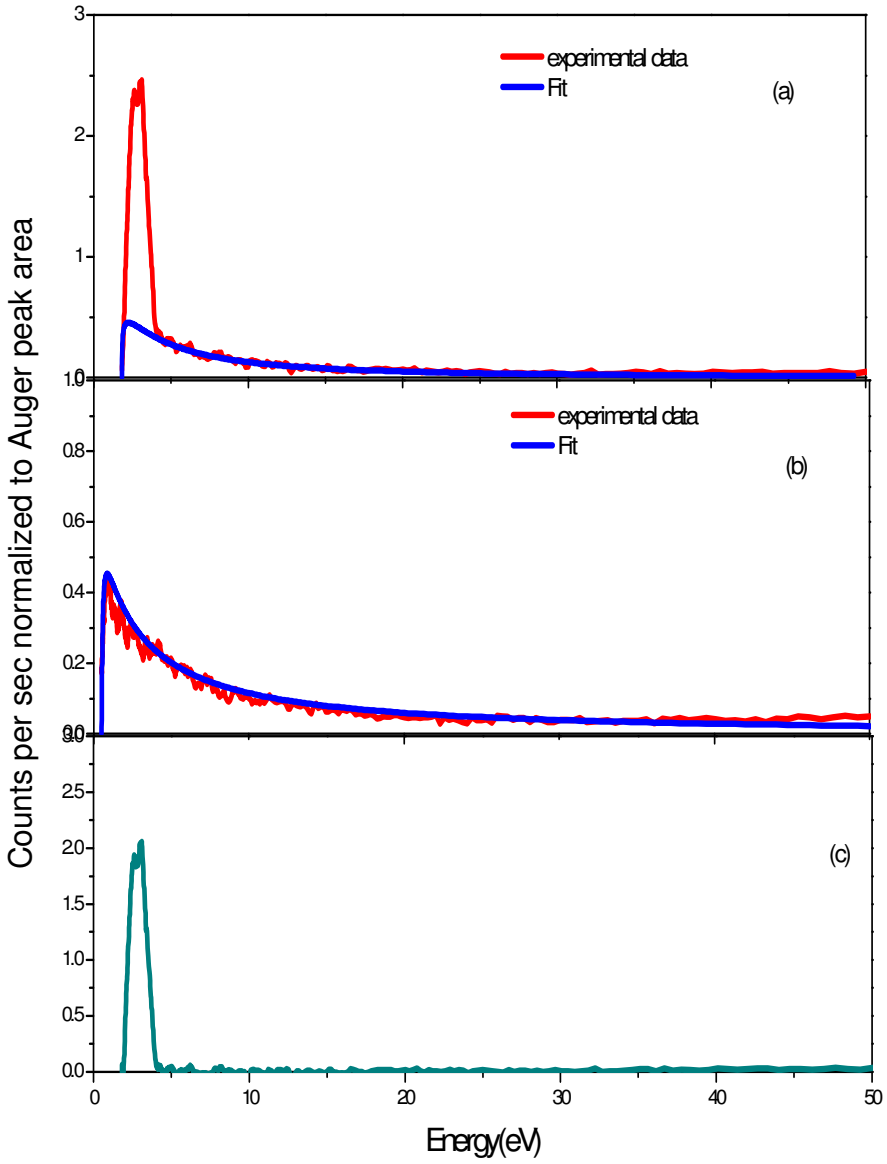

Figure 3.6 (a)Electron Energy spectrum from taken with beam energy 3eV.(b)Energy spectrum with beam energy 1.5eV.(c) same as (a) but with background, as estimated from (b), subtracted.

Note the absence of the low energy (AQSE) peak but the high energy Auger peak is present. A broad background between 5- 30eV can be seen which is due to the low energy secondary electron tail associated with the Auger transition. As discussed in detail in the next chapter, this

tail is from electrons that have lost energy on the way out or some intrinsic shakeup process that generates low energy electrons as a result of the large perturbation on the system represented by the sudden change in electrostatic potential resulting from the annihilation of a core electron. Note that in fig3.6 (b), we still get Auger transition because quantum sticking is still taking place although secondary electron generation is energetically prohibited. In this case quantum sticking is accompanied by electron-hole pair creation in which an electron at or below the Fermi level is promoted to an energy level above the Fermi level but below the vacuum level. Fig. 3.6 (c) shows the spectra from fig. 3.6(a) with the background due to the Auger electrons and associated Auger induced secondaries subtracted.

Background on the high energy side of the secondary electron peak in fig.3.6 (a) is primarily due to low energy electrons associated with the low energy tail of the Cu-MVV positron annihilation induced Auger transitions. Above the incident kinetic energy threshold at which it is possible to form Ps and produce an outgoing secondary electron (3.2eV for Au and 2.6 eV for Cu) there is another background due to positrons that have formed Ps. This background has two parts. One part is due to the ¼ of the Ps that are in the singlet state. These Ps annihilate in ~100 ps which is within the resolution time of the T-O-F spectrometer. These events will result in a narrow secondary peak in the T-O-F spectrum that cuts off at E_{beam} –2* φ^-+6.8 eV. The other part of the Ps background is due to the ¾ of the Ps that are in the triplet state and have a lifetime of 142ns. Other contributions include - gamma ray induced secondary electrons and Auger induced background.

The peak at the low energy side of the spectrum in fig 3.6(a) can be attributed to be generated by the electrons which came out with energies up to the limit given by eq.3.6 and above the limits given by equations 3.4 and 3.5. Hence the peak seen at the low energy side for 1.5eV, 2.3eV and 3eV can be ascribed to be the direct trapping of the positron into the surface state and transfer of the difference in between the initial and final state positron energy to an outgoing electron. As the beam energy increases the probability of the direct dropping of

positron in the sample bias decreases. Also at the cutoff energy (~5eV), collision induced secondary electrons begin to dominate the process.

To assure the true nature of the peak, triple coincidence spectrum were taken and compared with the normal coincidence spectrum (here called double coincidence).

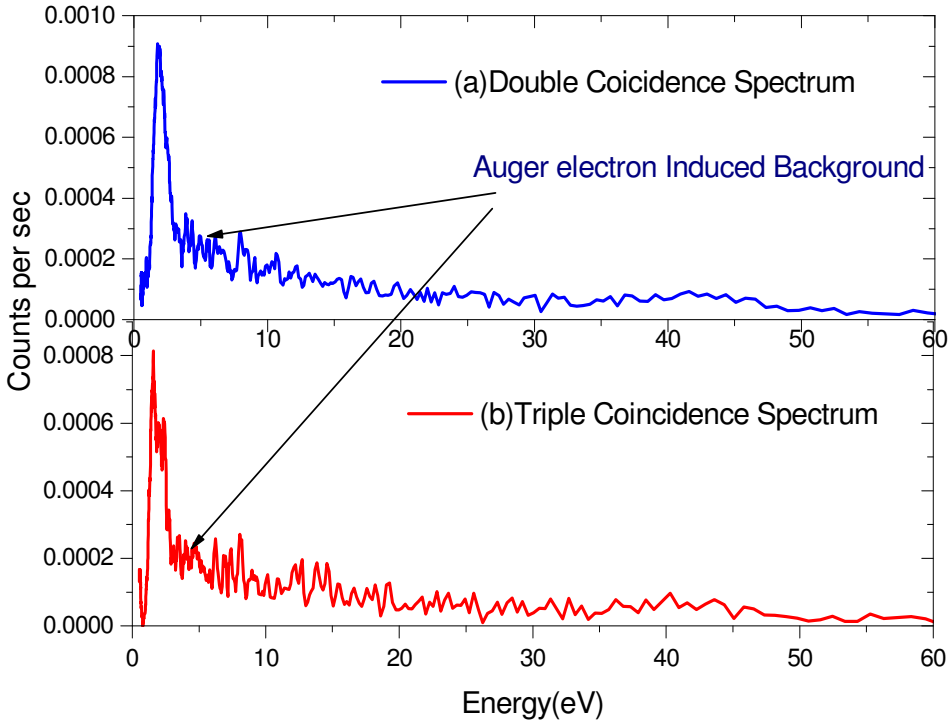

Figure 3.7 Comparison of the double coincidence (a) and triple coincidence (b) spectrum.

Since the triple coincidence gets the gamma ray signal only when both the gamma photons are detected in coincidence, any ortho Positronium induced background would be suppressed as would be signals from X-ray induced secondary electron emission. As can be seen the secondary electron peak is present in both the spectrum of fig 3.7 and the background at high energy side of the peak is not reduced. This confirms that this background is due to the Auger electrons.

To further verify the nature of the low energy secondary electron peak Cu was chosen as second sample because copper has the advantages of having known positron surface

properties. In addition Cu has a low sticking probability for O_2 and N_2 and was observed to stay clean for several days under UHV conditions. Cu sample was heated up to 720^{o}C and 650^{0}C and the data taken with incident positron beam energy above (fig 3.8) and below (fig 3.9) the threshold given by equation 3.6 respectively. At this temperature positrons in the surface state are desorbed as Positronium and are no longer available to annihilate with electrons at the surface [25]. Consequently heating the sample results in the elimination of the annihilation induced Auger peak as may be seen in the spectra shown in fig3.8. The Auger peak returns when the sample is cooled down. The secondary electron peak is present in the hot as well as the cold sample indicating that the peak is not associated with Auger process (fig 3.8). In the case of hot sample, the secondary electrons are created when the positron makes a transition into the surface state(the same as room temperature) The trapped positrons are then desorbed as Positronium thus leading to the absence of the Auger peak. This demonstrates that the narrow low energy peak of the secondary electron spectrum is indeed due to the sticking of the positrons to the surface state and not related to Auger electrons.

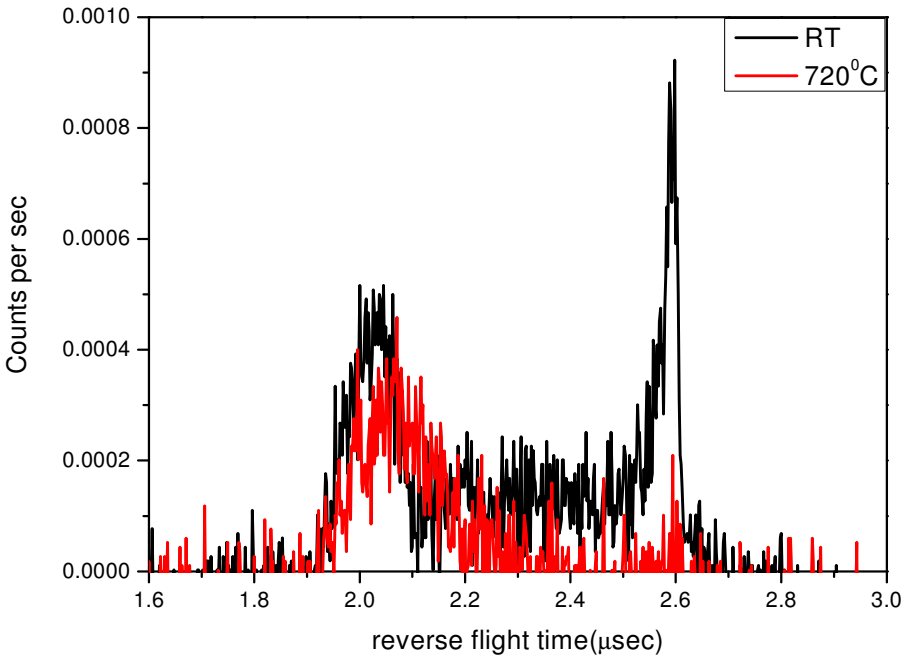

Figure 3.8 PAES Spectrum of Cu at 720^{o}C Room temperature with beam energy of 3eV.

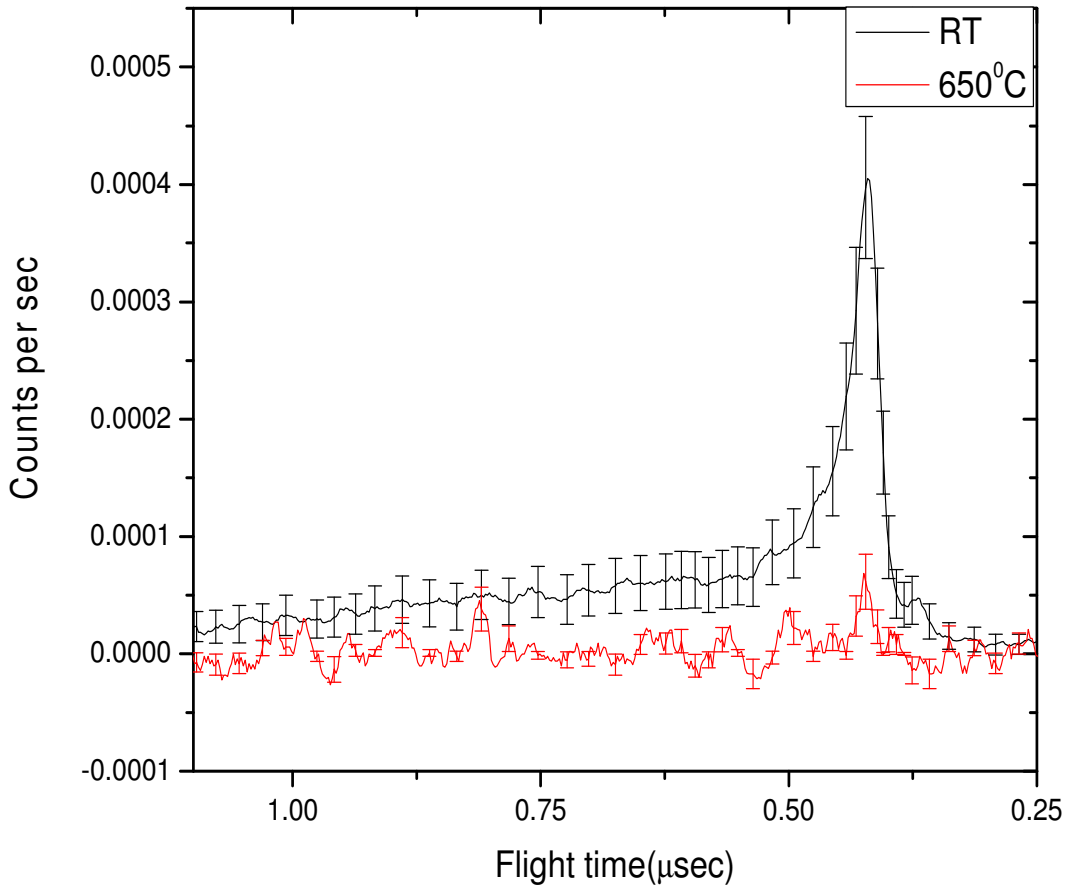

Figure 3.9 Channel spectrum of Cu (100) taken with positron beam energy 1.5eV. (a) Sample is kept at 650^{o}C (b) the same sample cooled down and data taken without any surface treatment.

Other contributions to the secondary electron spectrum can come from the annihilation gamma rays of energy 511 keV. The fact that AQSE peak goes away (fig 3.9) but the annihilation induced Auger peak remains when the beam energy is set below the threshold proves that the peak observed above threshold is not due to either the Auger process or gamma induced secondaries. As another check on the size of the gamma induced secondary electron background the sample was heated to 660^{o}C and the incident positron beam energy was kept below the threshold given by Eq3.6. In this case both the annihilation induced Auger peak and the AQSE peak are not present. However there are still annihilation gamma impacting on the surface due to the annihilation of Positronium. Hence any contribution from gamma

induced secondaries should still be available. The resulting timing spectra (fig3.9) show that the average gamma induced background is negligible. To verify that the sample surface was not contaminated, it was cooled down to room temperature and the Au -O_{23}VV peak came back. The Auger peak intensity normalized to the total peak area in the gamma spectrum as a function of beam energy is plotted in figure 3.10

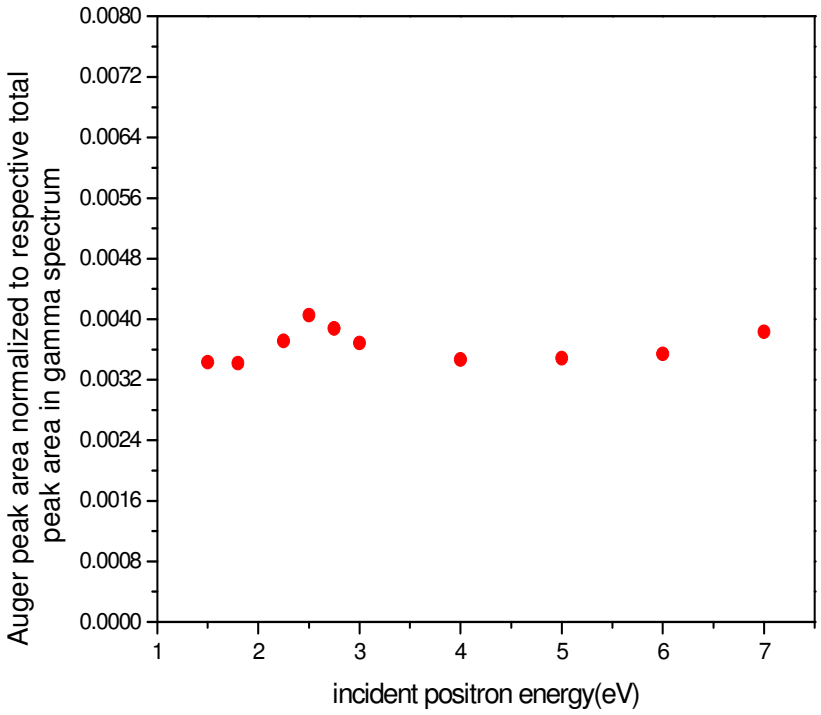

Figure 3.10 Auger peak intensity normalized to the total peak area in the NaI spectrum as a function of incident positron energy.

The functional form of the Auger induced background was determined from the spectrum taken at -0.5V sample bias.

$$N(E) = A * E * ((E + B)^{-1}) * ((E + \varphi^{-})^{-C}$$

where A,B and C are the fitting parameters derived from the plot at sample bias of -0.5V. The Auger induced background at various sample bias was fitted to the abovementioned function

and was subsequently subtracted (as shown in fig 3.6). The peak area thus determined is plotted as a function of beam energy in fig 3.11.

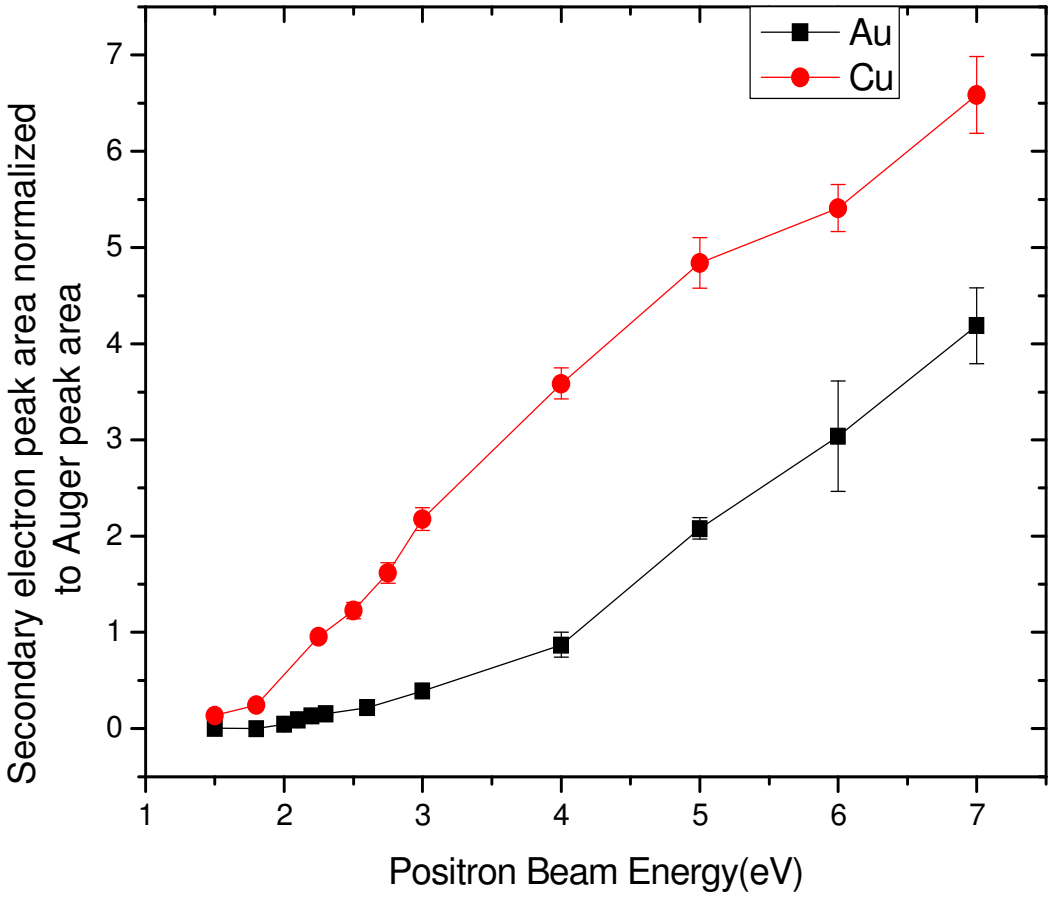

Figure 3.11 Secondary electron peak intensity as a function of maximum incident positron energy for Cu and Au.

3.7 Measurement of the Positronium fraction

This section presents the results of the measurement of the fraction of the incident positrons that form positronium, Ps. The positronium fraction (*f*) is defined as the percentage of the incident positrons that form Positronium [25].In order to estimate the sticking probability , we needed to determine the positronium fraction from a surface. The Positronium fraction is calculated from the NaI spectrum. A typical NaI spectrum consists of the 511keV Photopeak (P)

and a broad distribution of gamma counts at lower energies (T) (figure 3.12). The photopeak is due to the 2 gamma annihilation and the intensity less than the 511 keV peak contains contribution in which the $2m_e c^2$ energy of annihilation is distributed amongst three gamma photons leading to a broad distribution of energies. The photopeak also contains the contribution from the Compton scattering of the gamma photons in the detector . The contribution due to the Compton scattering is restricted to energies below the Compton edge.

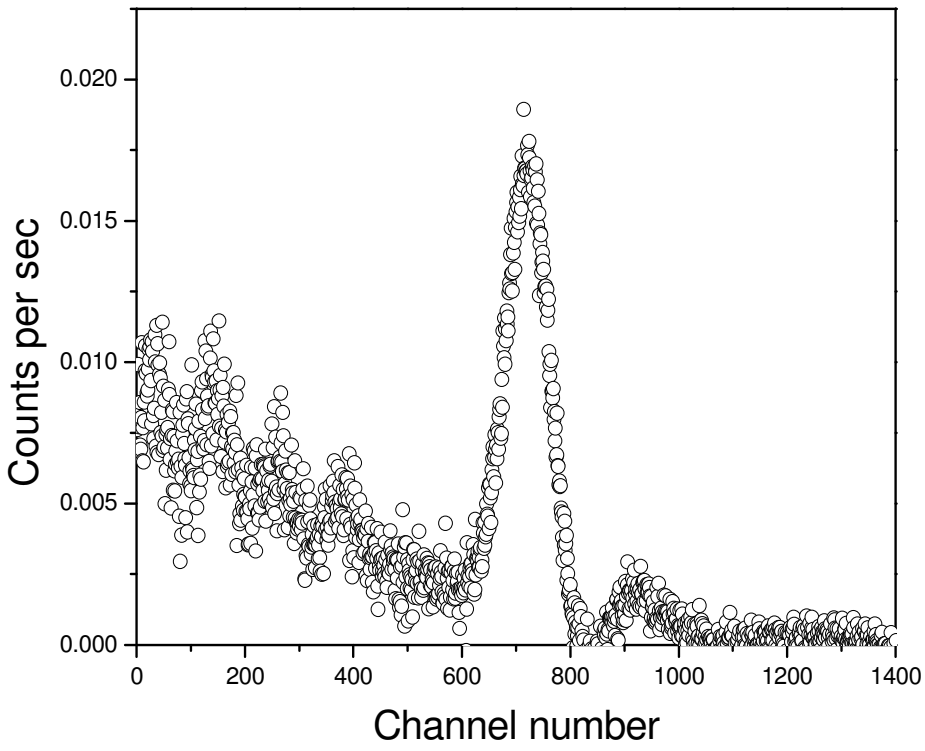

Figure 3.12 A typical NaI spectrum. The channel number is proportional to the gamma ray energy.

Positronium fraction is related to the Photopeak (P) and total peak (T) by the following relation[25]

$$P = fP_1 + (1-f)P_0 \qquad 3.7$$

$$T = fT_1 + (1-f)T_0 \qquad 3.8$$

Where $P_1(T_1)$ is the Photopeak (total peak) intensity when all the positrons incident on the sample form Positronium while $P_0(T_0)$ is the intensity when there are no Positronium formed. Defining R, such that

$$R = \frac{T - P}{P} \tag{3.9}$$

$$R_0 = \frac{T_0 - P_{01}}{P_0} \text{ and} \tag{3.10}$$

$$R_1 = \frac{T_1 - P_1}{P_1} \tag{3.11}$$

Then f can be written as

$$f = \left[1 + \frac{P_1}{P_0}\left(\frac{R_1 - R}{R - R_0}\right)\right]^{-1} \tag{3.12}$$

Hence to determine the Positronium fraction three factors are needed- R_0, R_1 and P_1 / P_0. In case of Cu, P_1 and R_1 were measured by heating the Cu sample to 700^0C. The ratio P_1 / P_0 was taken to be 0.67[15, 25]. The resulting plot of Positronium fraction at different energy is shown in fig 3.13.

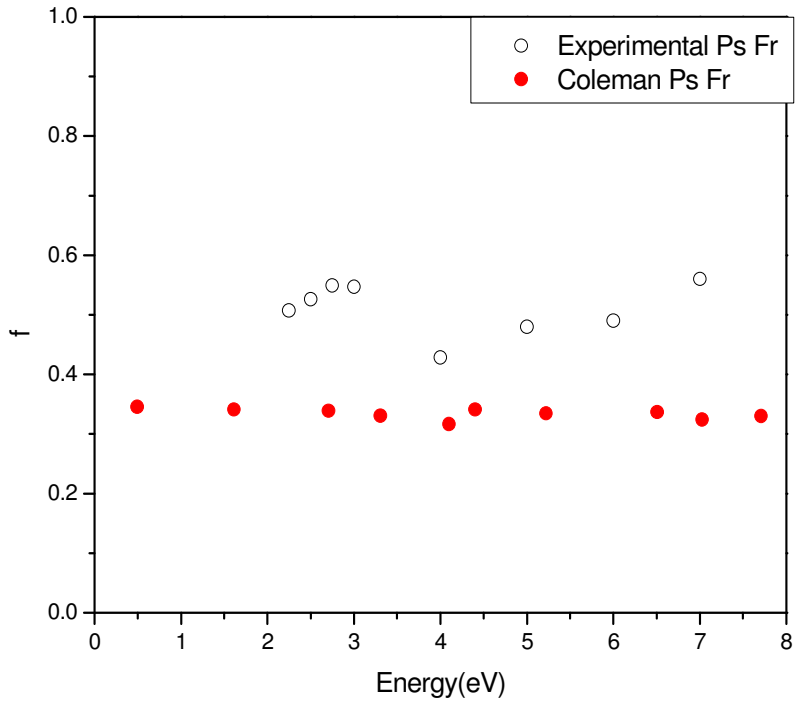

Figure 3.13 Positronium fraction variations with the incident Positron energy for Cu and comparison with data from reference 59.

3.8 Estimate of the Auger mediated Quantum Sticking Probability

In this section we present estimates of the sticking probability based upon an analysis of the intensities of the AQSE peak (figure 3.11). The assumptions in this analysis are as following-(a) The elastic reflection probability is small compared to the sticking probability (b) the incident positron has only two channels open to it- sticking and transmission into the bulk (c) the positrons can return to the surface state without being thermalized. The last assumption is valid because at low energy (<10eV) the mean free path of positron in matter is ~100Å. Hence it will have multiple chances of encountering the surface before significantly losing its energy to phonons or electron hole pair mechanism.

If we assume that the positron reflection or reemission probability is negligible, then the total incident positron intensity can be written as

$$N_{e^+} = N_{Ps} + N_{ss}\,, \qquad 3.8$$

where N_{e+} is the incident positron intensity, N_{Ps} is the number of positrons which form Positronium and N_{ss} is the number of positrons localized in the surface state. Number of positrons trapped in the surface state is related to the number of Auger electrons by the following relation

$$N_{ss} = (1/C)N_{Aug} \quad , \qquad 3.9(a)$$

where N_{Aug} is the Auger electron intensity and C is the annihilation probability of positron with Cu $M_{2,3}$ core level [13] .If *f* is the Positronium fraction [25], then the Positronium intensity is related to the number of positrons trapped in the surface state by

$$N_{Ps} = \left(\frac{f}{1-f}\right)N_{ss} \quad . \qquad 3.9(b)$$

In this process the electron emission can be compared to photoemission process with low photon energy (~12eV) [37]. The low energy photoemission results were chosen since they are more reflective of the surface DOS then the high energy photoemission results. The positron sticking probability is then given by

$$P(E) = \frac{N_{\sec}(1-f)C(T_{Aug}/T_{\sec})}{N_{Aug} \times \left(\sum_{E+E_{ss}-\varphi^-}^{E_F} DOS \Big/ \sum_{E+E_{ss}-\varphi^-}^{E_F} DOS \right)} \qquad 3.8(c)$$

where surface DOS has been taken to be proportional to the valence band photoemission measurements of Eastman et al. [37]. This has been shown schematically in fig 3.15. In fig 3.14(a) DOS is plotted as a function of energy below the Fermi level. As the positron makes a

transition from the scattering state to the surface state bound state it can excite electron-hole pairs in an energy range from E_F to $-(E+E_{ss})$. Of all these electrons only those with energy more than the electronic work function will escape the solid. These electrons are present in the DOS in an energy range from E_F to $-(E+E_{ss}-\varphi^-)$. Consequently the sticking probability is related to the ratio of DOS's by

$$P(E) \propto \left(\sum_{E_F-(E_P+E_{SS}-\varphi^-)}^{E_F} DOS \Big/ \sum_{E_F-(E_P+E_{SS})}^{E_F} DOS \right)^{-1}$$

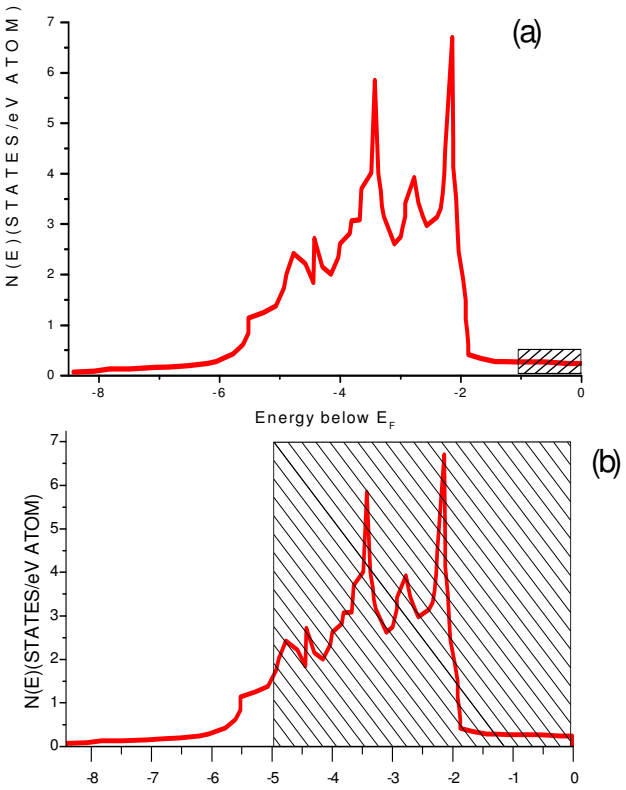

Figure 3.14 Schematic representation of the volume of DOS.excited by the positron making a transition to the surface state. Probability of sticking is inversely proportional to the ratio of shaded area in (a) and (b).

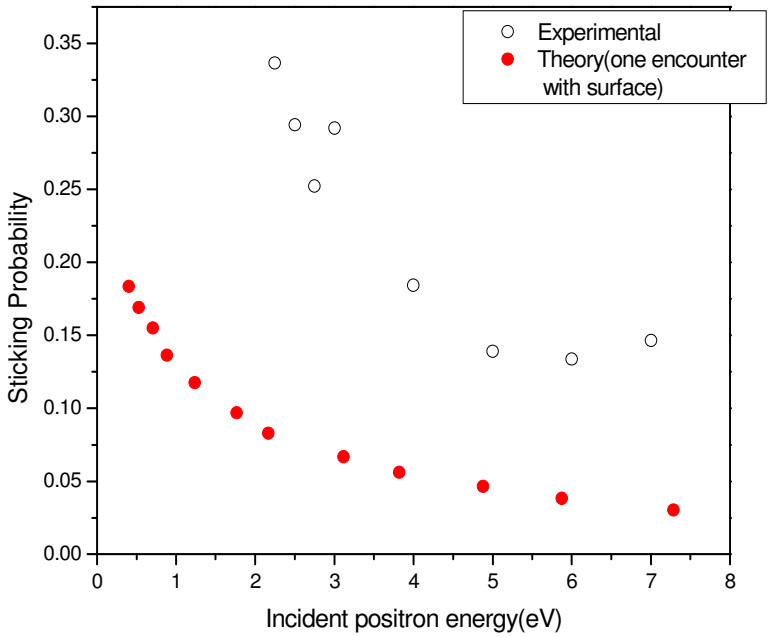

Figure 3.15 Probability of positron sticking to the surface estimated from AQSE peak intensity and compared with the theoretical calculation of theoretical value from ref 18.

3.9 Determination of surface state binding energy

In this section we present an analysis which is used to provide an independent determination of the positron surface state binding energy. The binding energy is determined from the intensity of the AQSE peak intensity as a function of incident positron energy. Till now this has been estimated from the Positronium thermal desorption experiments [25]. In such an experiment, the Positronium fraction (f) is measured as a function of the sample temperature. For a thermally activated process [11],

$$f = (f_o + f_\infty \gamma^{-1} z)/(1+\gamma^{-1} z) \qquad 3.9$$

where f and f_∞ are the low and high temperature limit of f, γ is the annihilation rate of positrons at the surface, z is the positron desorption rate. z is related to the depth of the surface state well, E_{ss} by $z = z_0(T)\exp[-E_{ss}/kT]$. In the experiments done in this

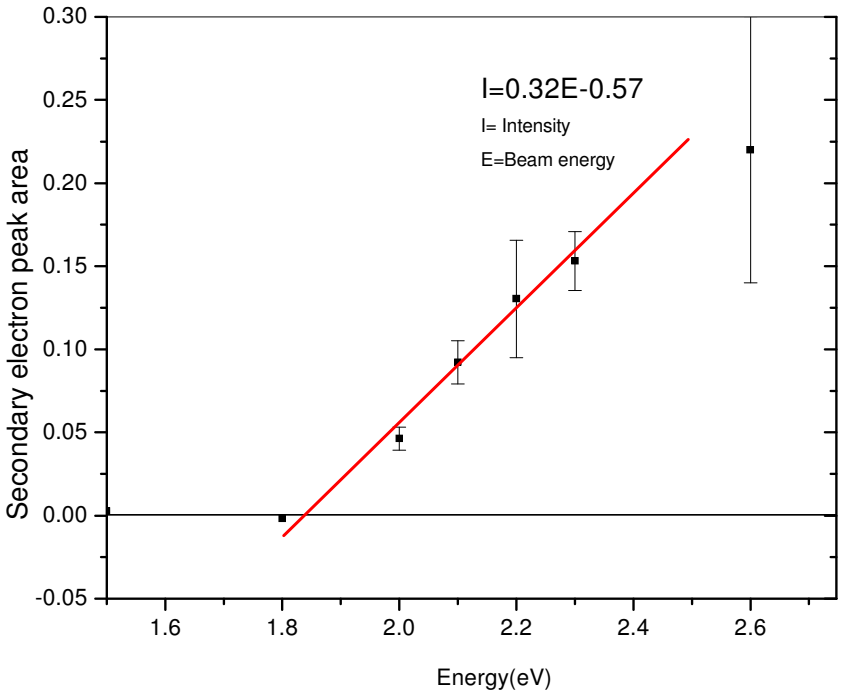

Figure 3.16 Secondary electron Yield vs. the incident positron beam energy for Au.

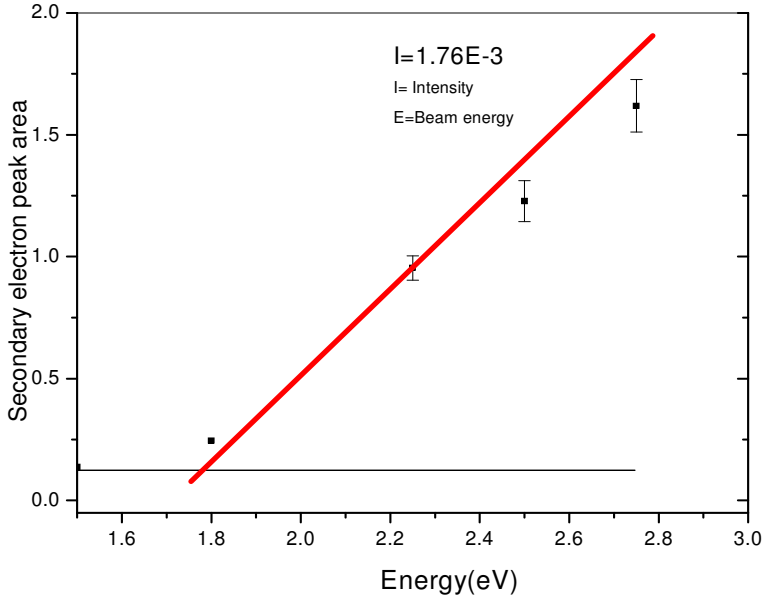

Figure 3.17 Secondary electron Yield vs. the incident positron beam energy for Cu.

dissertation, the AQSE peak has been shown to be related to the surface state potential depth. Near threshold an analysis similar to that used to deduce eq 3.8 results in a linear relation between AQSE peak intensity *Y* vs energy.

$$Y = AE - Y_o \qquad 3.10$$

where A and Y_o are the fit to the line and E is the incident positron energy.

The secondary electron yield will go to zero when the energy transferred to the electron at the Fermi level from a positron undergoing AQSE is less than or equal to the work function. Hence E_{ss} is given by

$$E_{ss} = \varphi^{-} - E_{\text{int}\,ercerpt} \qquad 3.11$$

Thus the potential well depth can be calculated by taking the y-intercept of the straight line fit to the AQSE secondary electron yield plotted as a function of the incident positron energy. The values calculated for Au and Cu via this method are – 3.22eV (Au) and 2.94eV (Cu). The corresponding values for Cu (100) surface measured using the thermal desorption process is 2.77eV [11].

3.11 Conclusion

In this section we provide a direct experimental evidence for the direct trapping of positrons into the surface state from a positive energy scattering state. This process is similar to the Auger process and is termed as Auger mediated quantum sticking effect (AQSE) The generation of a narrow secondary electron peak as a result of bombardment by positrons with incident energies less than 3 eV provides clear evidence that these electrons are due to the transfer of energy from positrons that make a transition from a positive energy scattering state directly into a surface state. There is not sufficient energy to boost an electron from at or below the Fermi level to a positive energy if the positron makes a transition from the scattering state to a final state in the bulk since the binding energies of the bulk state are close to zero. Gamma induced secondary electrons are allowed energetically but would not be expected to result in a

narrow energy peak. We also note that below the threshold of 1.8eV ,we still see an annihilation induced Auger signal proving that there are annihilation events at the surface (and hence annihilation induced gamma rays are still incident on the surface) but the narrow peak is absent which would not be the case if it were due to annihilation gammas. Transitions where the positron goes from the scattering state to an e+-e- bound state (Ps) do not release enough energy to generate a secondary electron. Below the threshold of 2eV we know the positrons are still hitting the surface because they are still generating Auger electrons from the surface. The Auger peak generated by positron incident at 1.5eV is verified by the spectrum taken when the sample is at heated to high temperature. When the sample is heated the positrons in the surface state are desorbed as Positronium and hence the Auger peak is absent.

CHAPTER 4

BACKGROUND FREE AUGER SPECTROSCOPY

4.1 Introduction

Auger spectra provide important information about the chemical properties of surfaces. Conventional Auger spectroscopic excitations rely on creating the core hole excitation that result in Auger electron emission with a beam of electron or photons. For ionization to take place the energy of the incident electron or photon must exceed the binding energy of respective core electrons. Hence in such a process, the Auger peak is accompanied by a background of inelastic and elastically scattered electrons. The range of energies of the primary beam induced electrons extends from 0eV to E_{beam} in case of electrons and up to $E_{beam} - \varphi^{-}$ in case of photons. This is because as the primary electrons go in the bulk, they pick up energy equal to φ^{-} and hence there will be secondary electron emission even with incident electron of vanishing energy. In the case of photons, this is not true and hence there is no secondary electron emission with photon energy less than work function, φ^{-}. A typical electron induced electron spectrum is shown in fig 4.1. The electrons are divided into three types based on the energy- I. true secondary electrons II. Inelastically scattered electrons and III. Elastically scattered electrons. As can be seen, the incident beam excites electrons from 0 eV to the beam energy.

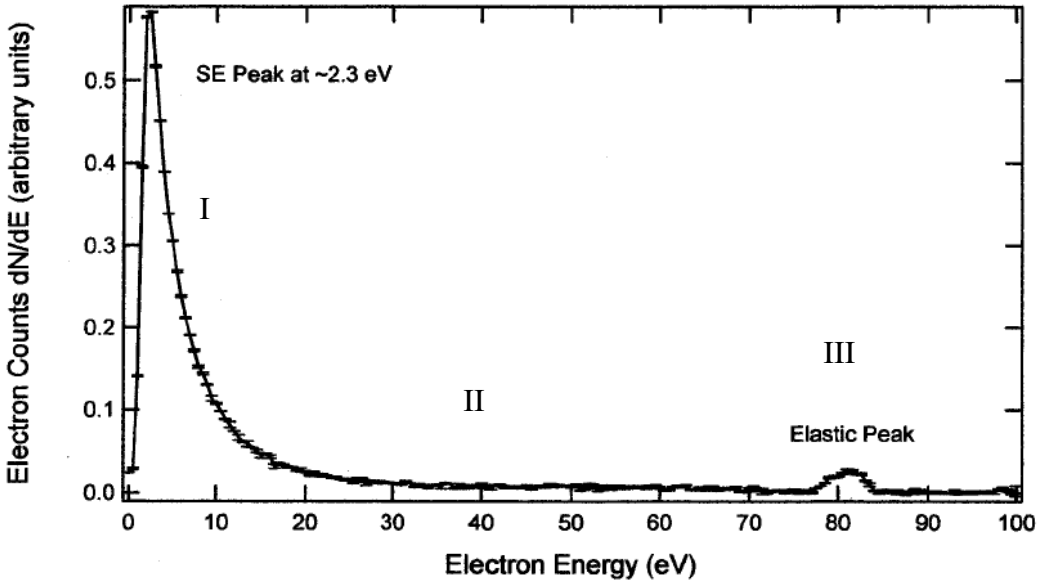

Figure 4.1 Electron induced Secondary electron spectrum of Gold with incident beam energy of 80eV taken from ref 26. Regions I, II and III have been labeled following Seah [27].

In EAES, the core hole is typically created with incident beam energies of several keV's. In such a case the Auger peaks appears as small bumps on the top of a large background of secondary electron in the energy spectrum. Often such a spectrum is differentiated to get rid of the smoothly varying background and to bring out the Auger signal. Other techniques model the background with a polynomial of the nature [27]

$$N(E) = A * E * ((E + B)^{-1}) * ((E + \varphi^{-})^{-C} \qquad 4.1$$

where A, B and C are the fitting parameters. This assumed background is then subtracted to reveal the true Auger peak which then is studied for the chemical information contained in the Auger line shape. This process relies on the assumption that the background (inelastic or elastic) is due to the interaction of the primary beam with the valence electrons in the sample and hence has no intrinsic relation to the Auger process. So while an excited atom in the solid may decay via processes that result intrinsically in low energy electron emission, there is no way to study this conclusively with conventional excitation techniques. Thus the origin of the

electrons with energy less than the Auger electron cannot be ascertained with certainty. This low energy tail (LET) has been shown in fig 4.2

In PAES, the core hole is created by matter antimatter annihilation. Theoretical and experimental work have shown that due to positron tunneling into the core region , annihilation with the core electrons accounts for several percent of the total annihilation events[13]. Weiss et al.. have demonstrated that thermalized positrons trapped in the image potential well at the surface can be used to excite Auger electron emission from the surface[39-35]. This suggests that if the surface state can be efficiently populated with positrons using low energy beam of positrons (as was demonstrated in chapter 3) then Auger transition at the surface can be excited using positron beam whose energy is below that necessary to excite secondary electron emission.

Thus the Auger transition can be achieved by using a positron beam of vanishingly low energy. This will reduce the background associated with the regions I, II and III in fig 1. A typical PAES spectrum is shown in fig 4.2[28]. The beam energy here is ~15eV. Thus the different regions of the spectrum can be separated based on their origin. Based on the energetic considerations, the primary beam induced secondaries must have energy $E \leq 15eV$.

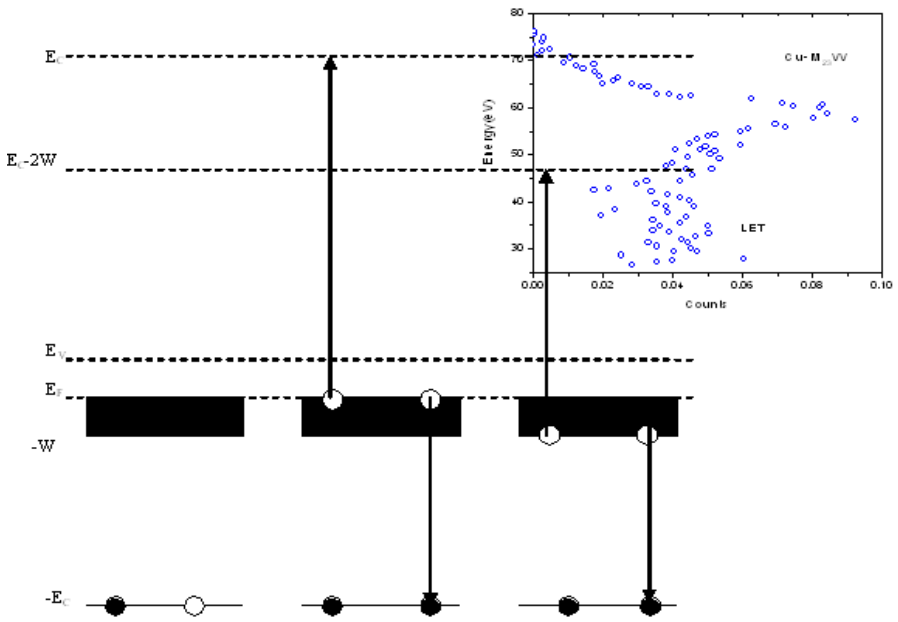

Figure 4.2 Band Diagram showing the minimum and maximum energy of Auger electron of Cu. Positron beam energy is ~15eV and the spectrum in the energy region from 25eV to 55eV is labeled as Low energy Tail (LET) [28, 30].

Figure 4.2 describes the Auger process from a material with valence band width of W and shows the maximum and the minimum energy that the Auger electron can have. Referencing to the zero of energy to the top of the valence band the maximum energy is given by $E_{Auger,Max} = E_C$ while the minimum is given by $E_{Auger,Min} = E_C - 2W$. Hence the width of the Auger peak will be 2*W*. In case of fig 4.2, the positron beam energy is ~15eV. Based on this argument neither Auger electrons nor beam induced background should be present in the region 25-45eV. But as can be seen, there is significant spectral weight in the low energy tail (from 25-45eV)associated with the Auger peak. The argument is made in the following sections that based on the large spectral weight of the LET in relation to the Auger peak, this feature is an intrinsic process associated with the Auger process.

4.2 Elimination of secondary electron background in PAES

Earlier PAES spectrums were taken with positron beam energy ~15eV and thus the beam induced secondary electron background was present from 0eV to ~15eV. In this

dissertation, positron beam energy was reduced below the secondary electron emission threshold (as discussed in chapter3) and the background free Auger spectrum of Cu and Au were obtained (fig 4.2 and fig 4.3) with incident positron beam energy of 1.5eV. Counting time for Au spectrum was 220hrs while for Cu it was 183hrs.

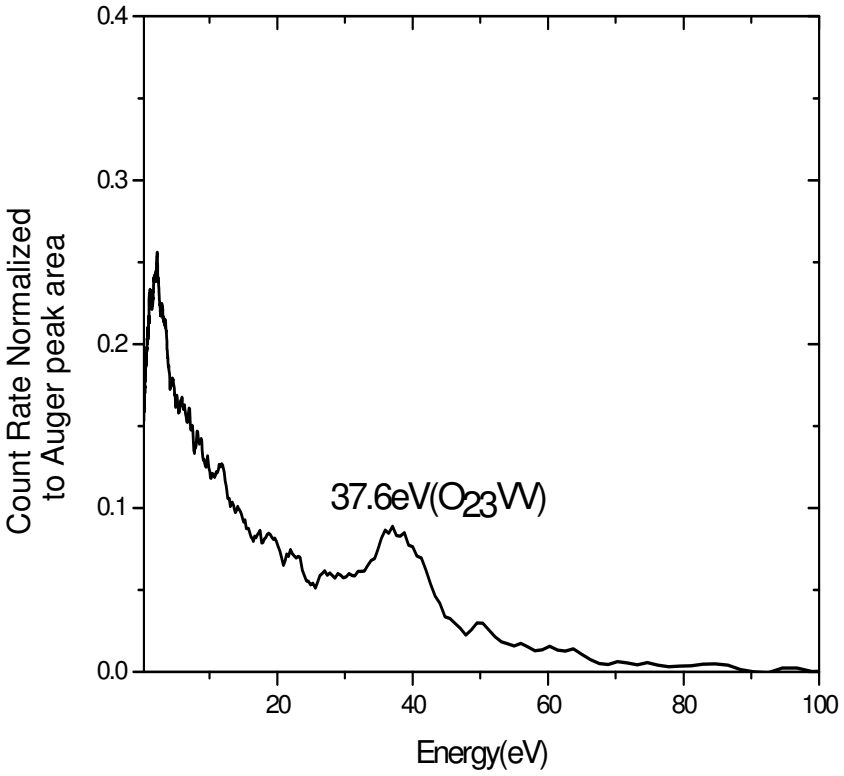

Figure 4.3 TOF-PAES spectrum of Au with positron energy of 1.5eV.

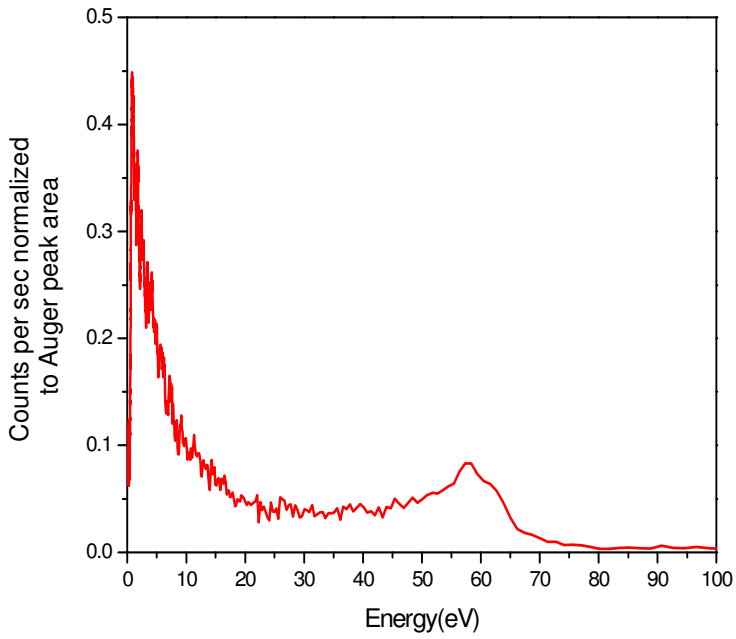

Figure 4.4 TOF-PAES spectrum of Cu with positron energy of 1.5eV.

4.3 Sources of inelastic electron in PAES

In Positron annihilation induced Auger electron spectrum the positron energy is much less than the core electron binding energy. In previous studies the beam energy was between 10-30eV. The LET associated with the Auger spectrum must be expected to contain contribution from- 1. Auger induced background 2. Gamma ray induced background 3. Positronium induced background 4. Primary beam induced background 5. Accidental background. The nature and magnitude of these different channels will be discussed below.

1. Auger induced background- The Auger electrons are emitted in 4π steradian. They can be divided into (a) those whose velocity normal to the surface will take them towards the detector and (b) those that will go opposite to and inside the sample. The electrons that are going in the forward direction will scatter inelastically with the valence electrons at the selvedge layer and generate inelastic electrons. The percentage of electrons that will pass through the selvedge

layer without suffering inelastic collision is defined as the Transmission factor [31]. This number can be estimated by the following formula

$$T = \frac{\int_0^{2\pi} d\varphi \int_0^{\pi/2} \exp\left(\frac{-d}{\lambda_{Cu,Au}.\cos\theta}\right)\sin\theta\, d\theta}{\int_0^{2\pi} d\varphi \int_0^{\pi/2} \sin\theta\, d\theta} \qquad 4.2$$

here $\lambda_{Cu,Au}$ is the inelastic mean free path of the Auger electron from Cu or Au[NIST handbook].Since in PAES the Auger electrons originate at the top most atomic layer ,d which is the distance the electrons travel in the solid can be taken as the half atomic layer thickness ~1A. This gives the transmission factor =0.45. This means that the 55% of the Auger electrons will inelastically scatter from the surface electrons. Hence the ratio between the extrinsic background and the Auger peak intensity is 1.2:1.

The resulting electronic excitation can be estimated as shown later.

(b)If we assume that half of the Auger electrons are going in the direction away from the detector and into the sample, then they can be thought of as a beam of electrons from the outside with energy equal to the Auger electron energy. The contribution of the backward directed electrons that could backscatter inelastically out of the sample and contribute to the LET may be estimated by considering the secondary electron yield. This yield for most of the metals as a function of the electron energy is known [32] .It has already been shown that the positron and electron induced secondary electron yield follow similar pattern [53,54]. Hence the secondary electron spectrum was taken with sample biased at -60V. The resulting spectrum was normalized to the electron induced secondary electron yield and the number of Auger electrons and is shown in fig 4.5

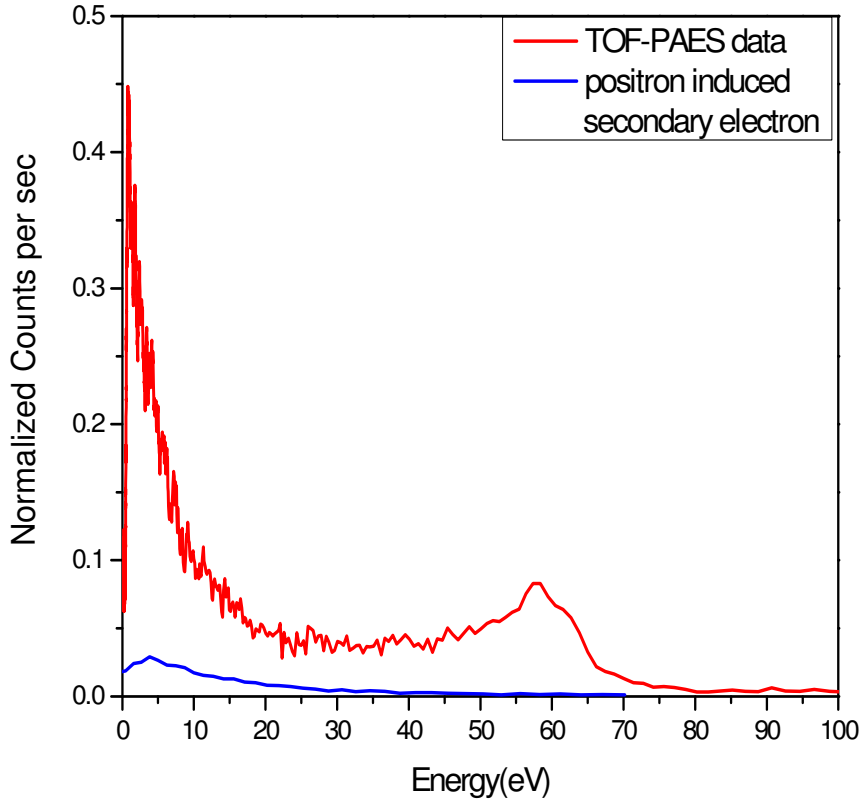

Figure 4.5 TOF-PAES spectrum of Cu. The blue line is the secondary electron spectrum with ~60eV incident positrons.

2. Gamma ray induced background- Matter- antimatter annihilation in solids or at their surfaces result in emission of two gamma rays of energy 511keV. The positron may escape as ortho or para-Positronium which annihilate by two or three gamma processes respectively. The o-Ps decay results in gamma ray of energy 0-~511keV. These gamma rays might produce secondary electrons by bremmstrahlung with the sample or the wall of the surrounding chamber. The intensity of the gamma induced background has been estimated here by measuring the TOF-PAES signal in the case where all the positrons desorbed as Positronium. Mills [25] et al. showed that when the Cu sample is heated to ~790^{o}C, almost all the positrons trapped in the surface state can be desorbed as Positronium. Once desorbed there will be two types of Positronium- ortho-Ps(o-Ps) and para-Ps(p-Ps). Hence ¼ th of the Positronium will be p-Ps and the other 3/4th will be o-Ps. The p-Ps has a lifetime of 125ps and hence will annihilate right in

front of the sample. The o-Ps has longer life time – 142ns. They o-Ps may drift away some distance before annihilating. The spectrum observed at high temperature (fig4.6) will provides a means to estimate the contribution to the background of the secondary electron produced by the gamma rays.

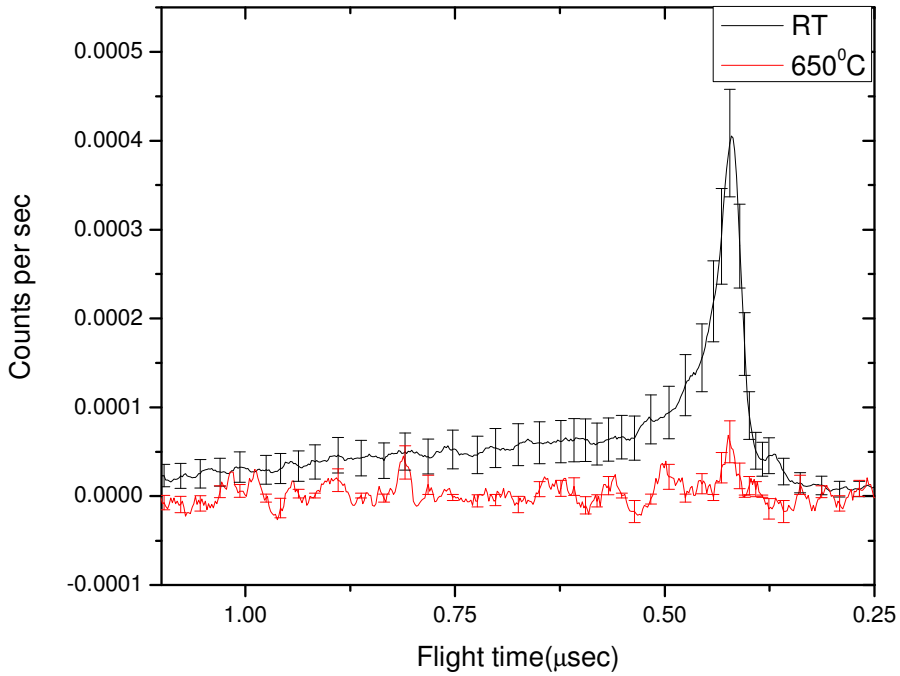

Figure 4.6 Comparison of the PAES spectrum of Cu obtained at room temperature and at 650°C.

In figure 4.6 the spectrum at room temperature has the Auger peak present and the LET will have, amongst other factors, the contribution from the secondary electrons due to gamma rays. However the high temperature spectrum has no Auger peak and hence the LET will be completely due to the secondary electrons due to gamma rays. The average count of the high temperature spectrum is almost zero and hence the gamma ray induced background is negligible. Zhou [28] et al. has also estimated the gamma ray induced background using a Cs covered sample. From such a surface, positrons desorb as Ps at room temperature and the

situation is exactly like the one where the sample surface is heated to high temperatures. They concluded that the gamma induced background was negligible in agreement with our results.

3. Positronium induced background- This channel presents a major complication, including the low energies, in TOF-PAES. It is present when the incident positron knocks out a secondary electron as it hits the sample and then leaves the sample bound to another electron as a Positronium atom. Fig 4.7 shows the time of flight spectrum of Graphite taken with a different setting of the detector and the beam energy of 15eV. The Positronium induced background shows up as an exponentially decaying tail.

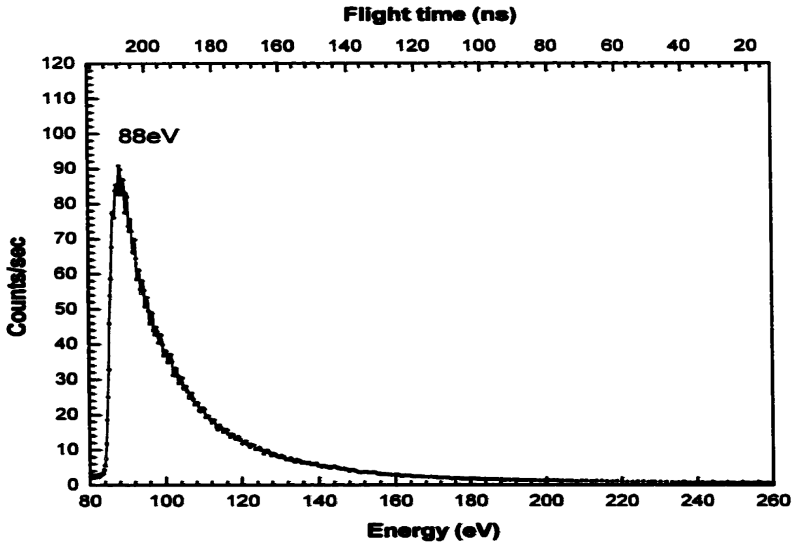

Figure 4.7 Secondary electron spectrum measured with PAES using a 15eV beam and the graphite sample is biased at -85V [from ref 15].

The measured timing spectra can be modeled by the following equation

$$N(t) = N_0 \exp(-t/\tau) \qquad 4.3$$

where τ is the effective lifetime of the long lived component of Positronium and *N(t)* is the number of detected gamma rays per unit time. In Time of flight PAES experiments this

introduces an exponentially decaying background. The time of flight of an electron, t_{flight} , is related to the time calculated by the spectrometer t_{neg} by

$$t_{neg} = t_{delay} - t_{flight} \quad 4.4$$

In case of secondary electron emission followed by Positronium formation the time recorded by the spectrometer is

$$t_{neg} = t_{delay} + t_{Ps} - t_{flight} \quad 4.5$$

The measured intensity can be represented by

$$N_{measured} = \iint N_{\sec}(t_{flight}) N_{Ps}(t_{ps}) \delta(t_{neg} - t_{delay} - t_{Ps} + t_{flight}) dt_{flight} dt_{Ps} \quad 4.6$$

This can be simplified to

$$N_{measured}(t_{neg}) = \int_0^\infty N_{\sec}(t_{delay} - t) N_{Ps}(t_{neg} - t_{delay} - t) dt$$

Substituting $N_{ps} = N_0 \exp(-\lambda t_{Ps})$

$$N_{neg} = \int_0^\infty N_{\sec}(t_{delay} - t) N_0 \exp(-\lambda (t_{neg} - t_{delay} + t)) dt \quad 4.7$$

Hence it can be seen that the secondary electron peak in the time (and hence channel) spectrum is convolution of the true secondary electron peak and the exponential decay of the Positronium.

Since the energy of the beam in measurements made in figure 3.9 was less then the threshold of collision induced secondary electron production, this channel was not active. There is another channel in which the incident positron, before encountering the bulk, forms a Positronium at the vacuum side of surface .The binding energy of Positronium in vacuum is 6.8eV. In such a scenario it is possible that the Positronium binding energy and the incident positron energy is given to an electron at the Fermi level. This electron may escape as a secondary electron. The kinematics equation for this process is given by –

$$E_{K\max} = Ep + E_{b\,Ps} - 2\varphi^{-} \qquad 4.8$$

where, E_{Kmax} is the maximum energy of the outgoing secondary electron, E_{bPs} is the binding energy of the Positronium and φ- is electronic work function. The beam energy used for the measurements described in this section was less than the energy required to allow this channel.

4. Accidental coincidence- The accidentals are estimated by the following formula-

$$N_{Acc} = \frac{N_{BaF_2} \times N_{MCP} \times Numberofchannels}{TAC} \qquad 4.9$$

This assumes a flat background

5. Primary beam induced secondary electron background- This background is due to the incident positrons scattering inelastically with the electrons and the later are ejected into the continuum as a result. The kinematics equation for this phenomenon is given by –

$$E_{K\max} = Ep - \varphi^{-} + \varphi^{+} \quad , \qquad 4.10$$

where φ^{+} is the positron work function. Since the beam energy was 1.5eV, in the measurements described in this chapter, this channel is not active.

4.4 Auger Photoelectron coincidence Spectroscopy

Auger photoelectron coincidence spectroscopy (APECS) has proven to be very useful surface selective technique [33]. In this technique a monochromatic photon beam is incident on the sample and the resulting electrons are detected in coincidence. Hence it is a (e^{-}, e^{-}) experiment. These experiments were carried out at U16 beam line at National Synchrotron Light Source(NSLS) at Brookhaven National Lab . Schematic of the experiment is shown in fig 4.8.

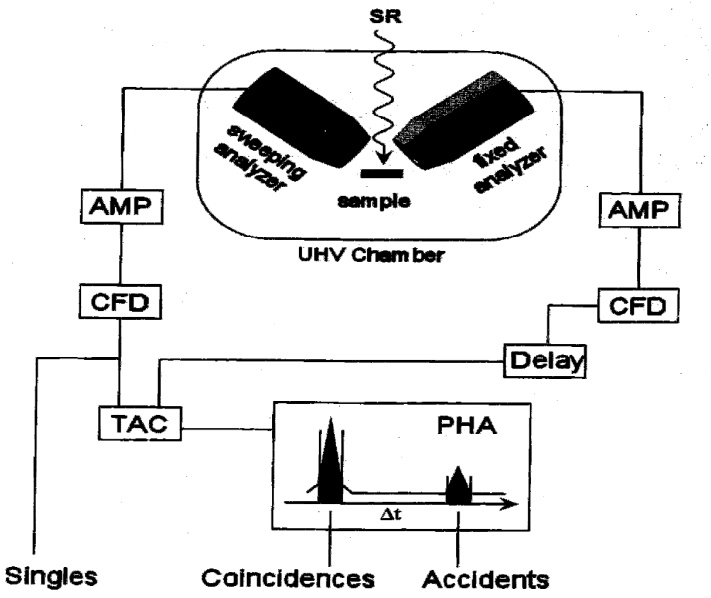

Figure 4.8 Schematic representation of the APECS experiment done at BNL [from ref 34].

Briefly, the electrons coming out of the sample are energy analyzed by two detectors kept at 45^0 to each other. Photoelectrons are produced when the incident photon energy is more than the threshold for core electron emission. In most of the metals and for shallow core levels (binding energy<2keV), such a core hole mostly relaxes by emission of Auger electrons. The time difference between the emission of Photoelectron and the Auger electrons is ~10^{-15} sec, hence with the timing resolution of the electronics (~10^{-10} sec) they appear to be simultaneous. One of the Channel Mirror Analyzer (CMA) is set at the Photoelectron energy while the other detector scans in the range of energy from 0eV to the Auger electron energy. Thus the Auger electrons are detected in coincidence with the photoelectrons. The timing coincidence technique also ensures that both the electrons are associated with the same atom. The accidental counts are removed by using the periodicity of the electron bunches producing the photons. The electrons from two bunches of electrons separated by one revolution time read in a timing spectrum gives the intensity of the accidental coincidences.

Jensen [30] was the first to study the LET associated with the Auger peak using APECS. In this experiment, the singles spectrum were compared with the coincidence spectrum to reveal the absence of the Plasmon peak. The presence of plasmon peak in electron spectroscopy is a signature of electrons losing energy to the plasmonic oscillations which are quantized with $n\hbar\omega_{s,b}$. The subscripts refer to the surface or the bulk plasmons. The absence of these periodic plasmon features was taken as evidence that the LET is not due to the interaction of the Auger electron with the surface[30]. Their result is shown in fig 4.9.

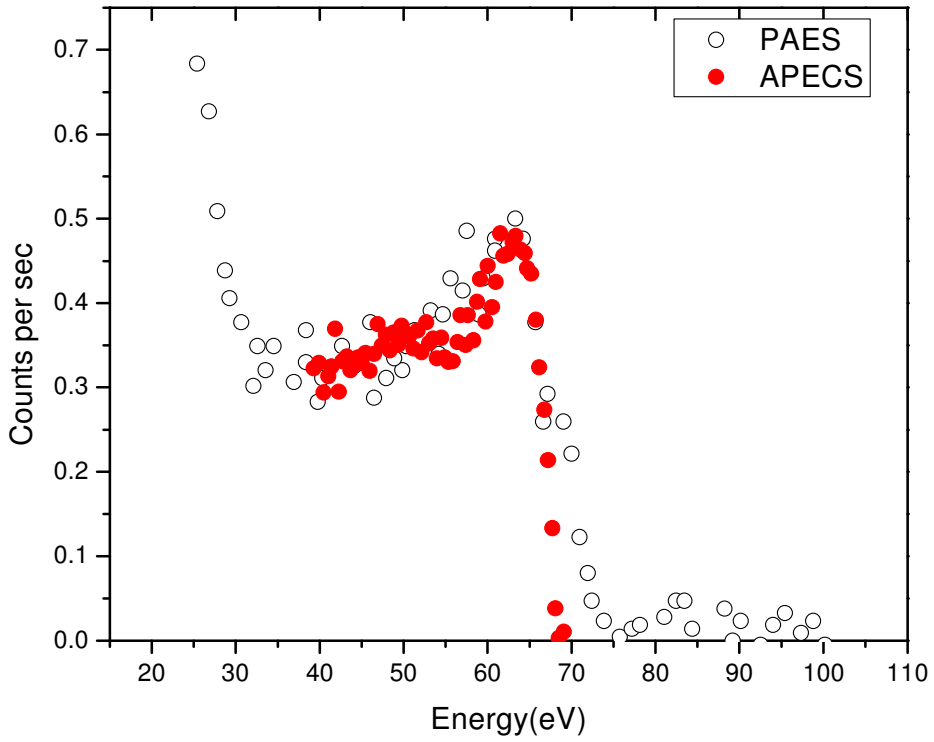

Figure 4.9 APECS data from Al [30] is compared to that of PAES [53]. The APECS data has been corrected for energy. The APECS data as well as the PAES data has no plasmon peak associated with the Auger peak.

The important observation in fig 4.7 is the spectral weight below 51.5eV which is forbidden by the two-hole final state assumption. In the single particle approximation, the matrix element for the two- hole state forbids final state transition to the n-hole state. Hence the

appearance of the LET was explained by the Core-valence (CV) interaction or the valence-valence (VV) interaction.

The enhanced surface selectivity of APECS stems from the fact that the joint probability of detecting two electrons from the surface in coincidence is proportional to the product of the escape probability of each electron. The mean free path for coincident detection will be $\frac{1}{\lambda} = \frac{1}{\lambda_{photoelect\ \ ron}} + \frac{1}{\lambda_{auger}}$. If $\lambda_{photoelectron} \cong \lambda_{Auger}$ then this implies that $\lambda_{eff} = 1/2\lambda_{Auger}$. Hence the probability of simultaneous detection of both the photoelectron and the Auger electron from the bulk is very less. They explained the presence of LET due to the n-hole final state as opposed to the 2 hole state in the conventional CVV Auger process. They estimated that the intensity in the CVV part of the spectrum is 35% of the total intensity. The measurement done by Jensen et al. [30] were hampered by the limitation of the conventional CMA's to measure electrons of energy less than 20eV. Their conclusion of the absence of secondary electrons in the coincidence spectrum is based on the mean free path of the detected electrons and the conclusion that the electrons are from the surface. The experiments conducted in this dissertation are free from these assumptions. TOF-PAES is proved to be able to detect electrons with energy 0.5 eV (see section 2.4for detail). The surface sensitivity of PAES arises from the trapping of the positrons in the surface state while APECS scans ~4Å deep from the surface.

Similar APECS experiments were done using Cu as the sample [38]. The resulting spectrum is shown in fig 4.10 and is compared to the PAES spectrum from Cu. The Cu sample was sputter cleaned every 24hrs for 40 minutes and the singles spectrum (from one CMA) is used to monitor the cleanliness of the sample.

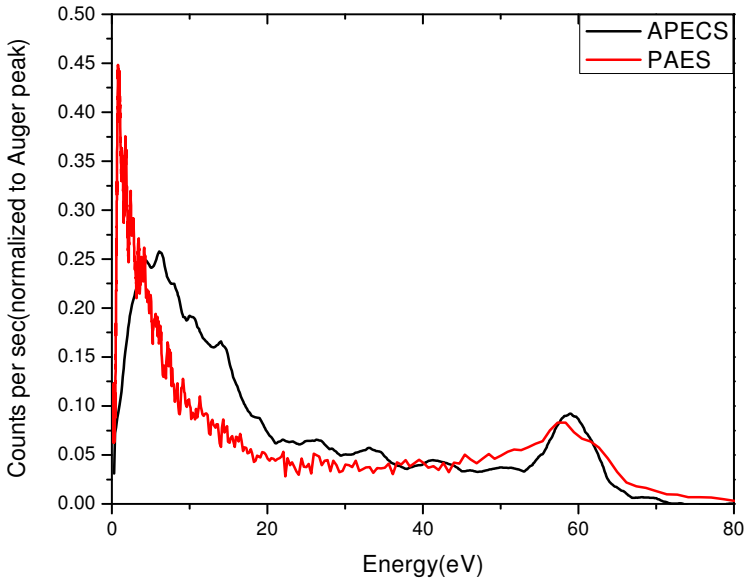

Figure 4.10 Comparison of the TOF- PAES and the APECS spectrum of Cu(100)[38].

The spectrum taken in fig 4.10 has the background estimated as follows. If one imagines two photons incident on the sample then one might lead to the photoelectron and hence Auger peak while the other leads to the extrinsic background. Such extrinsic background will be present all the way from 0eV to photon energy minus the work function. Hence the coincidence data will have contributions from such events where the fixed analyzer detects an inelastically scattered electron of same energy as the photoelectron. This background is estimated by taking the Auger spectrum in coincidence with the fixed analyzer which is now fixed at higher energy side of the photoelectron peak. The same experiment was repeated but with the fixed analyzer now looking at the low energy side of the photopeak. The resulting accidental coincidence is subtracted from the total counts to reveal the true coincidence as shown in fig 4.10

4.5 Estimation of the intrinsic background in PAES

After elimination of the respective channels for inelastic electrons, the resulting spectral weight in the energy forbidden region can be ascribed to :- 1.Inelastic scattering of the outgoing electron 2.Inelastic scattering of Auger electrons going the wrong way 3.an intrinsic LET. These factors are described below.

1. Inelastic scattering of the outgoing Auger electrons with the selvedge layer- In PAES 90% of the Auger electron originate in the surface layer and hence the one which are going in forward direction will inelastically collide with the electrons in the selvedge layer only. In our case the Auger electrons have an inelastic mean free path of 5 Å. Hence there probability of collision should be very small. This number has already been estimated and the increased probability is due to the fact that as opposed to CMA based detectors, our acceptance angle is ~ π. So the electrons which are coming at a large angle with respect to the surface will suffer more scattering then the one which are coming out almost normal to the surface as shown in fig 4.11.

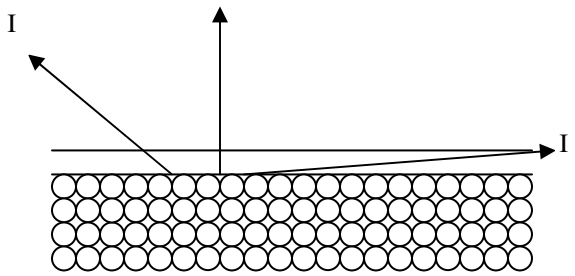

Figure 4.11 Schematic description of the scattering of the Auger electrons with the electrons in selvedge layer. The higher the angle from the surface normal more is the secondary electron generation.

A conservative estimate of this contribution can be made by comparing the spectrum from clean Cu and oxidized Cu surfaces as shown in fig 4.12. The monolayer coverage corresponding to the Cu+O spectrum in fig 4.12 has been estimated by using the data from ref 35. In this the Si

core annihilation rate is calculated as a function of the oxygen coverage and if it is assumed that the annihilation rate in Cu will follow the same trend as in Cu, then the coverage of oxygen at Cu surface is 0.5-1 monolayer.

The outgoing Cu Auger electrons will scatter inelastically from the selvedge layer in case of clean Cu surface while in the case of oxygen coverage, the interaction will be from the selvedge layer as well as the oxygen atoms. The comparison of the two spectra will thus give an estimate of the scattering due to the oxygen atoms. Here we have assumed that the interaction of the Auger electrons with the selvedge layer can be simulated by the interaction of the electrons with oxygen atoms on the surface and the low energy contribution of the oxygen KVV (516 eV) Auger electron is negligible.

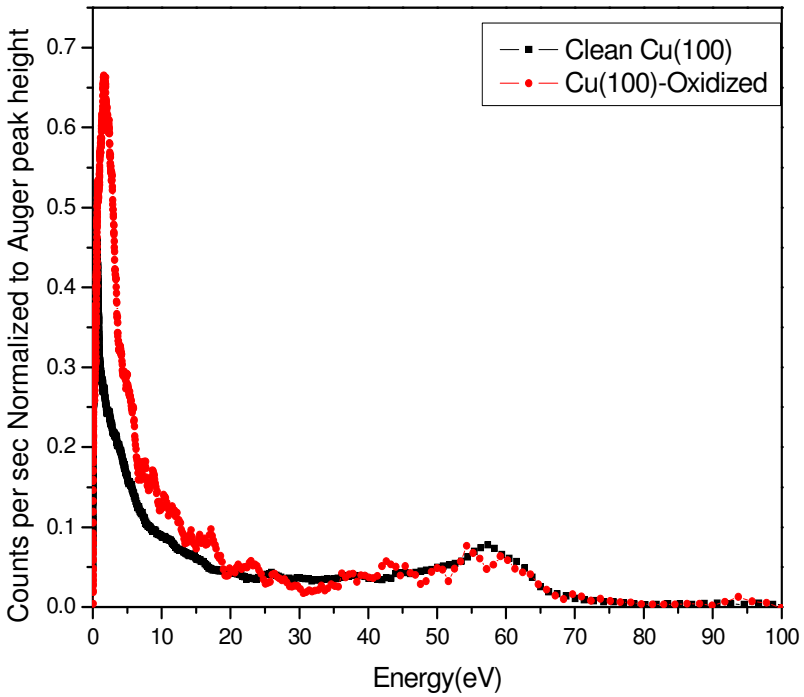

Figure 4.12 Comparison of TOF-PAES spectra from clean Cu(100) and Cu(100) with oxygen overlayer The spectra are normalized to the Auger peak area.

The LET in case of Clean Cu is represented as I_{LET}^{Cu} while that of Cu with O on the surface is given by I_{LET}^{Cu+O}. The intensity due to the Auger electrons going away from the detector and into the bulk is represented by $I_{Auger,bulk}$. The secondary electrons excited by the Auger electrons in the selvedge layer are represented by $I_{Auger,selvedge}$. Hence the following relation can be written,

$$I_{LET}^{Cu} = I_{\text{int}\,rinsic}^{Cu} + I_{Auger,bulk}^{Cu} + I_{Auger,selvedge}^{Cu} \quad 4.11$$

And the similar expression for LET in Cu+O surface is

$$I_{LET}^{Cu+O} = I_{\text{int}\,rinsic}^{Cu+O} + I_{Auger,bulk}^{Cu+O} + I_{Auger,selvedge}^{Cu+O} \quad 4.12$$

The assumptions that are made in following calculations is-(a) the LET due to the O Auger in Cu+O system is negligible compared due to LET of the Cu Auger and (b) the intrinsic part of the LET is proportional to the intensity of the Auger electrons.

Hence

$$I_{\text{int}\,rinsic}^{Cu+O} = A \times I_{Auger}^{Cu+O},$$

where A is a constant. Then a similar expression for clean Cu surface yields, $I_{\text{int}\,rinsic}^{Cu} = A \times I_{Auger}^{Cu}$. Further assuming that the secondary electron yield due to the Auger electrons going into the bulk will be similar for Cu and Cu+O surfaces, then

$$I_{Auger,bulk}^{Cu} = I_{Auger,bulk}^{Cu+O}.$$

Thus subtracting eq 4.11from eq 4.12

$$I_{LET}^{Cu+O} - I_{LET}^{Cu} = I_{Auger,selvedge}^{Cu+O} - I_{Auger,selvedge}^{Cu} \quad 4.13$$

Hence the subtraction of the two spectra shown in fig 4.9 will give an estimate of the interaction of the outgoing Auger electrons with the surface with O coverage. This will give an estimate of the inelastic scattering of the outgoing Auger electrons with the selvedge layer. This is shown in fig 4.13

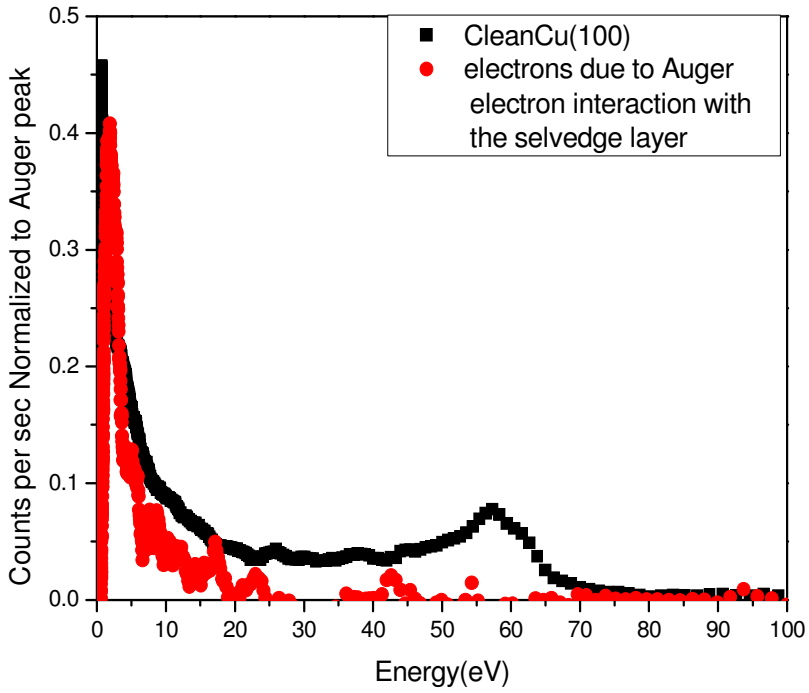

Figure 4.13 TOF-PAES spectrum of Cu. The secondary electrons produced by the interaction of Auger electrons with the selvedge layer is shown in red.

An important feature is the absence of the surface plasmons in the TOF-PAES (as well as the APECS data). This suggests that the interaction with the selvedge layer is not the dominant factor in the production of LET [30]. Hence the dominant contribution of the secondary electrons from selvedge layer should be in the low energy part and not extend all the way to the Auger peak. Additional evidence of the validity of our way of estimating the extrinsic contribution from the selvedge layer since in Fig 4.12 the spectral weight of the part of the spectrum presumed to be from inelastic collision with the overlayer. This also means that the two processes- scattering of the outgoing Auger electron with the surface electrons and the intrinsic decay of the core hole producing a wide spectrum of low energy electrons- are different both in origin as well as spectroscopically.

The Auger spectrum with the extrinsic background subtracted is shown in fig 4.14. The ratio of spectral weight area of the core holes decaying via the usual Auger mechanism to those which decay via an intrinsic multi-electron process is calculated to be 1:2.3.

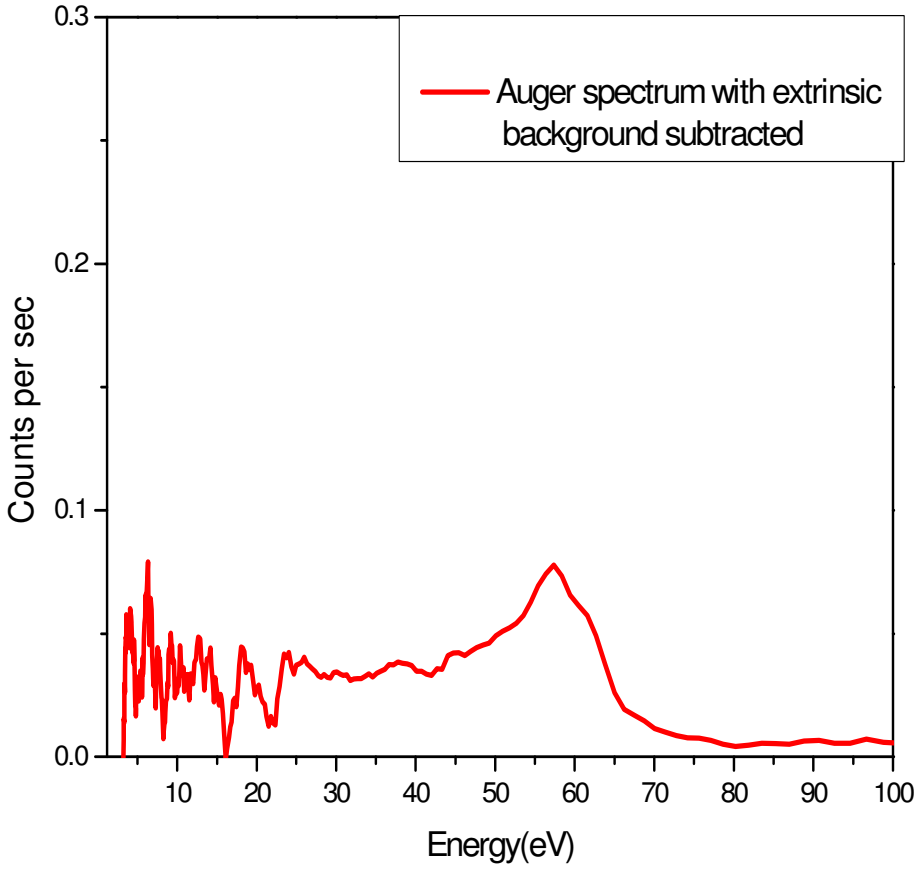

Figure 4.14 Auger spectrum of Cu with the extrinsic background subtracted.

4.6 Conclusion

Up till now in normal Auger spectroscopy (CVV) the spectral intensity below the low energy peak has been considered to be from the inelastic scattering of the primary beam and the outgoing Auger electrons. This smoothly varying background was subtracted to reveal what was thought to be the true Auger shape. In our studies, we found that most of the spectral

weight at low energies is due to the Auger process in which the core hole decays by emission of more than one Auger electron. This process is analogous to the Double Auger process found in rare gases [5]. The background associated with the Auger spectrum was eliminated using a positron beam with energy less than the secondary electron production threshold. The gamma ray induced background was found to be small based on the consideration of the Auger spectrum from Cu surface at high temperature. Hence the resulting background, which makes up the LET, is made up of (a) Auger electrons going into the bulk (b) Auger electrons scattering inelastically with the electrons in selvedge layer. The spectral intensity due to process (a) was estimated from the secondary electron yield using a positron beam of energy equal to the Auger electron. The intensity associated with process (b) was estimated by comparing the TOF-PAES spectrum from a clean Cu and Cu with submonolayer oxygen coverage. The assumption here is that the Auger electron scattering from the oxygen overlayer will be very close to the scattering off the selvedge layer. The resulting estimated was subtracted from the Auger spectrum to reveal the true Auger spectrum of Cu. The intensity on the low energy side was found to be more than twice that of the main Auger peak. This was used to calculate the percentage of the core hole which decays via usual Auger process as 30%.

CHAPTER 5

DISCUSSION

5.1 Conclusion

This dissertation presents the first demonstration of Auger mediated quantum sticking of low energy positrons to surfaces. As a positron encounters a surface from vacuum side, it can take part in number of different processes namely, penetrate below the surface and make a transition into bulk state, reflect from the surface, bind to an electron and leave the surface as Positronium or make a transition into the surface state. Earlier experiments have focused on the process of the positron penetrating into the bulk and the resulting phenomena. This dissertation has focused on the process of the positrons making a direct transition from the scattering state to the surface state and the energy spectra of the electrons emitted in this process including secondary electron and annihilation induced Auger electron.

The initial process of sticking is comparable to an Auger recombination process in semiconductors where an electron and hole recombine and give the resultant energy to another electron in the conduction band. Unlike the electron making the transition from the conduction band to the valence band, here the positrons is making a transition from the scattering state to the bound state. Furthermore this sticking process involves a transition from one quantum state to another. Hence we term this process Auger mediated quantum sticking.

An incident charged particle can lose energy either by phonon creation or electron-hole pair creation. We have experimentally verified that it is the latter that is the dominant process for the incident positron energy range of 1.5-7eV as the sticking is accompanied by secondary electron emission. The Time of flight method employed in our experiments is known to be efficient at detection of low energy electrons. The use of this technique allows us to detect the secondary electrons emitted as a result of the Auger mediated quantum sticking of

positrons. To verify that the secondary electrons are not related to core valence (CVV) Auger transition (also observed), the spectra from the hot sample (~700^{o}C) and sample at room temperature was compared. The secondary electron peak was present in the hot as well as the cold sample but the Auger peak was missing from the hot sample which means that the positron was trapped in the surface state and then desorbed. From this observation we can put an upper limit on the positron transition rate to the surface state. When the positrons at the surface are thermally desorbed, the Positronium fraction has been written as [55]

$$f = (f_0 + f_\infty \gamma^{-1} z)/(1 + \gamma^{-1} z) \qquad 5.1$$

where f_0 and f_0 are the low and high temperature limit of Positronium fraction, γ is the positron lifetime in the surface state and z is the Positronium desorption rate. Mills et al.. [55] calculated the value of $\gamma^{-1} z$ for Cu(100) surface as 4.3×10^{3}. If the positron lifetime in surface state is taken as $\sim 10^{-9}\,\mathrm{sec}$, then z is $\sim 4.3\times10^{12}\,\mathrm{sec}^{-1}$. Thus the incident positrons have to make the transition at a rate faster then z. We can estimate this number by taking the ratio of the well width to the incident positron speed. Hence the transition rate, Γ, is $\sim 6\times10^{5}/2\times10^{-10}\,\mathrm{sec}^{-1} = 3\times10^{15}\,\mathrm{sec}^{-1}$. This can be thought of as the upper limit on Γ.

The sticking process is modeled in terms of a quantum scattering problem [18]. Here we estimate the probability of this process. The probability of direct trapping of positrons was estimated from our experiments by taking the ratio of the integrated secondary electron signal to the integrated Auger signal. This has been compared to the estimates of the theoretical model giving a qualitative agreement between them. The spectrum of the electrons emitted during the Auger mediated quantum sticking is reflective of the surface density of states of the sample and may be useful in studying the local states at the surfaces and for studying two dimensional systems like graphene.

The second part of the dissertation deals with the low energy tail (LET) associated with the Auger peak. The data presented in this dissertation is the first background free Auger

spectrum from Cu ($M_{23}VV$) and Au ($N_{23}VV$). Time of flight Positron Annihilation induced Auger Spectroscopy has been used to make first measurement of Auger spectrum free of primary beam induced secondary electron background down to 0 eV. The detection of low energy electrons is possible in TOF-PAES because the electrons are detected in parallel as opposed to CMA where detection of electron is a function of its energy.

The experiments reported in this dissertation present the first experimental evidence that PAES is possible with very low energy positrons. Earlier experiments with PAES involved positrons beam energy ~ 15eV while here the experiments are with beam energy ~1.5eV.

In a conventional Auger (CVV) spectroscopy, the inelastic background is dominated by large contribution from primary beam induced secondaries. This background is typically modeled using semi-empirical function and is subtracted from the spectrum to reveal what has been assumed to be "true" Auger shape. This model assumes that the Auger transition is confined in the energy space from $E_C - \varphi^-$ on the high energy side to $E_C - 2W - \varphi^-$ on the low energy side. Here E_C is the core binding energy, φ^- is the electronic work function and W is the valence band width. Thus any spectral intensity at energy less than $E_C - 2W - \varphi^-$ is considered as extrinsic background.

In this dissertation, we have presented Auger spectra from Au and Cu which are completely free of primary beam induced secondary electrons obtained by setting the incident positron beam energy below the energy threshold for secondary electron emission. The resulting Auger spectrum had significant spectral intensity till 0eV. This point to a phenomenon where the core hole decay by emission of multiple electrons as opposed to the usual Auger process. The spectral feature below the Auger peak is referred to as Low energy Tail (LET). The electrons in the LET has been categorized as extrinsic and the intrinsic electrons. In case of PAES, the entire Auger signal comes from the top layer of atoms. The extrinsic electrons, in

case of TOF-PAES, are produced by the inelastic scattering of the Auger electrons with the bulk and the selvedge layer electrons.

We conclude that the considerable spectral weight remains after subtraction of the extrinsic loss contribution. The intrinsic part is due to the core holes decaying via mechanisms other than usual Auger process namely creation of multiple electrons which share the usual energy of the Auger electrons. Another marked feature of the LET is the absence of surface plasmons. Since PAES is a highly surface sensitive phenomenon, if the LET were caused primarily by the interaction of the Auger electrons with the selvedge layer, then there should have been surface plasmon peaks in the LET. Both, TOF-PAES and APECS spectrum, were devoid of any plasmon peaks. This leads to the conclusion that the surface interactions are not the main contributing factor to the LET. In absence of a more complete theory, the Auger electron interaction with surface electrons was probed experimentally by studying the effect on the Auger spectra of an added submonolayer surface coverage of O. The assumption here is that the outgoing Auger electrons will scatter off the oxygen atoms on the surface and will produce an effect similar to that produced by the electron gas of the selvedge layer. The contribution of the Auger electrons going into the bulk was estimated by biasing the sample to -60V and recording the secondary electron spectrum. The resulting spectrum was normalized to the Auger peak integral and the secondary electron yield from 60eV electrons (0.48). These two estimates were then subtracted from the background free Auger spectrum to yield an estimate of contribution to the intrinsic contribution to the LET. This spectra was then used to estimate the fraction of core holes which decay via the two-hole final state (Auger process) compared to the ones which decay via the emission of multiple electron for the first time for Cu-$M_{23}VV$ processes.

5.2 Future work

Positron Annihilation induced Electron Spectroscopy has been demonstrated with incident beam ~1eV. This can be used to study the magnetic surfaces such as Gadolinium in

which the core levels are extremely shallow (8eV). The positrons in our lab are produced by radioactive source and hence the beam is polarized [58]. Consecutively the Auger transition involving polarized electrons in the sample can be used to monitor the surface magnetism. The measurement of the low energy Auger lines of Gd with a spin polarized positron beam would be the first demonstration of the spin polarized positron Auger spectroscopy and will be adjunct to the conventional electron induced spin polarized Auger spectroscopy. Such a characterization technique could be very useful in the study of surface magnetism.

In the Asymptotic limit as $E \to 0, T \to 0$ the quantum sticking of particles is still a subject of considerable interest and debate. Further research, in line with that presented in this dissertation, on the quantum sticking of positrons should be useful in settling the questions of asymptotic behavior of Quantum sticking. Measurement of the PAES intensities as a function incident positron energy can provide direct measurement of the number of positrons that trap in the surface state and a method from which the sticking probability can be determined.

Background free PAES measurements utilizing Multi Stop-TOF techniques can be used to simultaneously measure the energy of all the electrons participating in process of Multi-electron Auger emission process. Such measurements will provide significant information concerning electron-electron interaction energy in strongly correlated systems.

APPENDIX A

MEASUREMENT OF GAMMA SPECTRA AS A FUNCTION OF BEAM ENERGY USING A SODIUM IODIDE DETECTOR

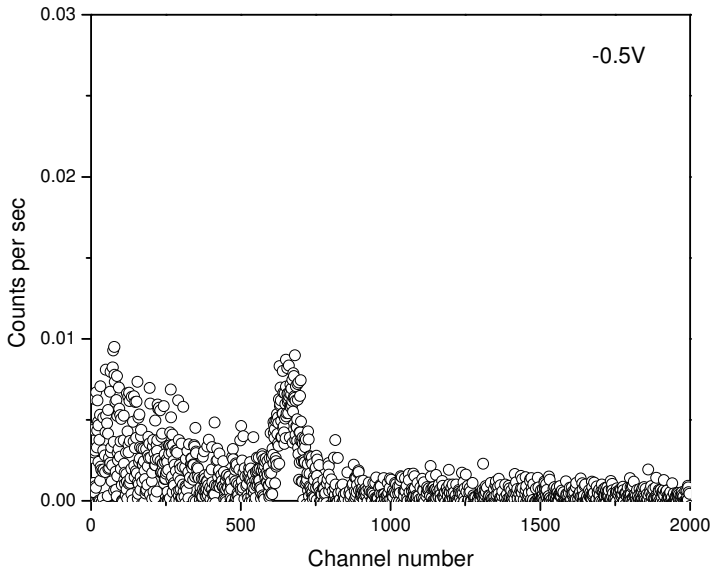

Figure A-1 NaI spectrum of Cu (100) with positron beam energy of 1eV. Sample bias is -0.5V.

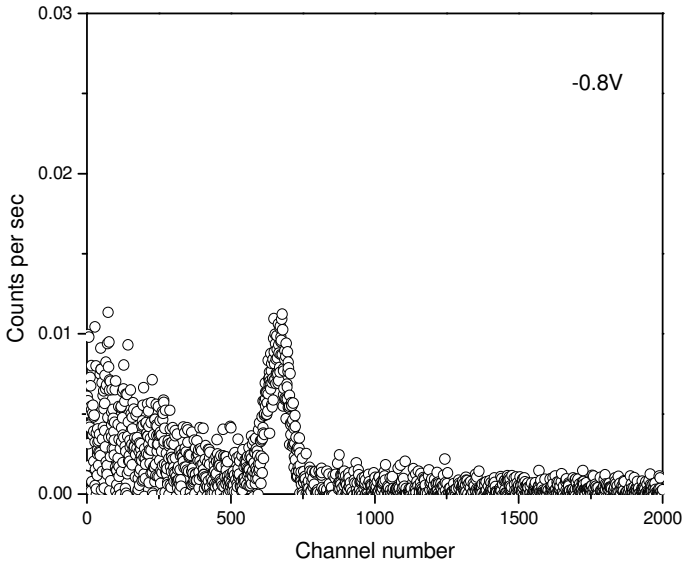

Figure A-2 NaI spectrum of Cu (100) with positron beam energy of 1eV. Sample bias is -0.8V.

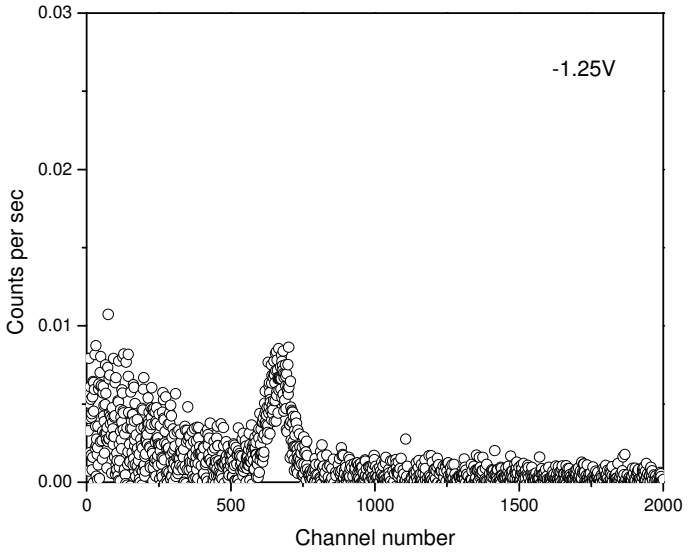

Figure A-3 NaI spectrum of Cu (100) with positron beam energy of 1eV. Sample bias is -1.25V.

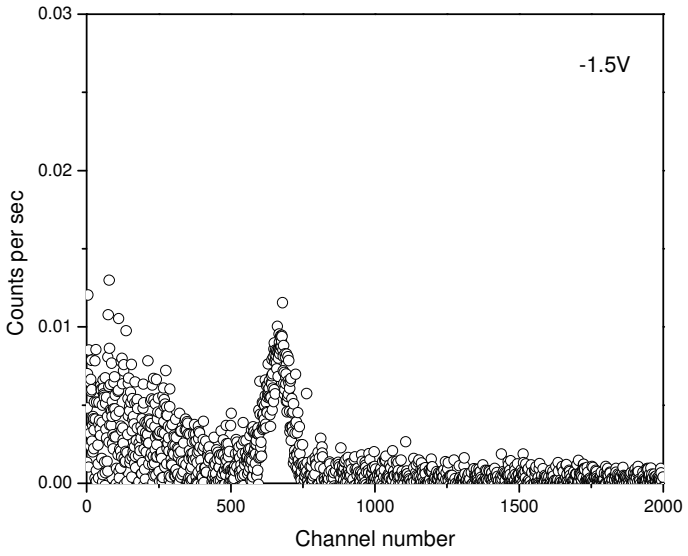

Figure A-4 NaI spectrum of Cu (100) with positron beam energy of 1eV. Sample bias is -1.5V.

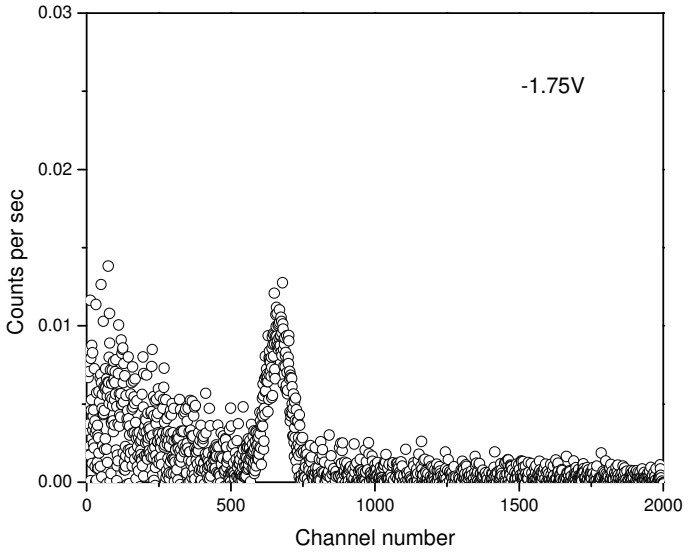

Figure A-5 NaI spectrum of Cu (100) with positron beam energy of 1eV. Sample bias is -1.75V.

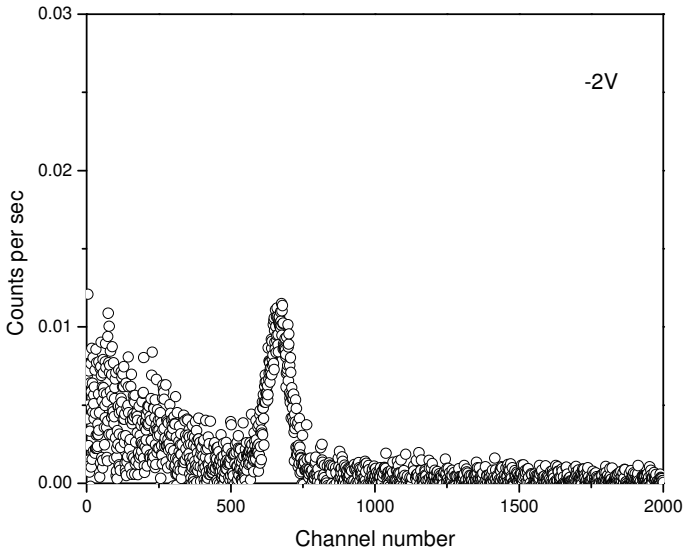

Figure A-6 NaI spectrum of Cu (100) with positron beam energy of 1eV. Sample bias is -2V.

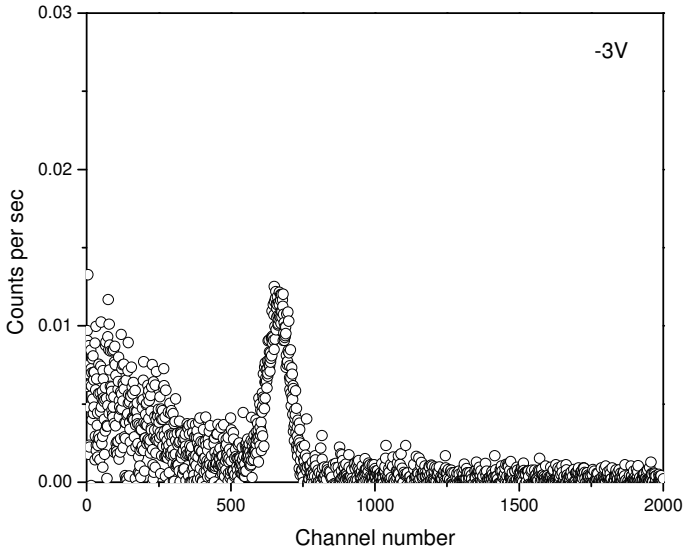

Figure A-7 NaI spectrum of Cu (100) with positron beam energy of 1eV. Sample bias is -3V.

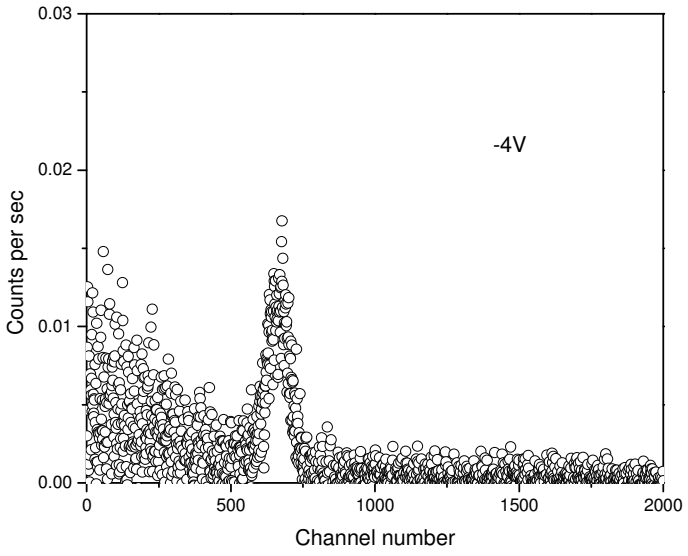

Figure A-8 NaI spectrum of Cu (100) with positron beam energy of 1eV. Sample bias is -4V.

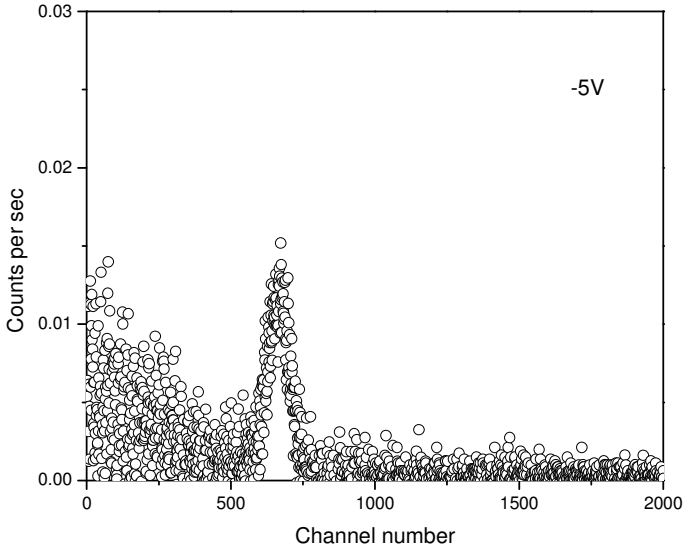

Figure A-9 NaI spectrum of Cu (100) with positron beam energy of1eV. Sample bias is -5V.

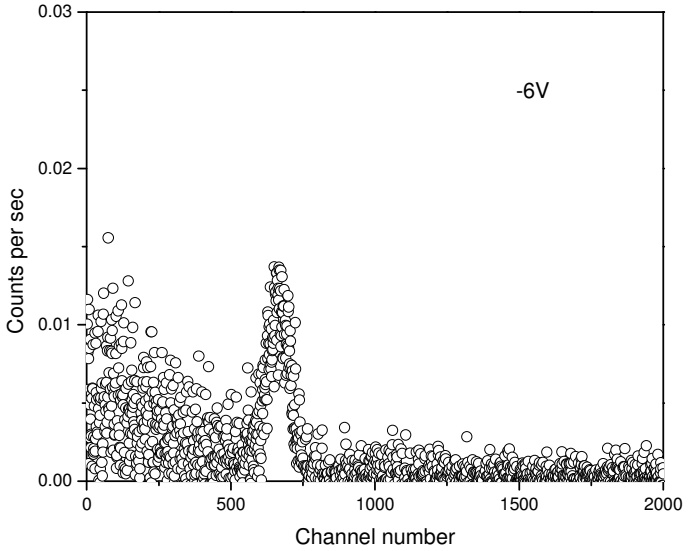

Figure A-10 NaI spectrum of Cu (100) with positron beam energy of 1eV. Sample bias is -6V.

APPENDIX B

MEASUREMENT OF THE POSITRON ANNIHILATION INDUCED LOW ENERGY OXYGEN AUGER (L_1VV) PEAK

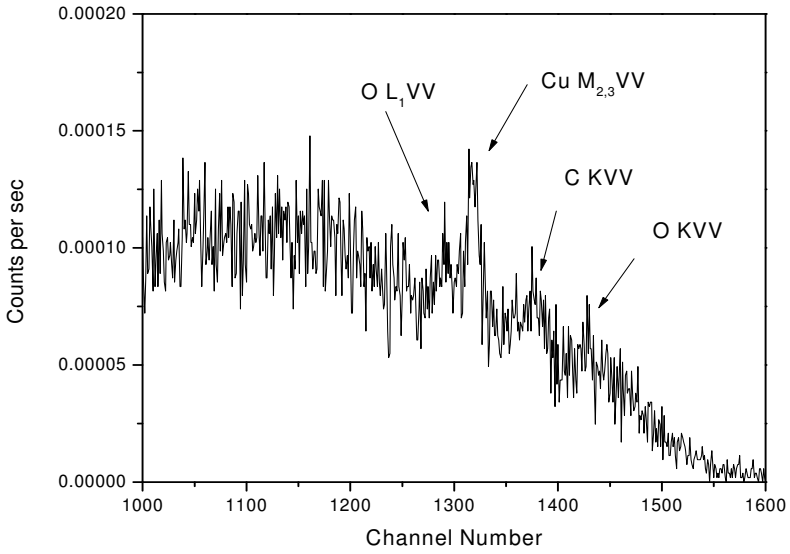

Figure B-1 TOF-PAES channel spectrum of Cu(100) showing O-L_1VV transition.

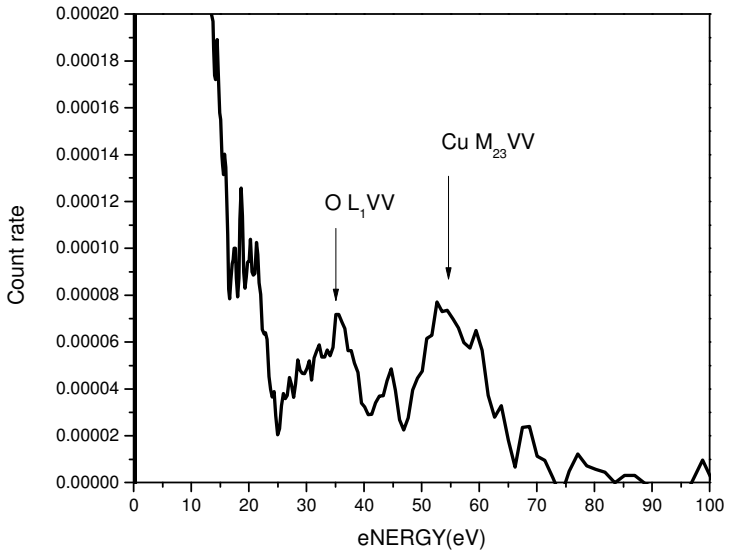

Figure B-2 TOF-PAES energy spectrum of Cu(100) showing O-L_1VV transition.

APPENDIX C

MULTI STOP TOF-PAES SPECTRUM OF COPPER

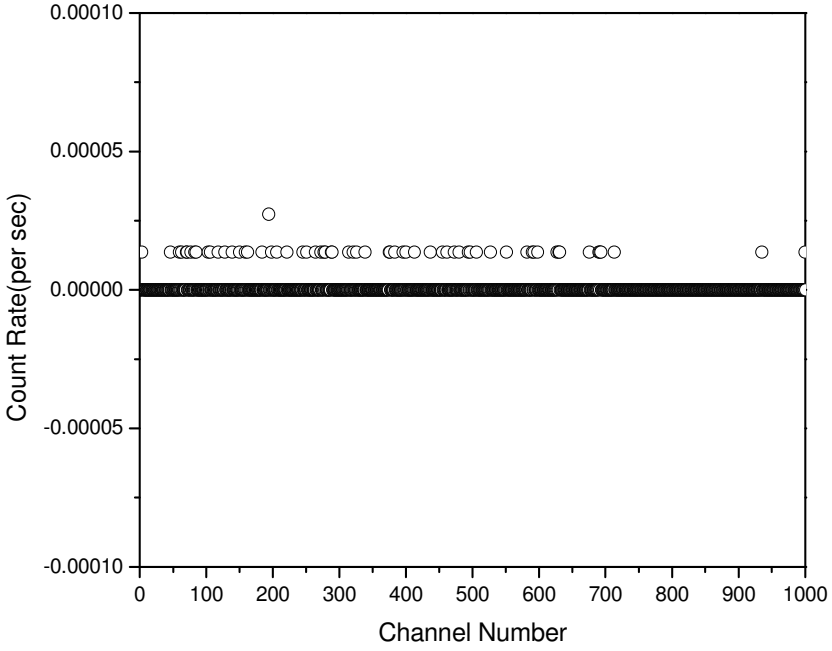

Figure C-1 Multi stop TOF-PAES spectrum of Cu(100).

APPENDIX D

POSITRONIUM LIFETIME CALCULATION

The ortho- Positronium lifetime has been calculated in this experiment from the secondary electron spectra from the hot sample (720^{o}C). At this temperature, the positrons trapped in the surface state are desorbed as Positronium before they can annihilate with the core electrons. Hence such a plot has no Auger peak while the secondary electron peak is present.

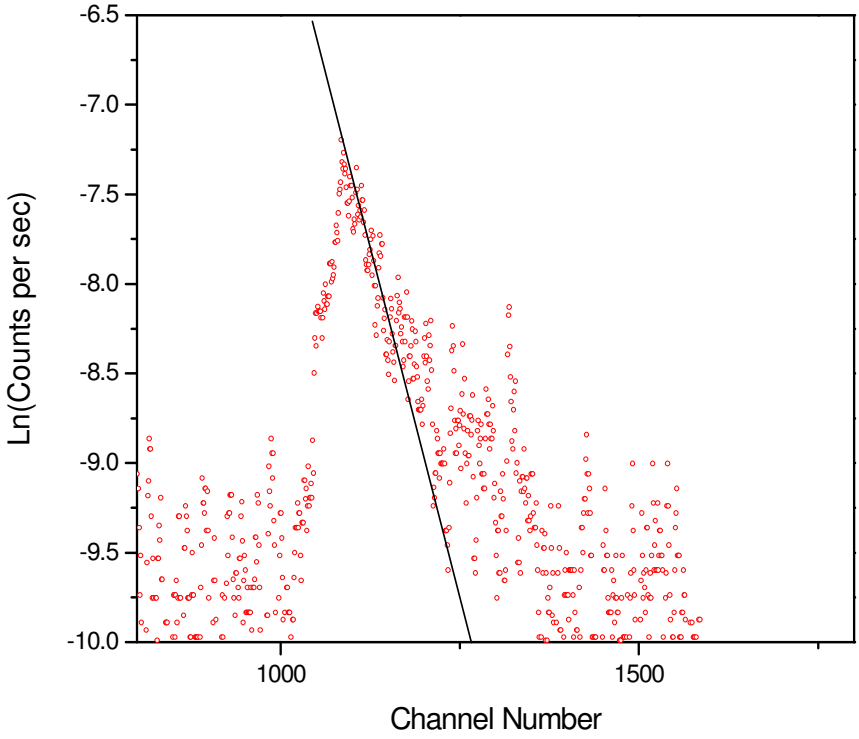

Figure D-1 Semi log plot of 5 point average of Channel Spectrum of Cu with sample temperature~720^{o}C. The slope has been fitted with a straight line of slope 0.0155.

The timing spectra when the positrons trapped in the surface state are being desorbed as Positronium is given by

$$N(t) = N_0 \exp[-t/\tau] \qquad 1$$

where τ is the ortho-Positronium lifetime. Equation 1 can be written as

$$\ln[N(t)] = \ln[N_0] - t/\tau \qquad 2$$

Now, the time is related to the channel number by a constant, $t = A\#$. Hence eq2 can be written as

$$\ln[N(t)] = \ln[N_0] - A\#/\tau \qquad 3$$

Hence the slope of the semi log plot in fig D-1 is related to the ortho-Positronium lifetime by $A/\tau = slope$. So the lifetime is given by,

$$\tau = A/Slope = \frac{\text{Range of TAC}}{\text{Total number of channels} \times \text{Slope}} \qquad 4$$

The lifetime of calculated this way is 125 nsec which is less then the actual lifetime of ortho-Positronium of 145nsec. The reduction may be explained by observing that the outgoing Positronium atoms may be annihilating on the walls of the surrounding vacuum chamber. It is interesting to note that straight line fit to the end of the TAC(fig D-2 and D-3.) and similar analysis as eq4 gives an estimate of the Positronium lifetime too.

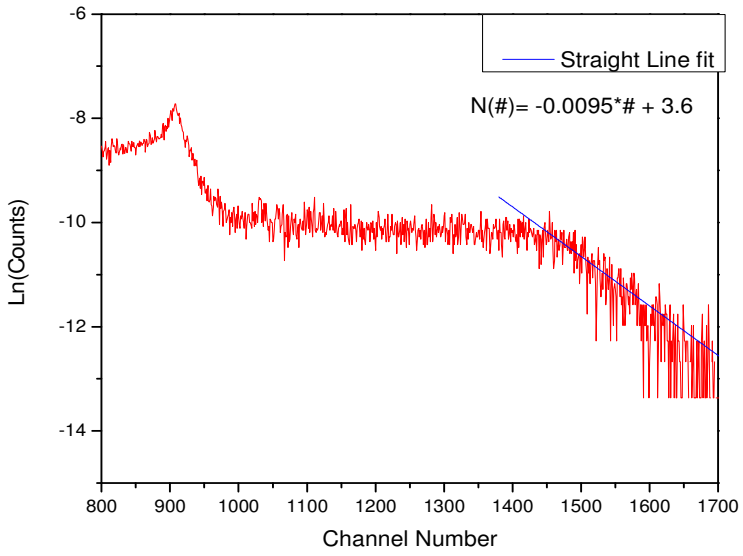

Figure D-2 Semi log plot of Channel Spectrum of Au with positron beam energy of 2eV and sample bias of -1.5V and TAC range of 2μsec.

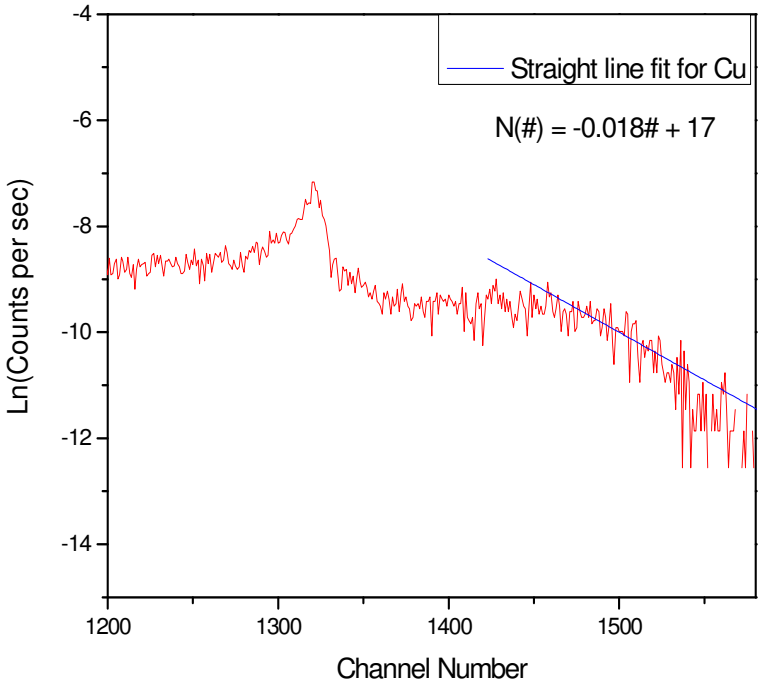

Figure D-3 Semi log plot of Channel Spectrum of Cu with positron beam energy of 1eV and sample bias of -1.25V and TAC range of 4μsec.

Here the secondary electrons from the source region provide the START signal of the TAC. In fig D-2, the range of the TAC is 2μsec while in fig D-3, it is 4 μsec. The lifetime calculated from these plots is 103nsec (fig D-3) and 109nsec (fig D-3).

REFERENCES

1a. K.H.Lee, Gimo Yang, A.R.Koymen, A.H.Weiss, Phys Rev. Lett., 72 (1994)

1b. J.H.Kim, A.H.Weiss, Surface Science, 460 (2000)

1c J.Zhu, Journal of Applied Physics, 97 (2005)

2. Th. Martin, R. Bruinsma, Phys.Rev.B, 39,16(1989)

3. Landau, lifshitz, Quantum Mechanic

4. A.P.Mills, Phys.Rev.Lett. 66, 735 - 738 (1991)

5. Thomas A. Carlson and Manfred O. Krause, Phys. Rev. Lett., 14, 390 - 392 (1965)

6. Thomas A. Carlson, Phys. Rev. 169, 27-36 (1968)

7. D.Chatterji, The theory of Auger Transitions, Academic Press (1976)

8. E. N. Sickafus, Phys. Rev. B, 16,1436-1447(1977)

9. M.P. Seah, Surface Science, 17, 132-160 (1969)

10. E. Jensen, Phys. Rev. B 45, 13636 - 13641 (1992)

11. A.P.Mills, Jr., in The Proceedings of the International School of Physics “Enrico Fermi”,p.432, North –Holland , New York (1981)

12. A.H.Weiss, Phys. Rev. Lett., 61, 2245 - 2248 (1988)

13. Kjeld O. Jensen and A.H.Weiss, Phys. Rev. B 41, 3928 - 3936 (1990)

14. Kjeld O. Jensen and Alison B.Walker, Phys. Rev. B 49, 2215 - 2217 (1994)

15. S.Xie, PhD Dissertation, University of Texas Arlington (2002)

16. F.Penent, Journal of Electron Spectroscopy and Related Phenomena , 7-11,144-147, (2005)

17. J.D.Jackson, Classical Electrodynamics, John Wiley & Sons 1998

18. Alison B. Walker, Kjeld O. Jensen, J. Szymański, D. Neilson , Phys. Rev. B 46,1687 (1992)

19. D.T. Britton, Phys. Rev. Lett. 62, 2413 - 2416 (1989)

20. Quantum Physics of Atoms, Molecules, Solids ,Nuclei and Particles, R. Eisberg and R Resnick

21. Rulon Mayer ,Alex Weiss , Phys. Rev. B 38 11927(1988)

22. N. Overton ,P. G. Coleman ,Phys. Rev. Lett. 79, 305 (1997).

23. A.P. Knights, P.G. Coleman, Surface Science, 367 , 238-244 (1996)

24. Mani Farjam and Herbert B. Shore, Phys. Rev. B 36, 5089 (1987)

25. A. P. Mills, Jr. and Loren Pfeiffer, Phys. Rev. Lett. 43, 1961 (1979)

26. Clint D Thomson, PhD Dissertation, Utah State University (2005)

27. M.P. Seah ,Surface Science ,17,132-160 (1969)

28. Haiqing Zhou, PhD Dissertation, University of Texas at Arlington (1996)

30. E. Jensen, Phys. Rev. B, 45,23 (1992)

31. David Mehl, PhD Dissertation, University of Texas at Arlington (1992)

32. Yinghong Lin, D.C. Joy, Surface and Interface analysis, 37 (2005)

33. E.Jensen, R.A Bartynski, Review of Scientific Instruments 63 ,3013-26 (1992)

34. Dario Arena, PhD dissertation, Rutgers University (2000)

35. N.G.Fazleev, Radiation Physics and Chemistry, v 58, n 5, p 659-665 (2000)

36. J.A.Knapp et al.., Phys Rev. B., 19,10, 1979

37. D. Eastman, J.K. Cashion, Phys. Rev. Lett., 24 (1970)

38. K. Shastry, to be published

39. J. H. Kim, G. Yang, A. H. Weiss, Surf. Sci., 396, 388-393 (1998)

40. N. G. Fazleev, J. L Fry, and A. H. Weiss, Phys. Rev. B. 57, 12506-12519 (1998)

41. N. G. Fazleev, J. L. Fry, and A. H. Weiss, Rad. Phys. and Chem. 58, 659-665 (2000)

42. N. G. Fazleev, S. Starnes, A. H. Weiss and J. L. Fry, Rad. Phys. and Chem. 58, 667-673, (2000)

43. J. H. Kim, A. Nangia, and A. H. Weiss, Rad. Phys. and Chem. 58, 655-658 (2000)

44. J. H. Kim and A.H. Weiss, Surf. Sci., 460, 129-135 (2000)

45. J.H. Kim, K.H. Lee, G. Yang, A.R. Koymen, and A.H. Weiss, Nucl. Instrum. and Meth. in Phys. Res.,. B 171, 231-235 (2000)

46. N. G. Fazleev, J. L. Fry, A. H. Weiss in Applications of Accelerators in Research and Industry, edited by J.L. Duggan and I. L. Morgan, AIP Conf. Proc. 576, 753 (AIP, New York, 2001)

47. J. H. Kim, G. Yang, S. Yang, and A. H. Weiss, Surf. Sci., 475, 37-46 (2001)

48. Alex H. Weiss , Mats. Sci. Forum, 363-365, 537-541 (2001)

49. N.G. Fazleev, J.L. Fry, and A. H. Weiss, Materials Science Forum, 363-365, 451-453 (2001)

50. W.-C. Chen, N.G. Fazleev, J.L. Fry, and A.H. Weiss, Mats. Sci. Forum, 363-365, 621-623 (2001)

51. Thomas A. Carlson, Manfred Krause, Phys. Rev. Lett., 17, 21 (1966)

52. Y.C.Jean, P.E.Mellon and D.M.Schrader, "Positron and Positronium Chemistry", World Scientific (2002)

53. R. Mayer, E. Gramsch, and A. Weiss, Phys. Rev. B.,40, 11287 (1989)

54. Rulon Mayer and Alex Weiss, Phys. Rev.B., 38, 11927 (1988)

55. A.P.Mills, Solid State Communications, Vol31,(1979)

56. A.H.Weiss, D.Mehl, A.R.Koymen, J.Vac.Sci.Tech.,8,3,(1990)

57. P Kruit, F.H.Read, 16, J. Phys. E (1983)

58. D.W.Gidley, A.R. Koymen, Phys. Rev. Lett. 49, 1779 - 1783 (1982)

59. J.A.Baker , M Touat, P.G.Coleman, J. Phys. C: Solid State Phys., **21** (1988)

BIOGRAPHICAL INFORMATION

Saurabh Mukherjee received his Bachelor of Technology degree in Ceramic Engineering from Banaras Hindu University in 2003. Then he moved to University of Texas at Arlington in Fall 2004 as a masters student in Materials Science and Engineering. He completed his Masters in 2006 with dissertation titled “SURFACE MODIFICATION OF 6H-SiC UNDER VACUUM ANNEALING STUDIED BY TIME OF FLIGHT POSITRON ANNIHILATION INDUCED AUGER ELECTRON SPECTROSCOPY”. He joined the Physics Department at UTA as a PhD student in Spring 2006 and completed his studies in December 2008.